Abstract

Title of Document: A TEMPERATURE-CONTROLLED ELECTROCHEMICAL MICROSCALE PLATFORM FOR BIOMOLEMULAR BINDING STUDIES

Zuliang Shen, Doctor of Philosopghy, 2014

Directed by: Professor Herman O. Sintim,
Department of Chemistry and Biochemistry
Dr. Steve Semancik,
National Institute of Standards and Technology

Electrochemical detection of nucleic acids has been a very important research area in the past several decades. In this research field, the stability of the nucleic acid structure is important and crucial for many aspects of nucleic acid metabolism. Also the binding of small molecule ligands to nucleic acids and resulting increase in stability of the nucleic acids can play a key role in many context including DNA-targeted therapy against various cancers, bacteria or viruses. Melting curve analysis using electrochemical detection, as a new method to characterize nucleic acids' stability and interactions between small molecules, provides high sensitivity and is also well suited for high-throughput formats. This thesis describes efforts to develop melting curve analysis using electrochemical detection method on a temperature-controlled microscale platform. Three chapters are included in this thesis.

Chapter 1 is a literature review of electrochemical DNA biosensors and microdevices. The general concepts of electrochemical detection, the development of various electrochemical microdevices for nucleic acids detection, and the common microfabrication technologies to fabricate these microdevices were introduced.

Chapter 2 introduces two electrochemical junction probe (JP) detection methods using isothermal amplification to sense specific DNA sequence. First, we describe the design and detection of signal-off electrochemical JP detection using restriction endonucleases. Second, we discuss the screening of the restriction endonucleases and the best candidate for this electrochemical JP detection. Lastly, we discuss the design, nucleic acids mismatch using signal-on electrochemical JP and the detection limit of this signal-on electrochemical JP detection technique.

Chapter 3a describes the development of a new microscale electrochemical measurement system. Fabrication was achieved using lithographic technology to integrate all required electronic components in a compact device for measurements on small-volume liquid samples. The integrated approach lends itself to parallel fabrication, which can be readily adapted to realize arrays of individual devices for high-throughput screening. The microfabricated imbedded resistive Pt heater below the electrodes allows rapid temperature control, and independent current monitoring that enables melting temperature determination for DNA structures. The small size, thin profile and overall low thermal mass of our configuration have inherent advantages relating to effective heat transfer and minimization of thermal gradients. Proof-of-concept measurements made with our platform for DNA melting directly relate to SNP applications.

Chapter 3b demonstrates an application for anti-cancer ligand discovery using the microscale electrochemical measurement system developed in Chapter 3a. We describe the design and concept to achieve G-quadruplex/ligand melting curve analysis using electrochemical detection. And we tested telomere G-quadruplex structure with and without the presence of the SYUIQ-5 ligand. Upon ligand binding, the stabilized G-quadruplex structure results a melting temperature shift to a higher temperature.

A TEMPERATURE-CONTROLLED ELECTROCHEMICAL MIROSCALE PLATFORM FOR BIOMOLEMULAR BINDING STUDIES

By

Zuliang Shen

Dissertation submitted to the Faculty of the Graduate School of the
University of Maryland, College Park, in partial fulfillment
of the requirements for the degree of
Doctor of Philosophy
2014

Advisory Committee:

Professor Herman O. Sintim, Chair
Professor Steve Semancik
Professor Jeffery Davis
Professor Yuhuang Wang
Professor Zhihong Nie
Professor Don L. Devoe

Dedication

To my parents, Wei Shen and Gang Wang,

and my wife Tongyun Li

Acknowledgements

I would like to thank my Ph.D advisors Herman O. Sintim and Steve Semancik for their guidance throughout my graduate studies. Their knowledge, motivation and support have helped me a lot throughout my five year academic research.

It was my pleasure to work with supportive colleagues in the Sintim lab and Semancik lab. I want to express sincere gratitude to all of you. I want to thank Dr. Phillip Rogers, Dr. Shizuka Nakayama, Dr. Ryan West and Dr. Kurt D. Benkstein for their helpful discussion.

I want to thank the National Institute Standards and Technology (NIST) Center for Nanoscale Science and Technology NanoFab Facility and the staff members. The supportive NIST scientists are very important for my academic success. I would like to thank Dr. Christopher B. Montgomery for all the help for wire bounding the microdevices for me and teaching me all the essential knowledge. I especially want to thank Michael J. Carrier for all the guidance and discussion to help me start with microdevice design and fabrication. I also want to thank Gregory A. Cooksey for the help for microfluidic technology.

Finally, I would like to thank my parents and my wife. This accomplishment would have never been possible without your encouragement. I really appreciate everything you have done for me all these years.

Table of Contents

List of Figures

Chapter 1

Chapter 2

Chapter 3

Chapter 4

List of Tables

Chapter 2

Chapter 3

I. Chapter 1: Introduction to electrochemical detection of bioanalytes and microfabrication of measurement platforms

1a. Introduction to electrochemical detection of bioanalytes

1a.1. Introduction.

There has been tremendous interest in developing sensor devices for bioanalyte detection. These sensors are composed of three components, a measureable signal response from a recognition element that can selectively respond to a particular analyte and minimize the interferences from other components; another is the signal transducer that produces a signal; and finally a processor or readout that collects, amplifies and displays the signal.[1] Electrochemical biosensors represent a subclass of chemical sensors and is currently one of the most active areas of research in analytical chemistry.[1] An important goal in this field is the development of cheap miniaturized electrochemical sensors that can rapidly and sensitively detect bioanalytes.

1a.2. Electrochemical Detection

Bioanalyte detection that relies on electrochemical signals is desired due to the portability, low cost and simplicity of fabrication associated with electrochemical platforms. There are several ways to monitor reactions and interactions electrochemically: amperometry, potentionmetry, conductometry and electrochemical impedance spectroscopy. Amprometry measures the current generated from the reaction. Potentionmetry measures the potential or a measurable charge accumulation. Conductometry measures the conductive properties of the medium between the electrodes. Electrochemical impedance spectroscopy is used to monitor two

properties, resistance and reactance in the biosensors.[2] Electrochemistry offers low detection limits with little or no sample preparation. Also measurements can be done with very small volumes.[3] Electrochemical detection, unlike optical detection methods that suffer from high background noise due to the presence of biological chromophores or fluorophores, is not overly affected with interference from biological components. For example, colored whole blood sample can be measured without interference by red blood cells, hemoglobin or fat globules.[4,5]

Current measurement is one of the most important categories of electrochemical measurement techniques. Voltammetry and amperometry are current measuring techniques that are characterized by applying a potential to a working electrode versus a reference electrode. Electrochemical oxidation or reduction occurring at the working electrode surface produces the electrolysis current. The mass transport rate of the molecules to the electrode surface limits the electrolysis current.[6] The voltammetry method is used by applying potential to scan over a set potential range. The current peak appears at the redox potential that is proportional to the concentration of analyte. There are many voltammetric methods with a wide dynamic range used extensively in low level quantitation in electrochemical detection, such as cyclic voltammetry, square-wave voltammetry, alternating current voltammetry, linear sweep voltammetry, differential pulse voltammetry and stripping voltmmetry.[6] Amperometry requires a constant potential which is maintained at the working electrode with respect to a reference electrode and one measures the changes in current which are generated by the electrochemical oxidation or reduction with time. Potential is set at a desired value (redox potential) for current measurement. The current value is proportional to the concentration of the electroactive moieties in the analyte over time. [7]

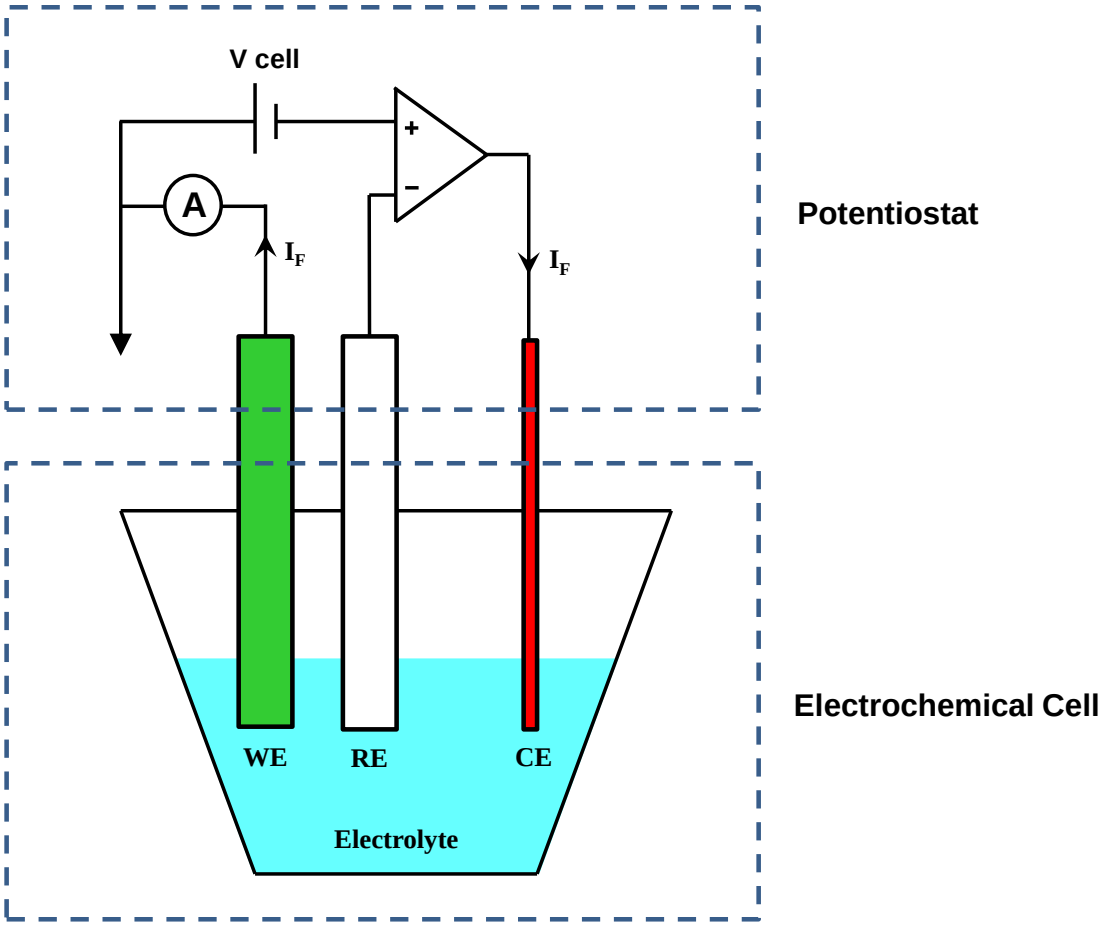

Figure 1.1. An electrochemical cell setup and connected to a potentiostat.

Electrochemical redox reactions take place in an electrochemical cell. There are two typical electrode systems, one is called three-electrode system, another is the two-electrode system. A three-electrode system consists of a working (indicator) electrode, a counter (auxiliary) electrode and a reference electrode.[2] The working electrode is a solid conductive material, e.g. graphite, gold or platinum, since the reaction of interest is occurring at that location, and these materials are chemically stable. The counter electrode allows the reaction current to flow, and the potential of the counter electrode is adjusted in order to balance the reaction occurring at the working electrode. The potential of the counter electrode is adjusted to balance the reaction at the working electrode; such a setup allows the potential of the working electrode to be measured against a

known potential reference electrode. The reference electrode requires high stability of the electrode potential by incorporating a redox system with constant concentration of each reactants of the redox reaction. An Ag/AgCl reference electrode is one of the choices, and it consists of a silver metal coated with a silver chloride layer. A two-electrode system doesn't have a reference electrode and a known current or potential is introduced to flow through the working and counter electrodes. This kind of system doesn't need long-term stablibity of the reference electrode and is usually created for disposable purposes, and reduces the cost for the system.

Electrode systems can be easily miniaturized by fabricating the electrode size on the order of micrometers, even nanometers.[8-10] The miniaturization of the electrode creates high sensitivity and leads to small sample volumes due to such small electrode surface area. Nanoparticles, nanotubes and nanowires provide these advantages and have been successfully applied into biosensor fabrication.[11] Miniaturized electrochemical detectors and portable control instrumentations are ideal components for biosensors applications. And this technology can be relatively low cost when one employs micromachining and microfabrication methods.[12]

1a.3. Electrochemical DNA Sensors

Electrochemical DNA sensors represent one of the important research areas in biomedical research. These devices can play a crucial role in clinical diagnostics of genetic diseases, analysis of forensic samples and monitoring of infectious bacteria.[13,14] Recently numerous innovative designs for DNA-based electrochemical sensors have appeared.[14] Electrochemical transducers that incorporate nucleic acid layers, can provide accurate, simple and inexpensive platforms for clinical diagnosis.[15]

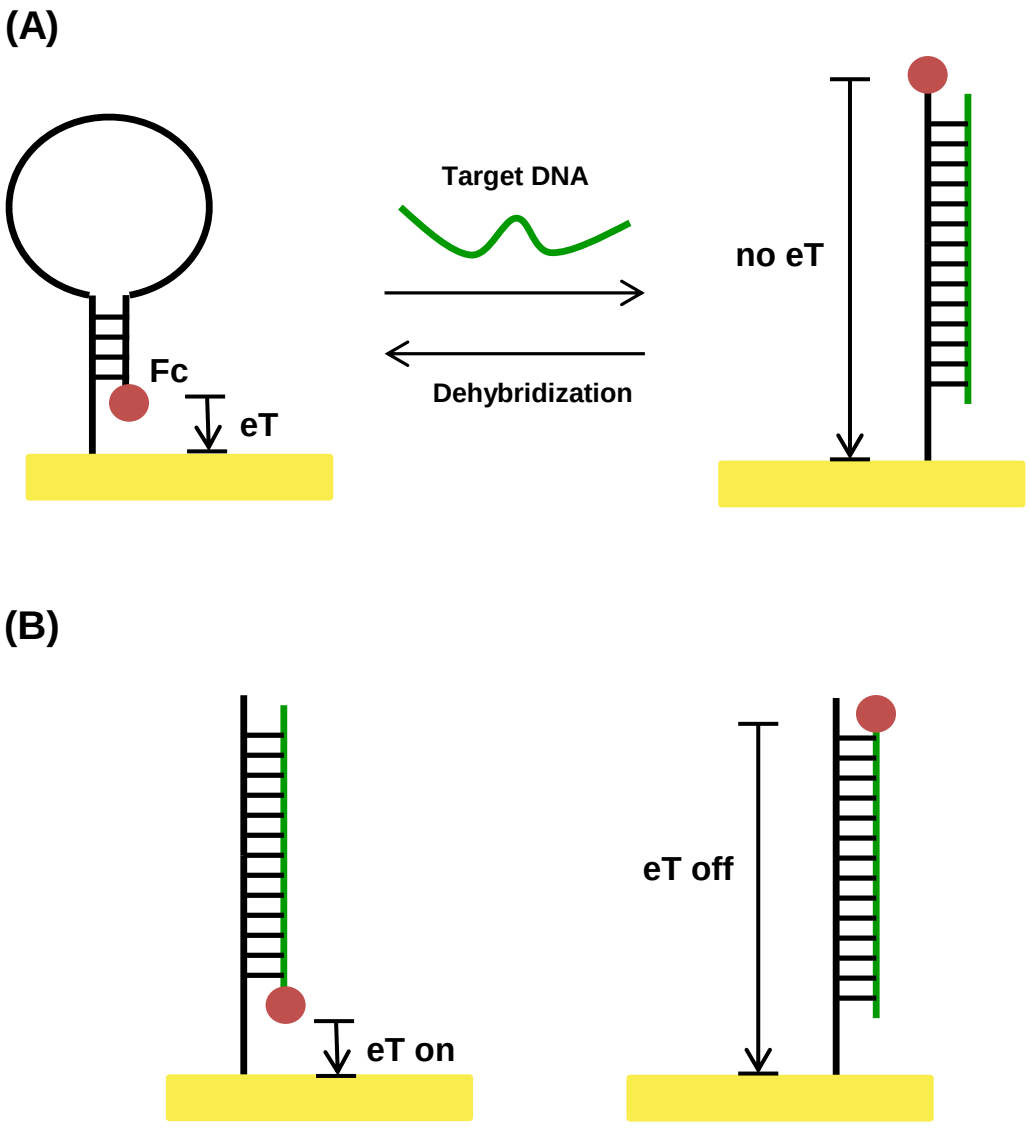

Figure 1.2. (A) An electrochemical DNA sensor realized by attaching redox ferrocene (Fc)-labeled stem-loop DNA probe on the gold electrode surface. Upon target DNA hybridization, the structural switching from stem-loop to double-stranded DNA resulted in inhibition of electron transfer (eT) between the Fc tag and the surface of the gold electrode. (B) Labeled Fc at different locations on surface-tethered DNA duplexes can change the eT of Fc significantly.

The earliest electrochemical DNA detection work involved sensing the oxidation and reduction of DNA on mercury electrodes. On the surface of the electrode, the amount of the

DNA captured was determined by the amount of the DNA oxidized or reduced. Palacek was the first to demonstrate that double-stranded DNA could be distinguished from single-stranded DNA using electrochemical means.[16] In 1993, Millan developed the first electrochemical DNA sensor using carbon electrodes and used electrochemically-active double-helix intercalators to discriminate between single-stranded DNA and double-stranded DNA.[17] One year later, a similar method was developed by Hashimoto et al. to assemble thiolated DNA probes onto gold electrode surfaces through Au-S chemistry.[18] Three years later, in 1997, Tarlov and co-workers improved the method and disclosed a two-step protocol for making a stable mercaptohexanol monolayer on a gold electrode.[19,20] Yu et. al developed a sandwich-type method with an electroactive ferrocene (Fc) reporter-labeled probe pairing with capture probe to distinguish target DNA sequences.[21] In 2003, Fan et. al designed a strategy by self-assembling a redox Fc tagged stem loop DNA probe on a gold electrode surface, as illustrated in Fig. 1.2A. The Fc redox tag was held very close to the gold electrode surface by the stem-loop and produced a strong electrochemical current signal. The strong electrochemical signal was altered via target DNA induced conformational change, which liberated the Fc tag from the gold electrode surface. This distance-based electron transfer (eT) limited the electrochemical signal and led to the detection of matched target DNA.[22] In order to prove that such small target-induced conformational changes of a surface-attached, redox tag labeled DNA would significantly affect the eT rates, as shown in Fig. 1.2B, a simple design was composed by self-assembling probe DNA on the gold electrode surface, followed by hybridizing the DNA target with electroactive Fc moiety labeled at different ends. This resulted in the Fc locations either close to or positioned away from the surface. After cyclic voltammetry measurements, such a small distance between

the electroactive moiety and the electrode surface showed a well-defined redox signal from the close target-version, but only featureless currents from the distant version.[23,24]

Most reported DNA detection using the transfer of electrons from electroactive groups to a conducting surface have used a signal-off approach and these signal-off designs have a limit of detection of around 10 pM level.[15] However in the real world, signal-off sensors are susceptible to false positives. To improve sensitivity, aptamer-based electrochemical DNA sensors and enzyme-based electrochemical DNA sensors were developed with signal-on detection technology. [24-28] These approaches can detect a range of analytes, such as proteins or small molecules.

The aptamer-based design is an extension of the previous signal-off DNA sensors shown in Fig. 1.2B. Signal-on detection can be incorporated by introducing an electrochemical aptamer switch strategy for an analyte, such as adenosine triphosphate (ATP), as shown in Fig. 1.3. For ATP detection, dually labeled 5'-Fc and 3'-SH anti-ATP single-stranded probe DNA was self-assembled on the gold electrode surface and then hybridized with its complementary sequence. The resulting duplex DNA positioned the Fc unit far away from the conducting surface (see Fig. 1.3A). However, in the presence of ATP, the analyte competes with the full-matched DNA strand for binding to the ATP aptamer. Upon ATP binding to the aptamer, the resulting conformational change for the aptamer structure brings the Fc redox moiety close to the electrode surface, resulting in the enhancement of the eT signal up to 10-fold. This approach provides high sensitivity with a 10 nM limit of detection for ATP detection. Another advantage of this signal-on approach is the excellent selectivity, where the aptamer structure only responds to ATP molecules. Furthermore, this signal-on technique is also suitable for ATP detection in

cell lysate.[24] Recently, other interesting signal-on designs that have detection limits in the picomolar and femtomolar range have been reportaed.[11]

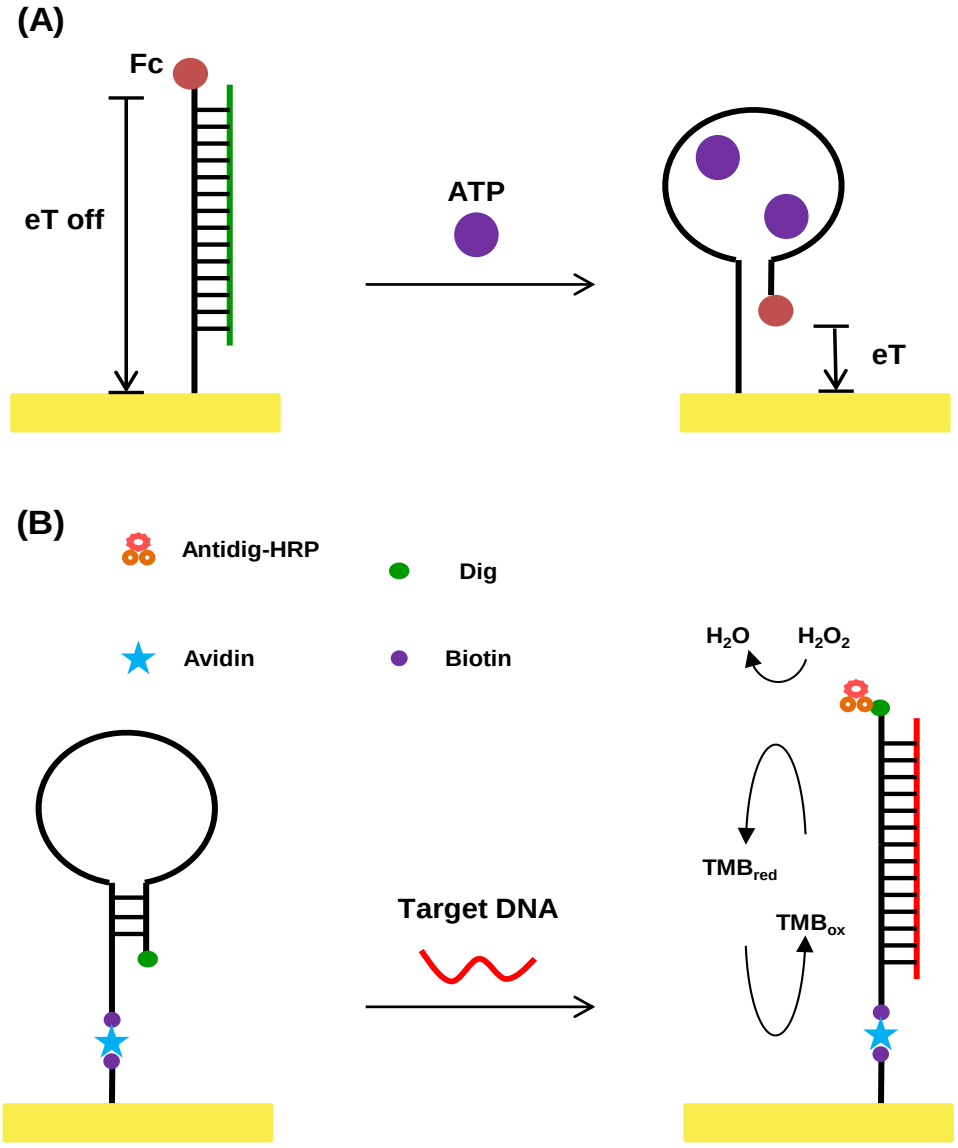

Figure 1.3. (A) An ATP signal-on electrochemical aptamer sensor that employs a Fc redox tag. The detection is based on target-induced conformational changes. (B) An enzyme-based electrochemical DNA sensor.

Enzyme-based electrochemical DNA sensors can achieve femtomolar sensitivity. The operating strategy also involves a signal-on approach, but not via the distance-dependent electron

transfer as described above for DNA or ATP sensing. The enzyme electrochemical sensor design is based on self-assembled probe DNA on the electrode surface with digoxigenin (DIG) -labeled at the 3'end (see Fig. 1.3B). The stem-loop structure at the initial state sterically prevents the conjugation between the DIG label and bulky anti-DIG-HRP (horseradish-peroxidase-linked-anti-DIG antibody). When a cDNA is introduced to hybridize and form a duplex structure with the surface tethered DIG-labeled probe, the exposed DIG becomes bound to the anti-DIG-HRP and turns on the catalyzed electrochemical current signal. The enzyme-based electrochemical DNA sensor can achieve a 10 fM limit of detection.[29]

The signal-on feature, excellent selectivity and high sensitivity brought by the aptamer-based electrochemical DNA sensors and the enzyme-based electrochemical DNA sensors open the door for single-nucleotide polymorphisms (SNPs) detection. Molecular beacons, which are capable of discriminating single-mismatch DNA from full match due to the internal conformational constraints of the stem-loop structure, can be coupled to electrochemical detection for sensitive sensing.[15,30]

Efforts have focused on improving the sensitivity of electrochemical DNA sensing. Researchers started to focus on amplification of the electrochemical signal dependent on the hybridization event. Use of nanoparticles (e.g. gold nanoparticles, quantum dots) based on catalysis or metal-based stripping has had a significant impact on electrochemical signal amplification. Recent developments include using AuNPs (gold nanoparticles) for heavy loading DNA probe reporters and employing $[Ru(NH_3)_6^{3+}]$ redox molecules for heavy binding to the charged DNA strands.[31] Quantitative measurements based on hybridization events lead to a detection limit of 10 fM. Signal amplification depends on the loading of one AuNPs and the amount of the binding $[Ru(NH_3)_6^{3+}]$ redox molecule. Each AuNP can carry hundreds of reporter

DNA strands, and a large number of small [$Ru(NH_3)_6^{3+}$] could bind to the charged DNA strands. Such binding dependent hybridizations can amplify the electrochemical signal by several orders of magnitude.

For these redox-active, self-assembled electrochemical DNA biosensors, the distance between the electrode and the redox reporter is key to controlling the electronic coupling. As Equation 1.1 shows, where k_{ET} is the rate constant for electron transfer, A is a preexponential factor, β is the decay constant, and d is the length between the electrode surface and the redox moiety center[32]

$$k_{ET} = Ae^{-\beta d} \quad (1.1)$$

As predicted by the equation, the rate of electron transfer (k_{ET}) decreases as the distance between the electrode surface and redox moiety increases. And the rate of electron transfer can be determined by using electrochemical methods such as cyclic voltammetry, alternating current voltammetry and electrochemical impedance spectroscopy.

1a.4. Summary

Since development began on electrochemical DNA biosensors, these sensors have played a continuously larger role in many clinical, pharmaceutical, environmental and food security applications, aided by the excellent sensitivity and selectivity provided. Both signal-off and signal-on electrochemical biosensors have great potential going forward to be miniaturized into portable devices for the consumer market. Strategies for building electrochemical sensors with modern nanotechnology and material science hold great potential. New designs with improved sensitivity and selectivity are expected to appear in the future.

1b. Introduction to Microfabrication for Bioanalytes Detections.

1b.1. Introduction

In the past 30 years, DNA sequencing and detection have attracted interest from many quarters. Because these analytical applications provide potential benefits related to the biomedical, environmental and forensics field, DNA sensors built on lab-on-a-chip (LOC) devices began to appear in the research field. The possibility of developing portable devices and instrumentation has caught more and more attention for medical diagnostics and screening. Analytical LOC devices are microfluidic devices that are capable of performing accurate and fast automatic laboratory DNA sequencing or detection. These LOC devices are miniaturized biosensors that convert biological and biochemical responses into measureable mechanical or electronic signals. Microscale experiments with tiny amounts of analytes can be conducted on these miniaturized low cost laboratories. By fabricating multiple biosensors on to the microscale devices, fast and parallel high sensitivity measurements can be conducted by incorporating microfluidic sample delivery systems. The use of the high-throughput screening opens the door for developing robust microsystems in biochemical and biomedical applications. Furthermore, the fabrication for building these miniaturized electrochemical transducers in the microsystem is relatively easy and compatible with most of the current detection methods.[33]

The first automated and integrated small devices that could perform laboratory operations were found in early 1990s. These devices had many advantages compared to the existing analytical system and can perform experiments with lower reagent consumption provide faster analysis time and has higher efficiency.[34] The first microfabricated microscale multifunctional closed system was reported in 1998.[35] The size of the device was only several square centimeters

and 1 mm in height. The device had built in hearers, temperature sensors, detectors and microfluidic channels for nanoliter-sized DNA samples preparation and analysis using gel electrophoresis. Reduced assay cost and sample contamination together with the minimization of harzaduos waste provided the motivation for developing microscale devices. Additionally, scaling down also provide shorter reaction time, better mixing efficiency, faster heat transport and higher reaction yields.[36]

Optical detection methods, using fluorescent dyes and surface plasmon resonance, have dominated the DNA sensor fields. But the relatively expensive sample and instrumentation cost, considerable labor cost for the analysts, and complexity of the procedures are the down side of the optical methods. Electrochemistry detection can be employed into LOC devices easily, and the simpler electrochemical readout is another main advantage. Integrated electrochemical LOC devices are excellent candidates for the DNA microchip industry since they offer easy signal integration, low fabrication cost, fast response, high sensitivity and small dimensions. By the end of last century, researchers in drug discovery, clinical diagnostics and pharmaceutical biomolecule screening showed an increasing demand for development and production of small, fast, cheap, easy to use and sensitive devices. The microscale electrochemical LOC devices concept can achieve this goal to fulfill the needs of biosensor industry.[33]

1b.2. Integrated Electrochemical DNA Biosensor Microfluidic Devices

There are four main types of electrochemical biosensors based on different electrochemistry concepts. We can divide them into voltammetric, potentiometric, amprometric and impedimetric operation. Due to the fact that biosensors are constructed according to the electrochemical detection working principle they rely on the design of the device, including dimension, shape,

material and surface properties, can have a big impact to the performance of the micro biosensors. The main detection concept involves monitoring reactions using either three- or two-electrode systems, with a stable potential having minimized interferences. The prior development of microfluidic technology promises high-throughput measurement possibilities with fast sample delivery chambers. Although the research field is getting much hotter due to the high demand of commercial biomedical application products, there are still challenges remaining for researchers to address.[33]

1b.2.1. Voltammetric DNA Biosensors

In voltammetric detection, the amount of current related to the analyte is measured as a function of applied potential during a redox reaction. The charge transfer between the electrode and redox reporting molecules is monitored while scanning within a potential range. The voltammetric technique can be applied to the microfluific DNA biosensors with both two- and three-electrode systems.

Motorola demonstrated an e-SENSOR^{TM} using the voltammetric technique and sandwich assay approach in 2001. In the following six years, the system was built into a plastic-based integrated biochip.[37,38] This biochip is an integrated cartridge and used a printed circuit board patterned with a 4x4 gold electrode microarray for SNP discrimination in real whole blood samples. The DNA microarray detection system in the chamber of the LOC chip integrated the units for the captured cell, enriched the target cell, purified, lysed and then performed PCR at the end. All the measurements could be done in 3 hours including both PCR processing and voltammetric detection. By using a Fc-labeled sandwich assay, the hybridization process was detected by alternating current voltammetry (ACV). Baeumner et al. developed an interdigitated

array microfluidic LOC device based on magnetic streptavidin-coated beads based on a sandwich assay for DNA detection. The poly(dimethylsiloxane) (PDMS) microchannel allowed hybridized targets to flow through and were attracted by the array patterned glass substrate using a magnet. The entrapped redox molecule after immobilization on the magnet was detected using volammetric technique. This kind of LOC system reported a detection limit of 10 nM.

Redox DNA intercalator molecules can bind between DNA base pairs due to their chemical structure (e.g. planar, aromatic and polycyclic) and appropriate size. These labeling molecules have certain advantages for replacing the sandwich assay methods described above. Upon the formation of the double-stranded DNA, the electrochemical signal of the redox molecules bound to the duplex can be obtained during this conformational change. Another microwell LOC silicon-based device with built in gold electrodes, heaters and temperature sensors was fabricatred by Lee et al.[39] The device had a glass sealed microchamber for DNA amplification and the target DNA hybridized with the cDNA probes immobilized on the gold electrodes. Different pulse voltammetry was used for the electrochemical detection with redox reporter intercalated into to the duplex. This microwell device reduced not only the size of the DNA LOC biochip but also the cost of the device fabrication.

In 2008, an electrochemical DNA microfluidic device was introduced by Pavlovic et al.[40] The device has a simple architecture with gold electrode array and PDMS microfluidic channels on the glass substrate. The Fc-labeled DNA probes were self-assembled on the gold electrode surface, and the target-induced conformation between the stem-loop and duplex structure altered the eT distance which could be detected by different pulse voltammetry.

Guanine bases can also be used as electroactive molecules for direct electrochemical reaction monitoring. Shiddiky et al. incorporated a separation and pre-concentration process into

the integrated electrochemical DNA sensors based on the electroactive guanine base principle.[41] The device has a Teflon microchannel for separation of different sizes of DNA analytes using colloidal gold nanoparticles. Hydroxypropyl cellulose was mixed with the gold nanoparticles and enhanced the guanine base current conduction upon DNA hybridization. This gold nanoparticle amplification method has a detection limit of 700 pM. Another approach, reported by Triroj, constructed a glass-mounted DNA sensor bound with a PDMS microfluidic network.[42] Thiolated capture probes were immobilized on the gold electrodes for target hybridization. The direct oxidation detection of guanine was catalyzed by adding a mixture of $Ru(NH_3)_6^{3+}/Fe(CN)_6^{3-}$. Cyclic voltammetry (CV) was used to monitor the electrochemical hybridization processes. After hybridization with 500 nM of target, a weak increase of the CV ruthenium peak proved the method was working.

In PCR amplification, the diagnosis of a disease requires knowledge of a specific sequence in order to amplify using the appropriate primers. In 2004, Ertl et al. developed a microfabricated electrocapillary electrophoresis chip incorporated with an electrochemical detector for the SNP diagnostic for hereditary hemochromatosis.[43] With the use of a Fc-labeled primer with a specific target sequence, the target could be amplified and labeled with Fc. These Fc labeled targets were detected by voltammetric techniques before exiting the channel.

Microfabricated device technology for electrochemical detection of DNA base changes in breast cancer cell lines was reported in 2013.[44] An electrochemical assay (μ-eLCR) with short motifs, which responded to the presence or absence of DNA bases in the target sequence were introduced to the detection system. The microscale working electrodes provided high sensitivity and had good reproducibility for DNA methylation in cell.

1b.2.2. Amperometric DNA Biosensors

In biochemical reactions, oxidations or reductions can be monitored using amperometric detection. This detection method generally requires the presence of enzymes. The enzyme catalyzes the reaction and converts the substrate into an electroactive product, which can generate an amplified electrochemical signal.

In 2004, Liu et al. fabricated a PDMS fluidic channel-based electrochemical biosensor.[45] Maleimide-labeled capture probes were attached on the active PDMS channel surface for silane-thiol coupling. After the immobilization, an enzyme was introduced to produce redox-active molecules that diffuse through the fluidic channel until arriving at the indium tin oxide interdiditated electrode for amperometric detection. The detection limit was 10 nM. This kind of combination using both integrated electronics and amperometric sensors was introduced to the biochip market through an array-based genetic system. An integrated multi-electrode array LOC device was commercialized for the biomedical market.[46,47] The complementary metal-oxide-semiconductor (CMOS) circuitry platform could process parallel immunoassays for bacteria and viruses detection in biological samples. The device had a platinum (Pt) electrodes microarray with a Pt counter electrode grid around the array. The electrochemical reduction signal of HRP was generated via an enzymatic oxidation of the electron donor substrate and showed a relatively low 0.75 pM detection limit, to be compared with the fluorescent detection limit (1.5 pM). Magnets have been widely used in these amperometric flow channel LOC devices because of the attractive feature they provide. Sandwich type assays that are linked by the enzyme were employed with magnetic beads during PCR amplification by Mascini et al.[48] After the target has been amplified, the hybridization occurred at the non-hybridized part of the target sequence. Amperometric detection measured signal from the third DNA probe bound to the streptavidin-

ALP for allergen detection. Another similar platform with integrated gold electrode deposited Si substrate encapsulated by silicon oxynitride.[49] The sandwich detection assay principle used was similar to the previous magnetic bead methods described. Capture probe selectively bound to the amplified target with a detection limit of 1 nM using amperometric detection.

Gao et al. designed, fabricated and tested a two-layer PDMS microfluidic device that could trap cells to measure cell exocytosis, as reported in 2013.[50] By patterning of double layer template using AZ photoresist, in a 2.5 μm deep fluidic channel was formed to stop the cells. Exocytosis measurement was achieved by targeting cells on indium tin oxide microelectrode arrays. 72 % of the trapping spaces could be fulfilled by the cells for the detection of amperometric signals. The device features simple, low-cost construction and the ease-of-use of the high-throughput detection allows sufficient sensitivity for cell applications.

1b.2.3. Potentiometric DNA Biosensors

Potentiometric LOC devices feature very small DNA biosensors that can be fabricated on silicon substrates using well-developed silicon manufacturing methods. The detection principle involves monitoring the voltage difference between the working electrode and reference electrode during the reaction process. Since the voltage change is the main focus, the current should be minimized to control interference during detection.

A potentiometric genetic field-effect transisitors (FET) microdevice was reported by Sakata et al. for the detection of DNA hybridization and intercalation. This kind of metal-oxide-semiconductor structure detected changes in charge density due to hybridization. Si_3N_4 surfaces provided the space for DNA probe immobilization. Even without DNA labeling, a viable electrochemical signal could still be measured. A voltage shift is detected due to the negatively

charged DNA probe on the Si_3N_4 surface. The hybridization of the cDNA probes further shifts the voltage after it is introduced to the Si_3N_4 surface.[51]

Nanotube technology can also be incorporated into FET structures employing single wall nanotube (SWNT) to conduct the current flow between the electrodes. A CNT network based NTFET LOC microchip was reported by Star et al. for the selective detection of DNA immobilization and hybridization processes.[52] SWNTs were grown on top of the SiO_2-coated Si substrate. The electric leads were made by Ti /Au films on the nanotudes. SNP detection could be accomplished by the charge transfer of the NTFET device after introducing the mismatch DNA into the microfluidic on-chip structure.

In 2011, Xue et al. reported a micro-potentiometric immunosensor that employed a self-assembled monolayer (SAM) with nano-spheres functionalized for the detection of hemoglobin-A1c level.[53] The surface of the immunosensor was attached by self-assembled SAMs nano-spheres array, so the antibody could covalently immobilize on the surface. The MEMS electrode array combined with FET-integrated device measured the level of hemoglobin-A1c according to the hemoglobin concentration. A linear concentration response was obtained, and furthermore, the utility of the MEMS LOC device was examined using blood samples from a hospital. This showed that such a LOC device can benefit the biomedical immunotechnology research in the near future.

1b.2.4. Impedimetric DNA Biosensors

This electrochemical technology has a detection principle involving sensing the electrical resistance of specific medium delimited by the electrode system. A common electrochemical detection technique is the use of impedance spectroscopy. The impedance spectroscopy features

a small alternating current potential excitation signal to monitor the resistance of the electrical current flow through the cell. Nowadays, a large number of impedance DNA LOC devices have been developed using nanotechnology (e.g. nanopores) for promising impedimetric detection.[54]

The detection of 8-hydrixydeoxyguanosine DNA adduct was used as a biomarker to monitor the oxidative stress. A capillary electrophoresis microfluidic device was introduced to separate and monitor the target signal inside the electrophoresis detection chamber. The separation efficiency and the detection limit (100 nM) were enhanced by using a palladium-plated chamber.[55]

There have been many published papers to introduce nanopore-based next generation DNA detectors. The nanopores have holes a few nanometers in diameter and the inner diameter is at the same scale as many single molecules, such as DNA and RNA strands. By the driving force generated from the electric field, particles (e.g. DNA, RNA strands) inside would face restriction. The detection process monitors the current changes that occur with a constant voltage applied. The principle is called "resistive-pulse sensing".[56,57]

A protein named "α-hemolysin" has been studied the most widely with nanopores sensing technology. High temperature can alter the function of this protein and a 1.4 nm diameter transmembrane channel was created. Unraveled ssDNA could generate a nucleotide signal during the crossing process through the pore.[58] Nanopore protein DNA sensors can also be chemically engineered to monitor DNA hybridization. Upon nucleotide oligomer bound α-hemolysin attaching to the matched sequence, sequence-specific single base detection is accomplished due to the delay of the pore translocation of the matched sequence.[59,60] The impedimetric DNA LOC devices show new and promising detection results. The potential

applications can be developed with modern nanotechnology to further invent other devices for biomolecular studies.

1b.3. Photolithography as an Enabling Technique in Microfabrication

Microscale LOC devices are one of the hottest research areas, not only in academic laboratories, but also in microelectronic-related industry, due to the potential applications for such devices in real world, such as clinical, biomedical, environmental, pharmaceutical, and food security. Photolithography is the most important production technology for microscale LOC device fabrication.

1b.3.1. Introduction

In microfabrication, photolithography is a process to pattern thin films on the substrate using an optical light source. There are several key components for the process including a light source, a photomask and a light-sensitive chemical photoresist. A photomask is an opaque plate with geometric patterns that allows light to pass through. Photoresists are light-sensitive materials that can form a patterned coating on a substrate. There are two types on photoresists: positive resists and negative resists, as shown in Fig. 1.4. Positive resist is a type of photoresist in which the light exposed region becomes soluble to the photoresist developer. The region that is unexposed remains insoluble to the developer. Negative resist is a type of photoresist in which the light exposed region remains insoluble to the photoresist developer. The region that is unexposed is dissolved to the developer.

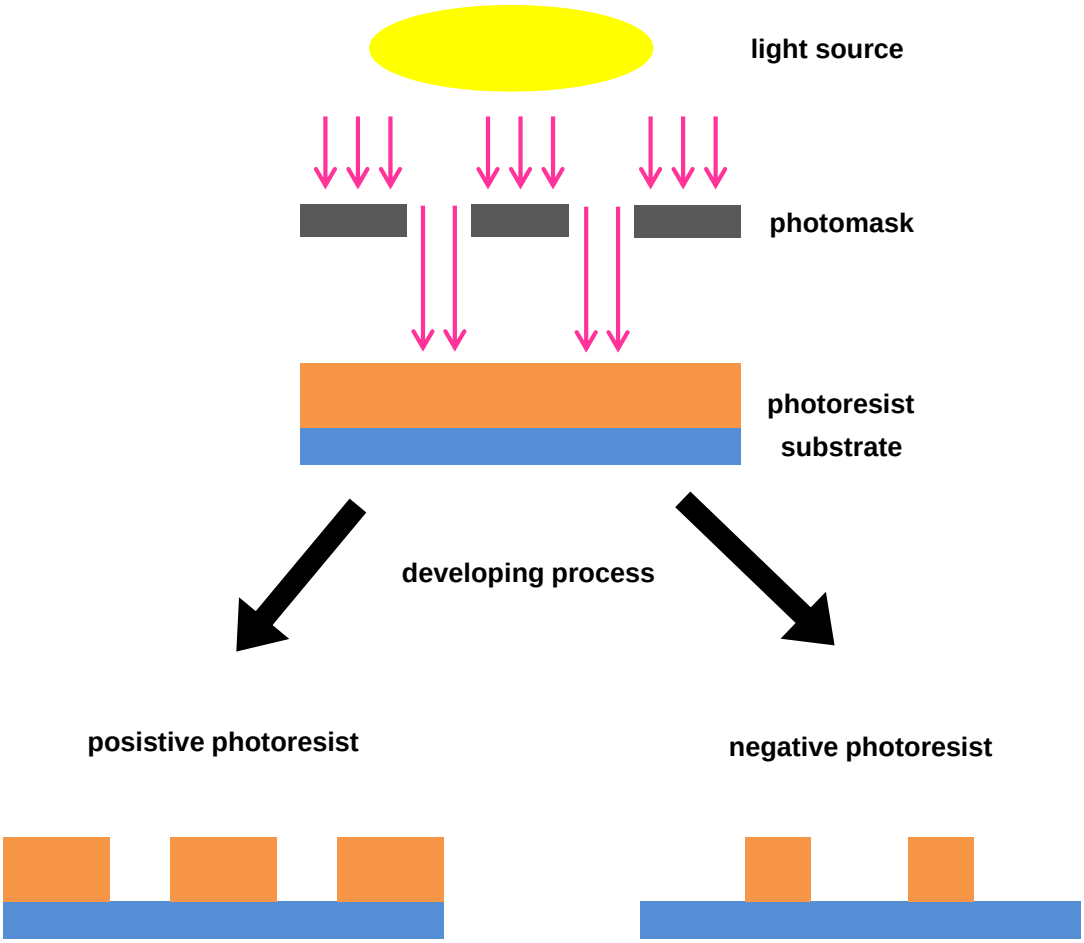

Figure 1.4. Illustration of photolithography process using positive and negative photoresist in microfabrication.

1b.3.2. Photolithography Basic Processes

A single photolithography iteration involves several steps (preparation, photoresist application, exposure, developing and removal) that are typically conducted in a modern cleanroom. Preparation often involves substrate pretreatment to clean the surface that will be photoresist coated. Then the substrate is covered with photoresist to form a uniformly thick layer using a spin coating instrument. This step is followed by a prebaking heating process. The thickness of the photoresist layer can be controlled by the spin speed and time. After the

prebaking, the photoresist-coated substrate is exposed to a pattern of light through the photomask. This exposure process causes a chemical change that allows exposed positive resist region to become soluble and the exposed negative resist region to become insoluble. Soluble regions can be removed by applying a special solution that can dissolve specific soluble photoresist, called "developer". After the developing, the remaining insoluble geometric patterned photoresist is ready for further treatment in different applications. The remaining insoluble photoresist can be stripped if no longer needed. A solution-based "resist stripper" is able to chemically remove the adhesive resist on the substrate. Another method is using oxygen plasma to etch the resist from the substrate.

1b.3.3. Multi-step of Photolithography in Device Microfabrication

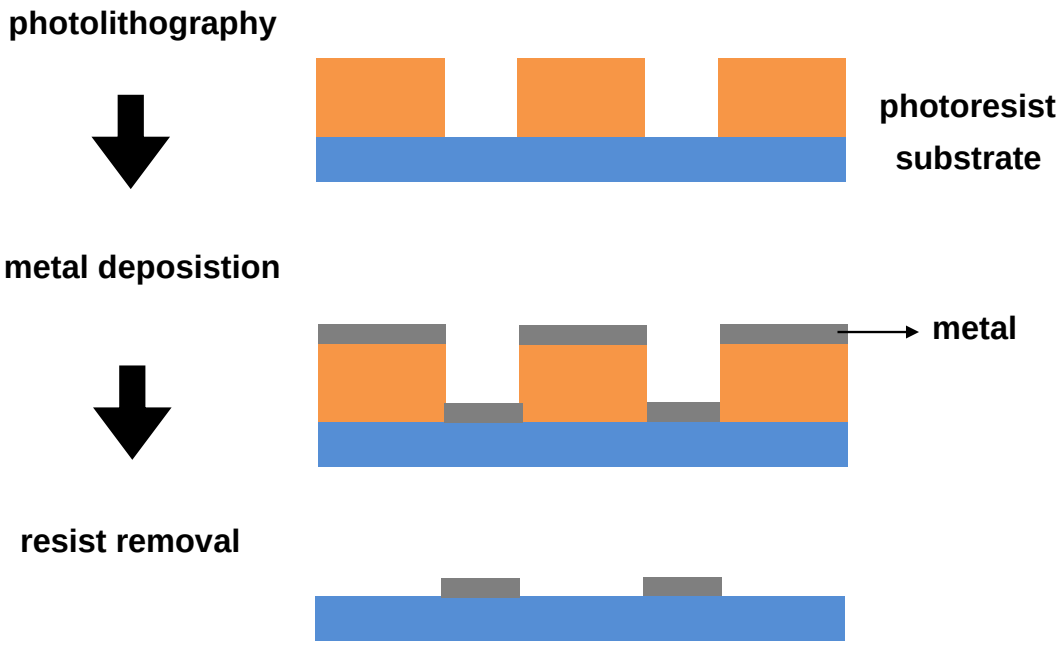

Figure 1.5. Thin-film deposition involving photolithography, metal deposition and resist removal.

Fabrication of a microscale LOC device is a series of steps involving photolithographic photoresist coating and removal with coupled additional microfabrication processes. For construction of a simple electrochemical LOC device, thin-film deposition and soft lithography are two major processes that can be important. Using a series of simple microfabrication processes, complicated electrochemical LOC device can be fabricated.

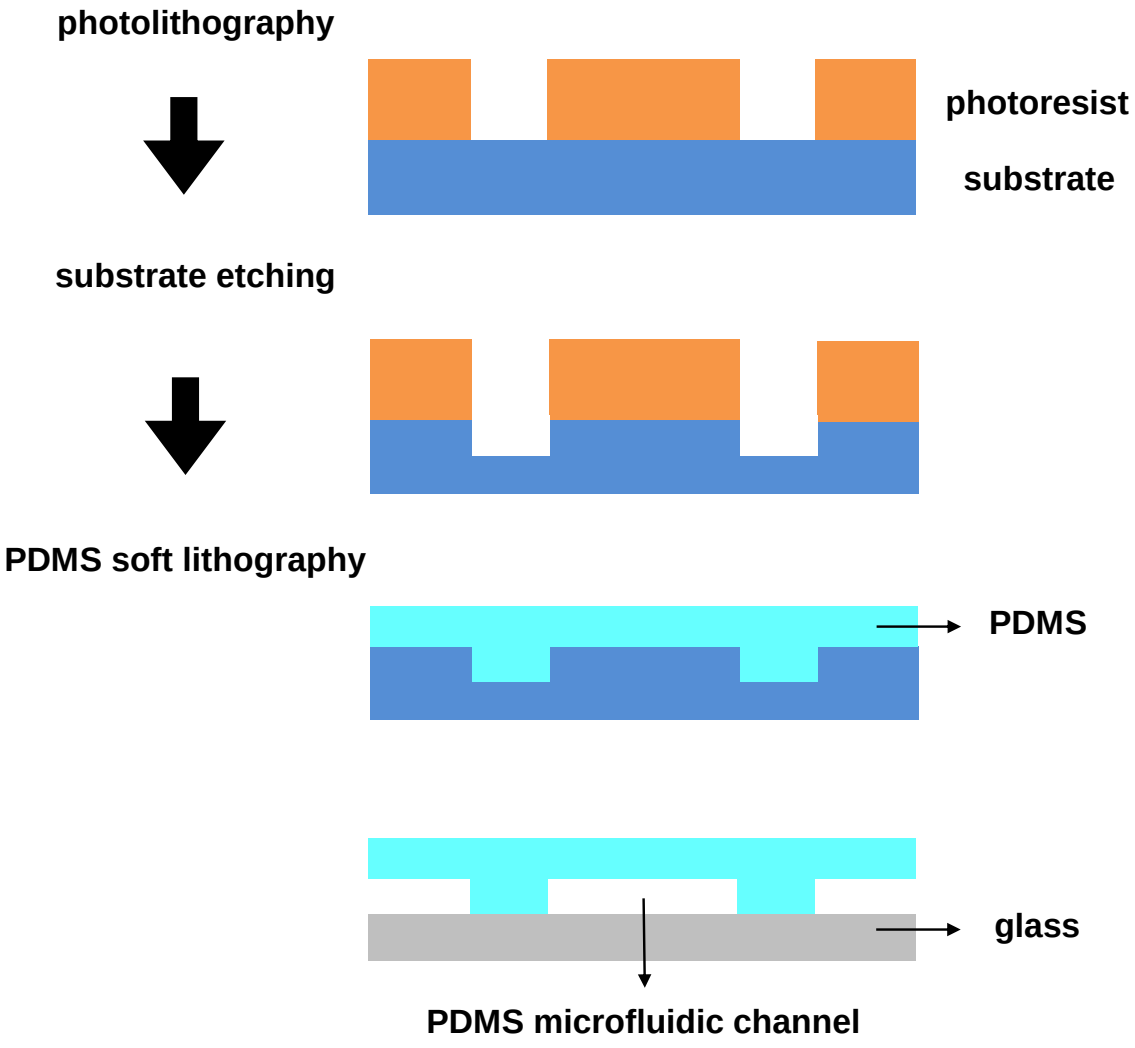

Figure 1.6. Soft lithography involving photolithography, substrate etching and soft lithography.

Thin-film deposition is widely used for source material such as metal device components. Micro electrodes (e.g. gold, platinum, silver) are deposited after photolithography. As shown in Fig. 1.5, the deposition process starts with coating the substrate with the photoresist. Then expose the resist is exposed using photolithography to create pre-designed geometric photoresist patterns with resist developer. An e-beam evaporator instrument is introduced to evaporate metal into vapor particles that travel directly to the photoresist coated substrate and condense back to original solid state form. Finally, the metal-coated substrate is treated by resist stripper to remove metal-coated photoresist regions and leave the geometric metal film on the substrate.

Soft lithography is a common technique used for fabricating microfluidic systems with elastomeric materials, as shown in Fig. 1.6. The deposition process starts with coating the substrate with the photoresist. Then the resist is exposed using photolithography to create pre-designed geometric (microfluidic channel geometry) photoresist patterns with resist developer. A reactive-ion etching instrument can be used to etch the substrate regions that aren't coated by photoresist. After the etching process, photoresist is removed by a resist stripper to attain a substrate with the desired regions etched away. Then PDMS is poured on to the substrate and left to harden in a heated environment. Finally the PDMS is peeled off from the substrate with all the details imprinted in the PDMS. One can apply the PDMS piece to form microfluidic channel on another substrate (e.g. glass).

Electrochemical microfluidic LOC devices can be fabricated based on these simple techniques involving photolithography. With more modern technology and instruments, LOC devices promise to have a bright future, providing required functionalities on a small scale.

1b.4. Summary

It is clear that the electrochemical DNA detection has many advantages over other methods that are suitable for integrated LOC devices. The low production cost, reduction in sample volume, array-based high-throughput fast measurements, high sensitivity and the small size of the device can bring these LOC devices into profitable commercialization. There have already been many commercial applications on the market, and the future of the new products based on these technologies is just round the corner.

.

II. Chapter 2: Electrochemical Y or junction probe detection of nucleic acid

2.1. Introduction

As introduced in the Chapter 1, since 1990s, the reported growth of sensing specific nucleic acid sequences has increased due to its impact on medicine and modern biology. Because it is very critical to detect the pathogenic bacteria, viruses or cancer genes in a patient's sample to help patient's medical care treatments, nucleic acid sequence sensing will continue to play a key role in the field for the next several decades. The development of simple chip-based DNA sensors capable of sensitive and selective detection of DNA sequences is likely to increase in importance for clinical diagnosis.[61-63] Isothermal amplification,[64-67] combined with the use of electrochemical detection promises to deliver portable genetic diagnostic devices that could be used in resource-poor areas of the world as well as for field testing.[68-72] Nucleases, especially restriction/nicking endonucleases are DNA modifying agents that are increasingly being used in DNA diagnostics.[71-75] One of the limitations for the use of restriction/nicking endonucleases in DNA diagnostics is the requirement for the target of interest contain a specific sequence.[70,72] Y- or junction probe (JP)-based detection platforms obviate the need for the target to contain a specific cognate sequence and are finding utility for the detection of single nucleotide polymorphism as well as for the detection of RNA, including shot microRNAs that are implicated in cancers.[73-75]

We recently became interested in the development of electrochemical junction probes with the ultimate goal of incorporating such probes into handheld or portable devices. In the course of developing our electrochemical junction probe detection technology, Wang et al. reported a ''signal-off'' electrochemical JP strategy using endonuclease.[75] However ''signal-on'' detection

is preferred over signal-off detection due to the higher propensity for interference problems in signal-off detection. Herein, we report the details of new signal-on, as well as signal-off, electrochemical JP detection.

2.2. Results and Discussion

This results and discussion section is organized as follows. First, we describe the design and detection of signal-off electrochemical JP detection using restriction endonucleases. Second, we discuss the screening of the restriction endonucleases and the best candidate for this electrochemical JP detection. Lastly, we discuss the design, nucleic acids mismatch using signal-on electrochemical JP, and the detection limit of this signal-on electrochemical JP detection technique.

2.2.1. Signal-off Electrochemical JP Detection

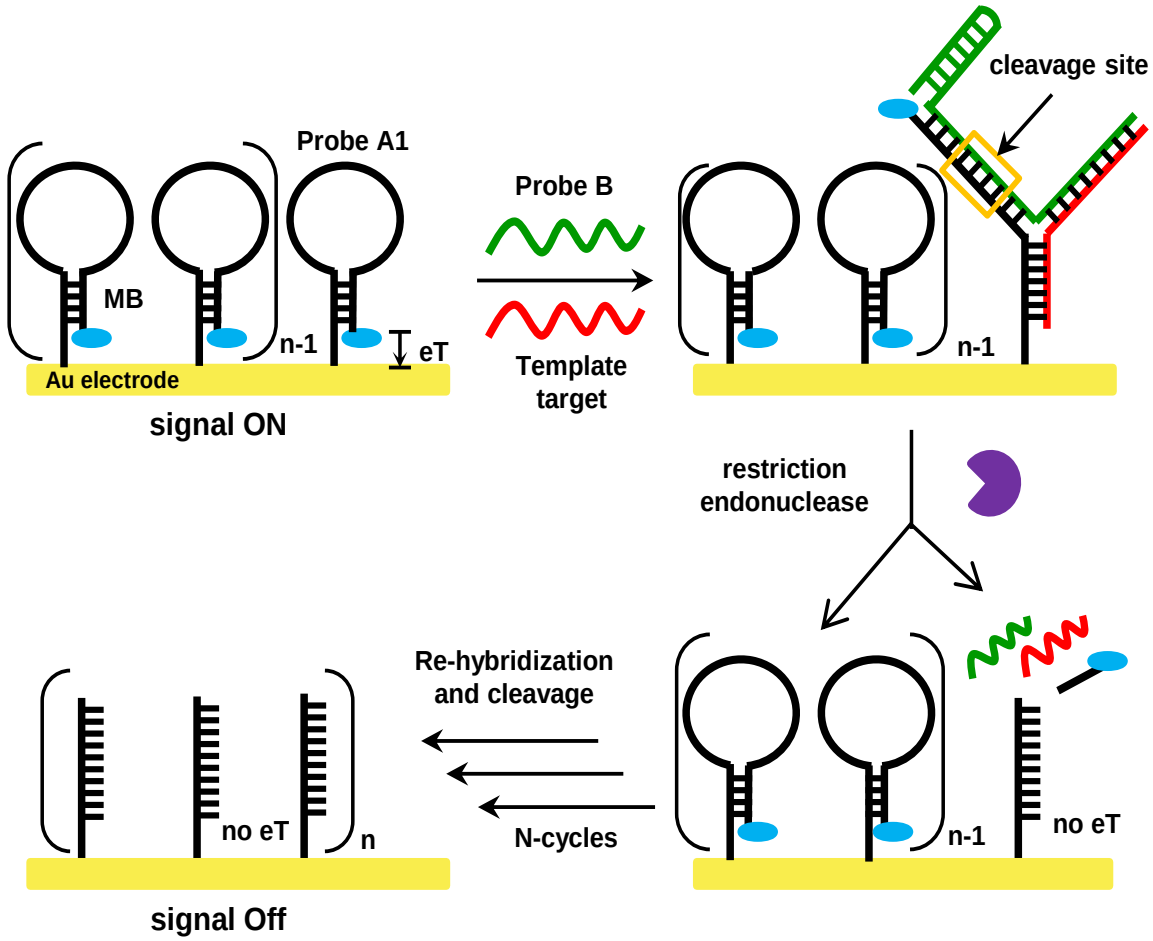

Figure 2.1. Electrochemical JP detection using a signal-off method. MB intercalates into the stem part of Probe A, leading to eT between MB and the gold electrode. The Probe A–Probe B duplex contains a restriction endonuclease cleavage site. In the absence of a template, Probe A and Probe B do not form a duplex because the T_m of Probe A–Probe B duplex (only 6 BP) is below 10 °C.[73] However upon the addition of a template, a Y junction structure forms, which now contains a restriction endonuclease (REase) cleavage site. Addition of REase would then lead to cleavage of Probe A, which destroys the MB labeled stem-loop structure of Probe A. In the absence of MB, eT is inhibited to the gold electrode, leading to a signal reduction.

For signal-off JP electrochemical detection (see Fig. 2.1), a redox-active methylene blue (MB)-labeled Probe A1 that is self-assembled on a gold electrode can hybridize with a helper probe (called Probe B, and colored green in Fig. 2.1) and template (target DNA, which is colored red in Fig. 2.2) to form a JP structure. Addition of restriction endonuclease to the probes and template then results in the digestion of Probe A. Because the MB label is cleaved during this process, the MB-derived peak current is reduced. Cleavage of the Y structure leads to a ternary complex that is less stable than the structure before cleavage, and therefore both the template and a fragment of the helper Probe B are released to start the cycle all over again. Cleavage during each subsequent cycle would further decrease the MB peak current (see Fig. 2.2). For the sequences of oligonucleotides used in this study, see 2.4. In our approach, we use a helper Probe B with duplex overhang as well as phosphorothioate ‘‘protected’’ helper Probe B.In our work we found that this gave a more consistent signal and with greater sensitivity.

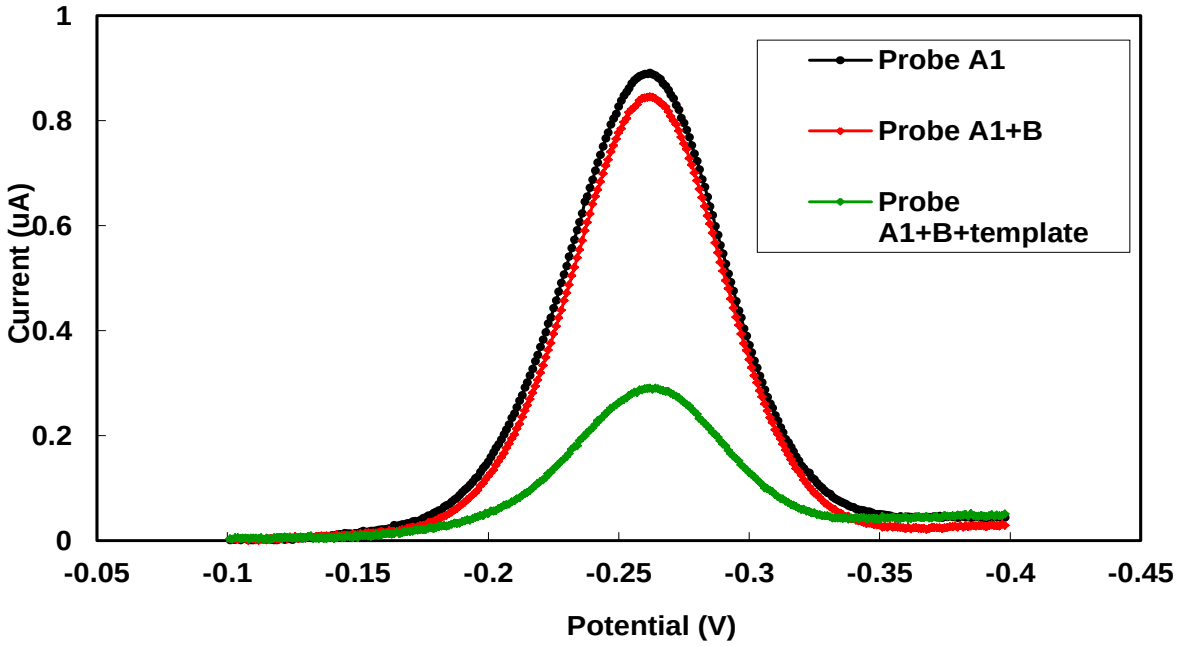

Figure 2.2. Square wave voltammogram of (a) Probe A1 modified on Au electrode; (b) 4 h after restriction endonuclease (Bsp143I) was added to Probe A and Probe B without template; (c) after restriction endonuclease (Bsp143I) treatment of Probe A and Probe B (4 h) in the presence of 20 nM template. Addition of template caused ~70% reduction in current at 0.26 V.

2.2.2. Restriction Enzyme Screening

We screened six restriction endonucleases (Bsp143I, BfuCI, NDEII, MboI, FD MboI and FD Sau3AI; FD stands for fast digest) to find the best enzyme for this electrochemical JP detection scheme (Fig. 2.1) and also to investigate if the proficiencies of some of the enzymes mirror solution-phase catalysis (see Fig. 2.3). FD MboI and NDE II were ineffective REases for the cleavage of surface-tethered JP structures. MboI and BfuCI only caused approximately 20% signal reductions. BfuCI could cleave the solid-supported JP structure but on some occasions failed to cleave the JP structure. Curiously, we did not observe such erratic cleavage behavior

when BfuCI was used in solution phase JP by optical detection[73,74], and we do not have a hypothesis at the moment to account for the inconsistency observed with BfuCI. Addition of Bsp143I and FD Sau3AI to the solid-supported JP caused significant signal reduction, and so Bsp143I was chosen for the development of the signal-on JP detection.

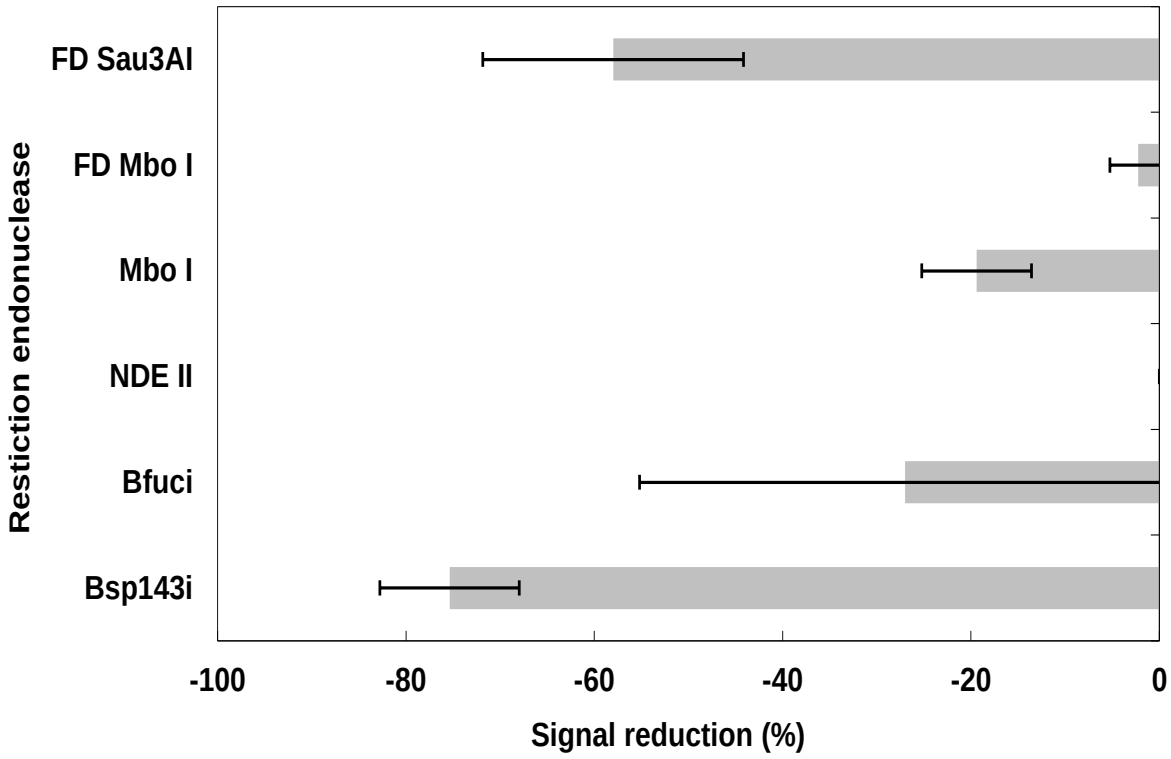

Figure 2.3. Percentage signal reduction with different restriction enzymes. Same condition as Fig.2.2. The percentage signal change was calculated using, $\{ (I)_{\text{with enzyme}} - (I)_{\text{without enzyme}} \} / (I)_{\text{without enzyme}} \times 100\%$, where I = current at - 0.26 V.

2.2.3. Signal-on Electrochemical JP Detection

Signal-on detection of bioanalytes is a superior detection strategy compared to signal-off methods. For the signal-off strategy shown in Fig. 2.2, if thiols that are present in biological fluids exchange with the immobilized MB-labeled probe A,[76] then this would also lead to a decay in current (signal-off) and essentially give a false positive response. Secondly, it might be easier to amplify an increase in current (signal-on) than a decrease in current (signal-off). With such motivation, we proceeded to develop an electrochemical signal-on junction probe detection strategy. It is known that when MB is positioned in single-stranded DNA regions, electron transfer (eT) to electrodes is significantly larger than when the MB is intercalated into a duplex DNA.[77] This has been attributed to the higher probability of MB approaching the electrode surface when attached to the more flexible ssDNA than when attached to the more rigid dsDNA.[77] We therefore hypothesized that if MB is positioned in the stem of Probe A of a molecular beacon junction probe, then eT should be inhibited (see Fig. 2.4). However, upon restriction endonuclease cleavage of Probe A, after hybridization with the helper Probe B and target template, MB would be left on a single strand oliginucleotide and eT to the electrode then be enhanced (Fig. 2.4). We were pleased to observe that the incubation of Probe A alone or Probe A and Probe B with Bsp143I did not lead to an increase in current at the relevant potential of -0.26 V. However, upon the addition of a matching template, there was an increase in the current at -0.26 V (Fig. 2.5). This electrochemical signal-on JP detection can also be used for single nucleotide polymorphism detection; whereas addition of the perfect matching template resulted in about a 90% increase in current (in comparison with when no template was added), templates containing a single mismatch only increased the current level by 15–30% (see Fig. 2.5). Signals generated from base pairs A–A and A–C mismatches were not significantly different

from the background (not greater than an increase of 15% of background) whereas the signal from an A–G mismatch was 30% more than background (no template added). It is not surprising that the A–G mismatch was more stabilizing than the A–A or A–C mismatches as it is known that adenine and guanine can form a wobble base pair.[78]

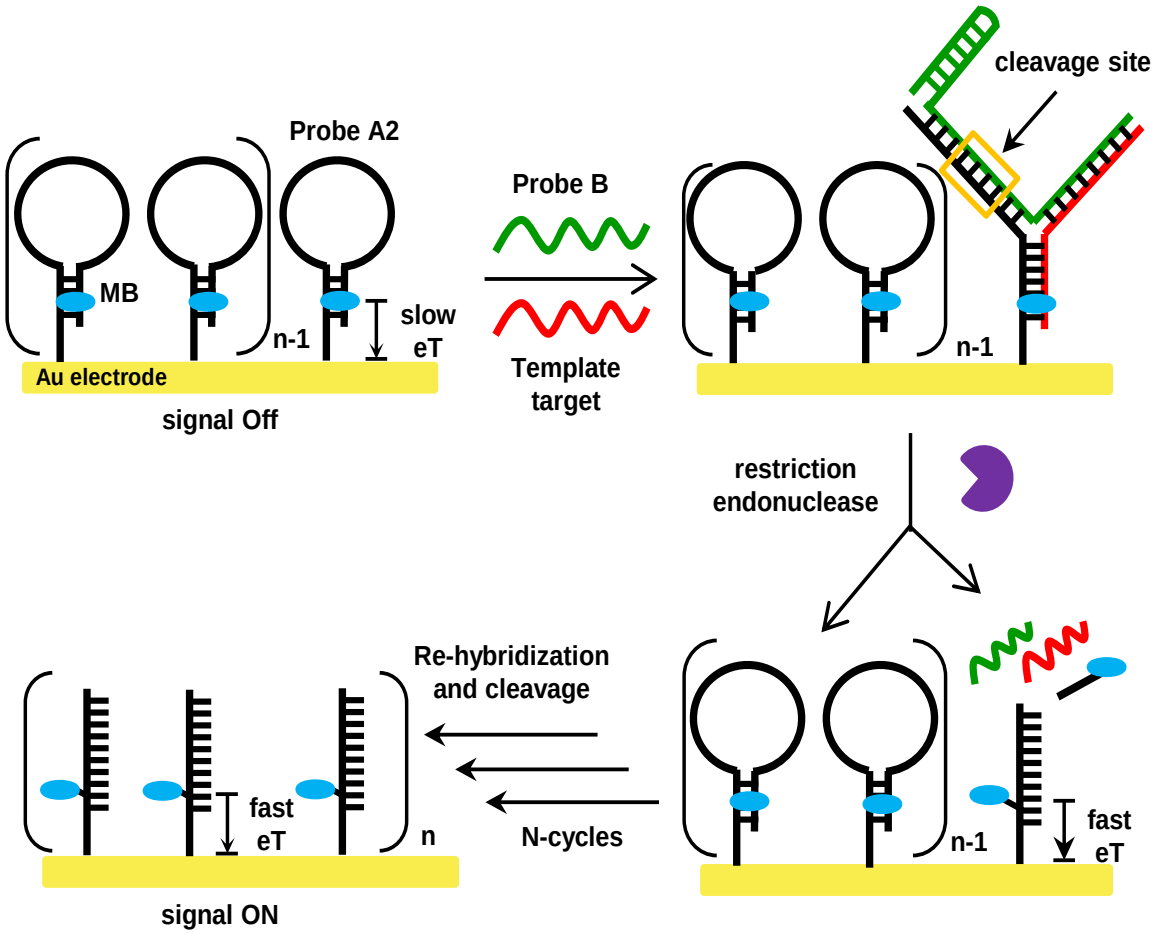

Figure 2.4. Electrochemical JP detection using a signal-on method. MB intercalates into the stem part of Probe A, leading to reduced electron transfer (eT) between MB and the gold electrode. Probe A–Probe B duplex contains a restriction endonuclease cleavage site. In the absence of a template, Probe A and Probe B do not form a duplex because the T_m of Probe A–Probe B duplex (only 6 BP) is below 10 °C.[73] However, upon the addition of a template, a Y junction structure forms, which now contains a restriction endonuclease (REase) cleavage site. Addition of REase would then lead to cleavage of Probe A, which destroys the stem-loop structure of Probe A. In the absence of a duplex region in Probe A, MB is not intercalated between base pairs anymore and hence readily transfers electrons to the gold electrode, leading to a signal enhancement.

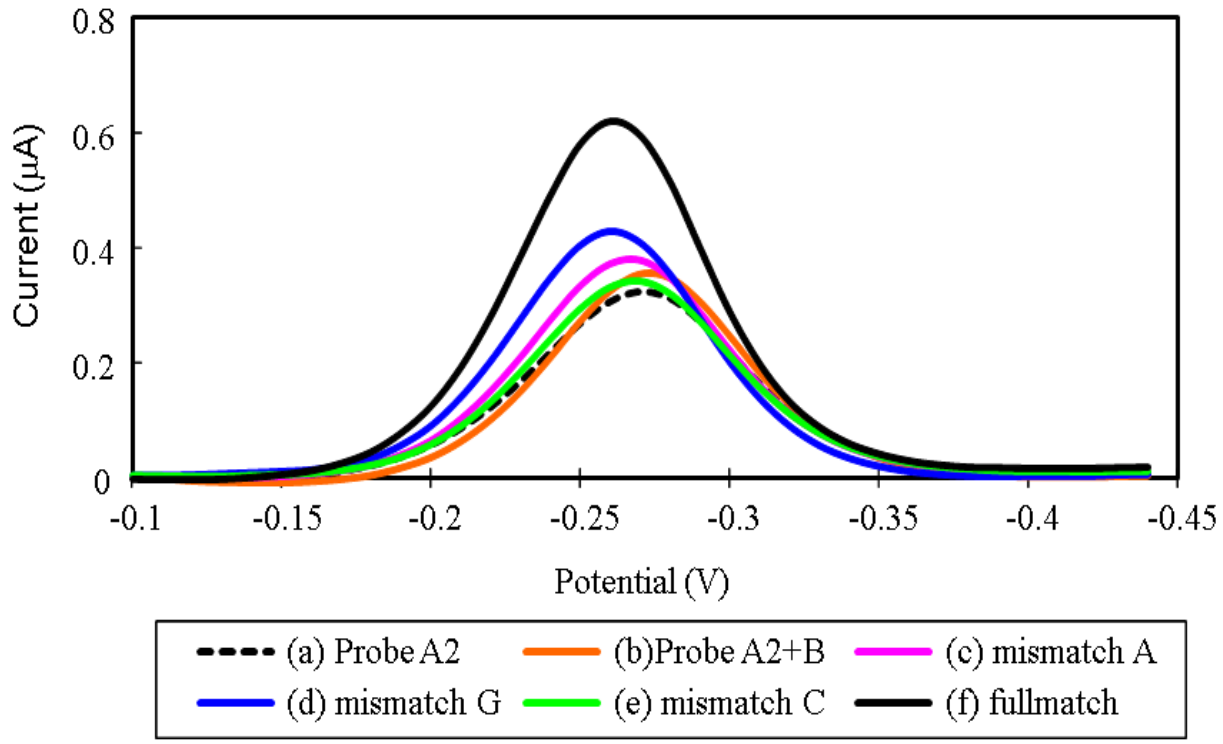

Figure 2.5. Alternating current voltammogram of (a) Probe A2 modified on Au electrode; (b) after restriction endonuclease treatment with Probe B after 4 h in the absence of template; (c–e) after restriction endonuclease treatment with Probe B after 4 h in the presence of 20 nM single mismatch (A,G, C) DNA template; (f) after restriction endonuclease treatment with Probe B for 4 h at 31 °C in the presence of 20 nM fullmatch DNA template.

To provide more proof that the increase in current at -0.26 V was due to the added DNA template, we added different concentrations of the fully-matched DNA to the Probes A and B and Bsp143I and then measured current at -0.26 V after 4 h incubations. As can be seen in Fig. 2.6, the increase in current was proportional to the amount of target DNA template that was added, (The small difference between the signals when template concentrations are equal to 10 nM and 100 nM is probably due to the fact that when [template] = 10 nM, the concentration of the template becomes comparable to the immobilized Probe A, hence the concentration of Probe

A, and not the template, is the determinant of the electrochemical signal and this provides further compelling evidence that the signal-on detection is due to the DNA template).

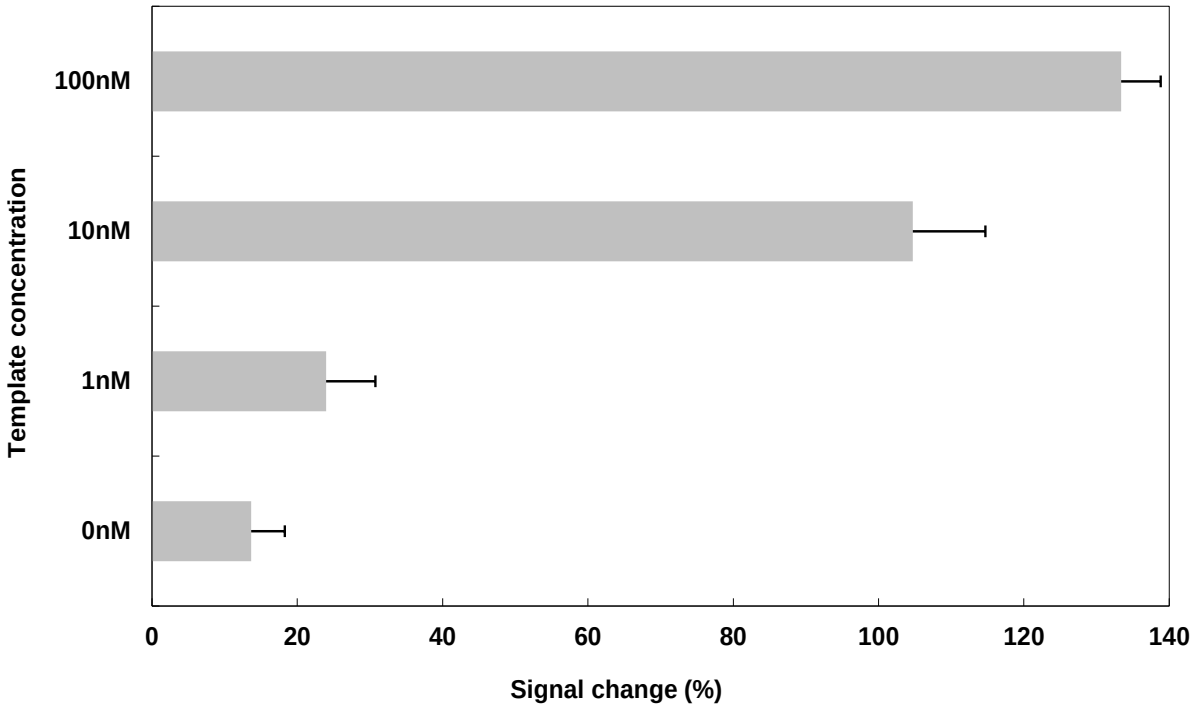

Figure 2.6. Increasing the concentration of target DNA increases the current, implying that the signal change arises from the added DNA template.

2.3. Conclusion

In summary, we have been successful in developing an electrochemical signal-on junction probe (or Y probe). We found that not all of the endonucleases that worked in solution phase junction probe detection assay could be successfully used when one of the probes was immobilized on a gold electrode. The limit of detection, which is currently around 1 nM and the long assay time, are not ideal for practical application. However, the potential exists to combine other isothermal amplification strategies, such as rolling circle amplification (RCA),[79–82] to first

pre-amplify the target before using the signal-on electrochemical junction probe technology. Efforts to improve upon this first-generation signal-on electrochemical junction probe would involve the screening of more restriction endonucleases to find candidates that can facilely cleave immobilized probes on electrodes and/or the engineering of Bsp143I to increase the rate of cleavage. Future work will also investigate if labeling probe A with multiple methylene blues would lead to more sensitive detection of both DNA and RNA using our electrochemical signal-on junction probe approach. This work adds to the current efforts to simplify nucleic acid detection assays.[83–91]

2.4. Materials and Methods

Materials

All unlabeled DNA oligonucleotides were synthesized in house whereas labeled oligonucleotides were purchased from Biosearch Technology. Restriction endonucleases were purchased from Frementas Inc. USA. 6-mercaptohexanol and tris-(2-carboxyethyl) phosphine hydrochloride (TCEP) were purchased from Sigma-Aldrich. All chemical reagents were of analytical grade or higher. Ultrapure water (18.2 MΩ·cm) was used as a pure source in preparations.

Au electrode surface cleaning and modification

Au electrodes (2 mm in diameter, CH Instrument, Inc.) were cleaned before DNA self-assembly. The cleaning procedures were done according to a published protocol (Nature Protocols, 2007, 2, 2875-2879).[92] Gold rod electrodes were prepared by polishing on a

microcloth-coated glass plate with a suspension of 1 μm diamond (Buehler) for 3 mins. The gold rod electrodes were processed further by polishing on a microcloth coated glass plate with a suspension of 0.05 μm Gamma Alumina (Buehler) for 3 mins. The polished gold electrodes were sonicated in absolute ethanol/water for 5 mins to remove any remaining polishing agent. A smooth gold surface is important to support efficient target binding.

The electrodes were then cleaned under basic conditions, with a 2 V/s scan rate and 0.01 V sample interval in 0.5 M NaOH, via oxidation and reduction scanning over a potential range from -0.35 to -1.35 V (versus a 3 M NaCl saturated Ag/AgCl reference electrode). The scanning was reported until peak heights or shapes are constant and have no further changes.

After finishing the electrochemical cleaning under basic conditions, an acidic condition cleaning was performed by 20 oxidation and reduction scans, at a scan rate of 4 V/s and a sample interval of 0.01 V in 0.5 M H_2SO_4, via a potential range from -0.35 to 1.5 V. Another four scans were followed, at a scan rate of 0.1 V/s and sample interval of 0.01 V, via a potential range from -0.35 to 1.5 V.

The final round of electrochemical oxidation and reduction scans were performed under acidic conditions again in 0.01 M KCl / 0.1 M H_2SO_4 for 10 segments, at a scan rate of 0.1 V/s and a sample interval of 0.01 V, under four different potential ranges sequencially: (1) potential range from 0.2 to 0.75 V; (2) potential range from 0.2 to 1.0 V; (3) potential range from 0.2 to 1.25 V; (4) potential range from 0.2 to 0.75 V.

200 μM Probe A (1 μL) was mixed with 10 mM TCEP (2 μL) at room temperature in the dark for 45 min. The mixture was then diluted with PBS buffer (10 mM phosphate-buffered saline pH 7.4 with 1 M NaCl and 1 mM Mg^{2+}) to a final Probe A concentration of 200 nM. Each electrode was immersed with 100 μL of 200 nM stock Probe A in PBS for 30 min. After rinsing

with deionized water, the electrodes were incubated in 2 mM 6-mercaptohexanol solution for 3-5 h at room temperature in the dark. The electrodes were rinsed for 3 min using deionized water to remove any remaining 6-mercaptohexanol solution. The electrodes were then soaked in PBS for 5 min before any electrochemical measurements.

Square wave voltammetry measurements (SWV) of signal-off JP and screening of different restriction endonucleases

All SWV measurements were performed with a CHI 660 electrochemical workstation (CH Instrument, Inc,). The normal three-electrode system consisted of an Au working electrode, a platinum wire counter electrode, and a 3 M NaCl saturated Ag/AgCl reference electrode. SWV was carried out in the 10 mM PBS (pH 7.4) from -0.1 V to -0.4 V with 0.001 V interval, 60 Hz frequency and 0.025 amplitude. The reaction conditions were as follows: 1μL of restriction endonuclease (stock solution from company), 1 μL of 20 μM Probe B, 1 μL of 2 μM template, 10 μL of 10x restriction endonuclease buffer, 87 μL of deionized water. The reaction time and temperature were 4 h and 31 °C, respectively. The final concentrations were 200 nM Probe B and 20 nM template.

Alternating current voltammetry measurements (ACV) of signal-on JP

All ACV measurements were performed with a CHI 660 electrochemical workstation (CH Instrument, Inc,). The normal three-electrode system consisted of an Au working electrode, a platinum wire counter electrode, and a 3 M NaCl saturated Ag/AgCl reference electrode. SWV was carried out in 10 mM PBS (pH 7.4) from -0.1 V to -0.45 V, with 0.01 V interval, 50 Hz frequency and 0.025 amplitude, 1 sec sample period. The reaction conditions involved 1μL of

restriction endonuclease (stock solution from company), 1 μL of 20 μM Probe B, 1 μL of 2 μM template, 10 μL of 10 x restriction endonuclease buffer, 87 μL of deionized water. The reaction time and temperature were 4 h and 31 °C, respectively. The final concentrations were 200 nM Probe B and 20 nM template.

Table 2.1. Sequences of oligonucleotides used in this study.

Oligonucleotide	**Sequences (5' to 3')**
Probe A1	5'-SH-C_6H_{12}-TTTTCCACCGCCAATATTTTT*GATC*TGTGG(MB)-3'
Probe A2	5'-SH-C_6H_{12}-TTTTCCT(MB)CCGCCAATATTTTTGATCTGAGG-3'
Probe B	5'TG(S)*GATC*GGAAAACC(S)*GATC*CA(S)*GATC*ATATACGTGCTGC TA-3'
Full match template	5'-TAGCAGCACGTA-AATATTGGCG-3'
Mismatch A template	5'-TAGCAGCACGTA-AATAATGGCG-3'
Mismatch G template	5'-TAGCAGCACGTA-AATAGTGGCG-3'
Mismatch C template	5'-TAGCAGCACGTA-AATACTGGCG-3'

The location of mismatched bases are colored blue.

Endonuclease cognate recognition sites are highlighted in italic and underlined.

(S) denotes phosphorthioate linkage.

III. Chapter 3: Rapid DNA melting analyses using a microfabricated electrochemical platform

3a. Introduction to nucleic acid binding studies.

3a.1. Introduction

Nucleic acids (DNA and RNA) are biopolymers that contain a phosphate backbone, sugar and nucleobase (adenine, A, cytosine, C, guanine, G, thymine, T, (for DNA) and uracil, U, (for RNA). Individual single strands of DNA or RNA can base-pair with another strand (A with T/U and G with C) to form a paired double stranded helical structure. The stability of the double stranded structure is important and crucial for many aspects of nucleic acid metabolism.[92] The binding of small molecule ligands to nucleic acids and resulting increase in stability of the nucleic acids can play a key role in many contexts including DNA-targeted therapy against various cancers, bacteria or viruses.[93] Most nucleic acids' stabilities and interactions between small molecules are characterized by melting curve analysis using classical optical methods. Melting temperature (T_m) can be measured and used as a key factor for nucleic acid thermodynamic analyses. The melting temperature (T_m) depends on its specific nucleotide sequence and also the length of the DNA sequence. The T_m is defined as temperature at which half of the DNA strands are in the single-stranded or coil state. DNA melting is also called DNA denaturation. This is a process by which double-stranded DNA separates into single-strands due to breaking of hydrophobic stacking attractions between base pairs. There are formulas that can be used to calculate T_m in predicting melting temperature of DNA duplexes[94]. The equilibrium

constant of a melting reaction from double-stranded nucleic acid AB to single-stranded A and B (AB ↔ A + B) is $K = \frac{[A][B]}{[AB]}$. The equilibrium constant relates free energy ΔG,

$$\Delta G° = -RT\ln K = -R\mathrm{T}\ln\frac{[A][B]}{[AB]}. \quad (3.1)$$

where R is the gas law constant, and T is the reaction temperature. The melting temperature is determined when half of the double-stranded DNA has denaturized, so single-stranded [A] and [B] will be equal to double-stranded [AB], which is the same concentration as half of the initial concentration of $[AB]_{initial}$. This gives a T_m expression for nucleic acid,

$$T_m = -\frac{\Delta G°}{R\ln\frac{[AB]_{initial}}{2}}. \quad (3.2)$$

After plugging in $\Delta G° = \Delta H° - T\Delta S°$,

$$T_m = \frac{\Delta H°}{\Delta S° - R\ln\frac{[AB]_{initial}}{2}}. \quad (3.3)$$

The formula can be rewritten into

$$T_m = \frac{\Delta H°}{\Delta S° + R\ln([A]_{total} - \frac{[B]_{total}}{2})}, where\ ([A]_{total} > [B]_{total}), \quad (3.4)$$

due to $\Delta H°$ and $\Delta S°$ are given for association reaction[94].

Melting temperature determination is done mainly by optical methods. Fluorescent intercalator displacement (FID) is one of the most important techniques used to determine the binding of a small molecule to a nucleic acid.[95] FID uses a fluorogenic compound, usually an intercalator to displace a bound small molecule from the nucleic acid, resulting in a change in fluorescent signal.[95] Alternatively if the nucleic acid binder is fluorescent, then binding to the nucleic acid could be monitored directly via changes in the fluorescence properties (change in quantum yield upon binding, which will lead to fluorescent intensity enhancement, or a Stoke

shift).[96] Also fluorescent anisotropy could be used to monitor the binding of fluorescent drugs to nucleic acids.[97] The binding of compounds that are UV-active could also be monitored via UV spectroscopy.[98] However UV is not sensitive enough to study the binding of high affinity ligands. These chromophore-based techniques have been implemented in microwell as well as microarray formats, and show capability in high-throughput screening.[99,100] However, the central difficulty with the widely utilized FID approach is that because FID introduces a competition between the intercalator and the small molecule, ligands that have lower association constants, but which could be developed into viable drugs nonetheless, are missed with FID screenings.[94] Label-free methods using surface plasmon resonance (SPR) and quartz crystal microbalance (QCM) techniques can measure the stability of the small molecule and nucleic acid complexes without the limitations described above.[101,102] However, these systems are costly and also non-trivial to set up high-throughput systems.

Electrochemical detection of nucleic acid provides high sensitivity and is also well suited for high-throughput formats. The electrochemical detection approach offers great potential and has many advantages for melting curve analysis. Small molecules do not need labeling and the interaction between a small molecule ligand and nucleic acid can be monitored using DNA that is labeled with electroactive redox moiety. The electrochemical detection is only sensitive to the redox moiety, therefore provides immunity to nonspecific binding adsorption of the small molecule. Experimental procedures are simple, and there is no wash or drying steps prior to measurement. Temperature in an electrochemical microwell can be accurately controlled by microheaters. Therefore electrochemical heated-microarray systems hold considerable potential to overcome limitations associated with optical methods with regards to DNA melting experiments.

Single nucleotide polymorphism (SNP) has been shown to account for differences between individuals. For example, in some instances SNP can predict drug metabolism and susceptibility to certain diseases, such as cancer.[103] Consequently, ample motivation exists for the development of measurement methods that can detect SNP.[104] Traditionally, SNPs have been detected after genomic amplification, via polymerase chain reaction, followed by melt-curve analysis of the amplified polynucleotide using optical methods. Electrochemical monitoring of nucleic acid melting, while generally underdeveloped, would be a complementary and potentially a cheaper and/or simpler alternative to optical monitoring. Electrochemical methods can utilize a surface-bound thiolated DNA/RNA capture probe that contains an electroactive moiety such as ferrocene or methylene blue (MB), and when a complementary strand binds to this probe, the resulting conformational change would also affect the distance between the electroactive moiety and the surface. If the surface is a conducting element, such as gold, then the nucleic acid conformational change can be monitored via changes in the rate of electron transfer from the electroactive moiety to the conducting surface.[105-109] Alternatively the bound probe could be devoid of an electroactive element, but if the complementary probe in solution contains an electroactive group, then a hybridization between the bound and unbound probes would bring the electroactive group close to the conducting surface.[110]

Being able to monitor the rate of change of electron transfer from electroactive moieties, which are attached to nucleic acids with respect to increasing temperature enables the determination of biomolecule melting temperatures (T_m), and hence facilitates the detection of SNPs, as SNPs are typically characterized as having different melting temperatures. Towards the goal of such electrochemical monitoring, Flechsig et al. developed a heated gold electrode to measure electrochemical melting curves using a 5 mL cell.[111,112] Also a recent report by Soh et al.

built on this precedent with decreased reaction volume and demonstrated that electrochemical melting curves could be obtained using microfluidic channels that are heated by a Peltier heater.[113] These approaches have the ability to perform electrochemical melting curve measurements for DNA structures, but there are also some limitations. The heated electrode method uses a regular electrochemical cell with a relatively large analyte volume; this is not ideal for developing array-based high-throughput screening. The microfluidic channel heated by Peltier heaters is capable of handling small analyte volumes, but fabricating individual micro-Peltiers for each microwell is impractical and so a single Peltier heater is usually used to heat many microwells, and this configuration may affect precise temperature control in each well. An alternative heating device that is easier to fabricate, such as that described below, can overcome this challenge.

This project has developed new microscale electrochemical measurement system. Fabrication was achieved using lithographic technology to integrate all required electronic components in a compact device for measurements on small-volume liquid samples. The integrated approach lends itself to parallel fabrication, which can be readily adapted to realize arrays of individual devices for high-throughput screening. The microfabricated imbedded resistive Pt heater below the electrodes allows rapid temperature control, and independent current monitoring that enables melting temperature determination for DNA structures. The small size, thin profile and overall low thermal mass of our configuration have inherent advantages relating to effective heat transfer and minimization of thermal gradients. Proof-of-concept measurements made with our platform for DNA melting directly related to SNP applications will be described below.

3a.2. Results and Discussion

This Results and Discussion section is organized as follows. First, the design and fabrication details of the 1st generation silicon-based and miniaturized 2nd generation glass-based microdevices are described. Second, DNA electrochemical measurements and rapid DNA melting analyses for duplex DNA detection using the microfabricated platform are discussed as proof-of- concept demonstrations. Lastly, rapid DNA melting analyses for SNP detection using the microscale devices is discussed.

3a.2.1. Design and Fabrication of the 1st Generation Prototype Device

For more than a decade, the Chemical/Biochemical Microsensor Science Group of National Institute and Standards Technology (NIST) has been developing MEMS microhotplate microsensor arrays for gas sensing. The sensors have wide applications in multiple areas including industrial process monitoring, building security and extraterrestrial exploration. The microhotplate was fabricated with polysilicon or Pt as a heater to control the surface temperature of the sensing thin films. Temperature of a sensing film is altered by many factors such as the film's conductance, the types of gases it will adsorb and the reaction rates between the adsorbates on its surface. These small microdevices have low power consumption and rapid temperature control technology to enhance the signal responses for sensitive gas phase sensing, These advantages can also be applied to biochemical sensing technology to develop thermal-related microscale biosensors for biochemical and biomedical studies. It should be noted that electrochemical sensors have great sensitivity and easy signal processing for fast chemical and biochemical sensing. Among majority of the electrochemistry instrumentation, the lack of temperature control is always a limitation for studying biochemical processes. Because the

thermal factor plays a very important role and can have a huge impact in biomolecular reactions, for development of a rapid temperature-controlled platform to examine the thermal characteristics in electrochemical biomolecular sensing. Such a tool holds great potential for many applications, such as clinical diagnostics, analysis of forensic samples and monitoring of infectious bacteria.

Based on the current NIST microhotplate gas sensor fabrication technology, a Pt heater-based electrochemical cell, 1st generation prototype platform was planned and designed (see Fig. 3.1 and Fig. 3.2) to investigate many heating and electrochemistry device parameters for accomplishing electrochemical measurements with temperature monitored for biochemical samples. The goal of the 1st generation prototype platform was to ensure the heating capability from 0 to 100 °C for liquid-based biochemical samples and control the temperature with small power consumption. Microfabricated electrodes were also tested to ensure the three-electrode system has the ability to immobilize biochemical samples and measure electrochemical processes as the temperature is changed. This prototype platform testing provided valuable data for developing components within the 2nd generation miniaturized platform.

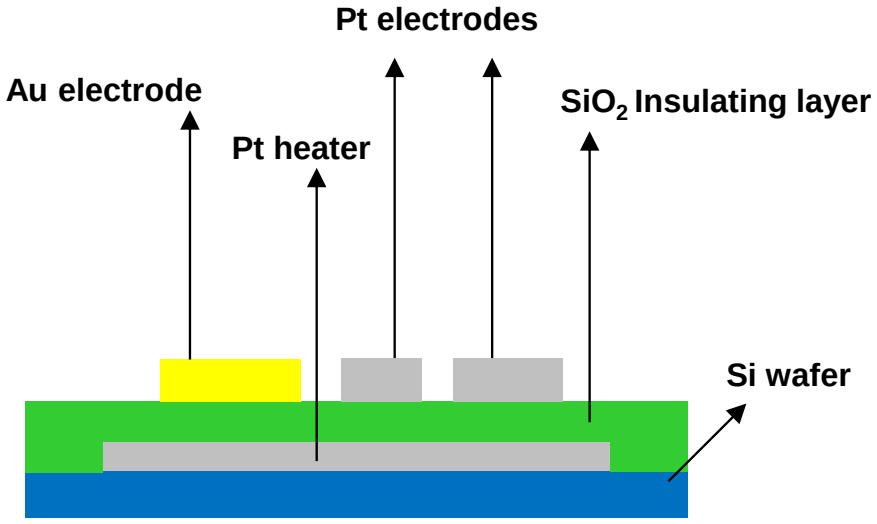

Figure 3.1. Schematic architecture of the 1st generation prototype device.

The 1st generation prototype device was designed and fabricated on a 100 mm silicon wafer. Fig. 3.1 shows the general architecture of each single device. First a 200 nm Pt heater layer (plus a 20 nm Ti adhesion layer) was deposited on to the silicon wafer substrate and then sealed by a SiO_2 insulating layer over to separate the electrode system and the Pt heater. 300 nm Pt counter and 300 nm reference electrodes (deposited onto a 20 nm Ti adhesion layer) plus one Au working electrode (20 nm Ti adhesion layer) were then fabricated on the insulating layer to form the three-electrode system. Because the Pt heaters were sealed by the insulating layer, the metal connection bonding pads for wiring up device components were opened by etching through the insulating layer. The photomask design for the platform fabrication used CAD software to draw all the mask layers for photolithography deposit different properly patterned layers to build the platform. As shown in Fig. 3.1, there are eight individual devices fabricated on the 1st generation silicon wafer. Each device was labeled from 1-8 going clockwise within Fig. 3.2. The metal contacts were designed on the outside of the wafer for wire bonding. Each of the mask layers are shown individually in Fig. 3.3.

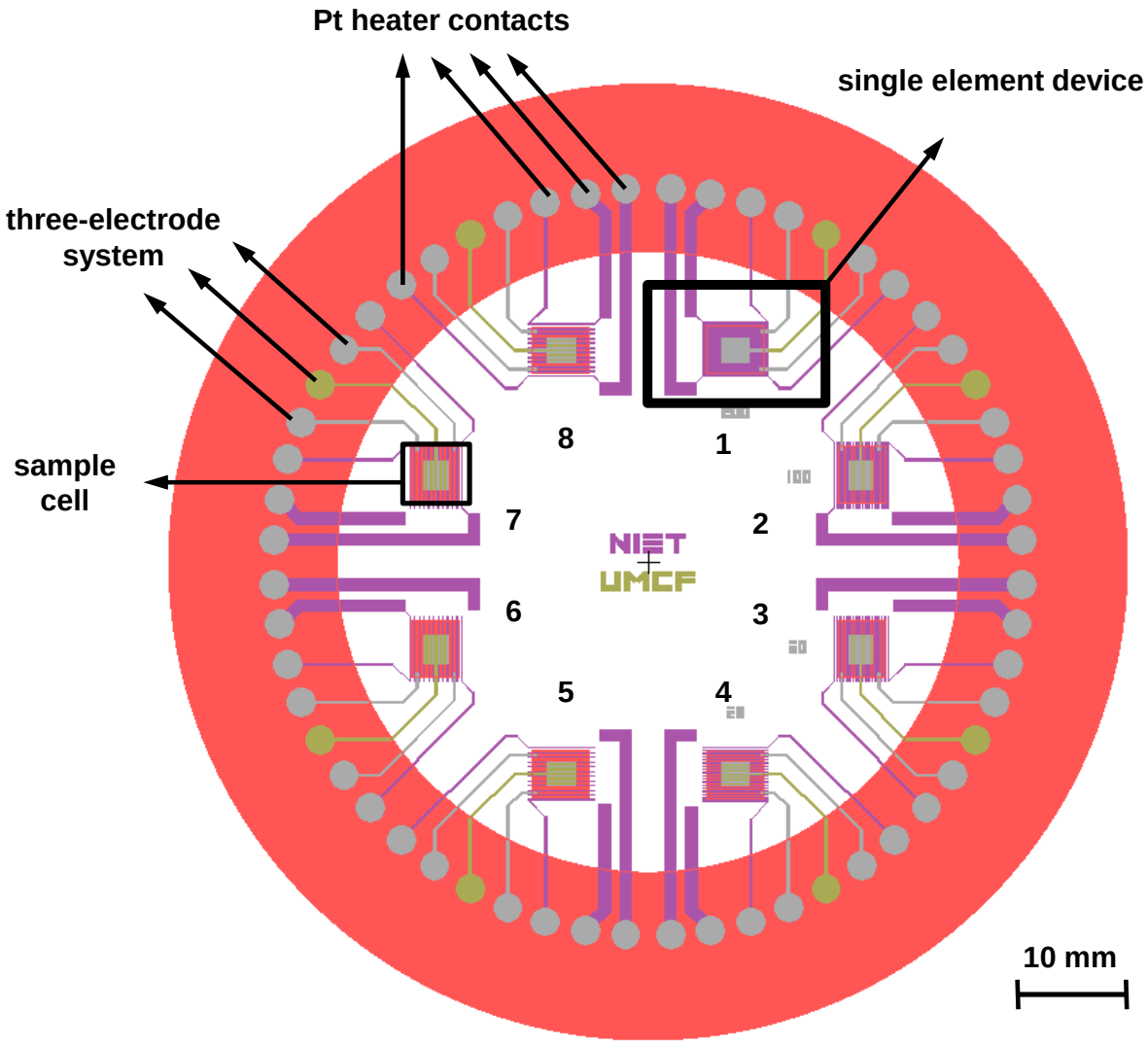

Figure 3.2. CAD drawing of the 1st generation silicon based prototype platform. The wafer includes eight individual single-element devices (labeled through 1-8). Each individual device has its own Pt heater with different parameters (width and separation) and three-electrode system (Au working electrode, Pt counter and reference electrodes).

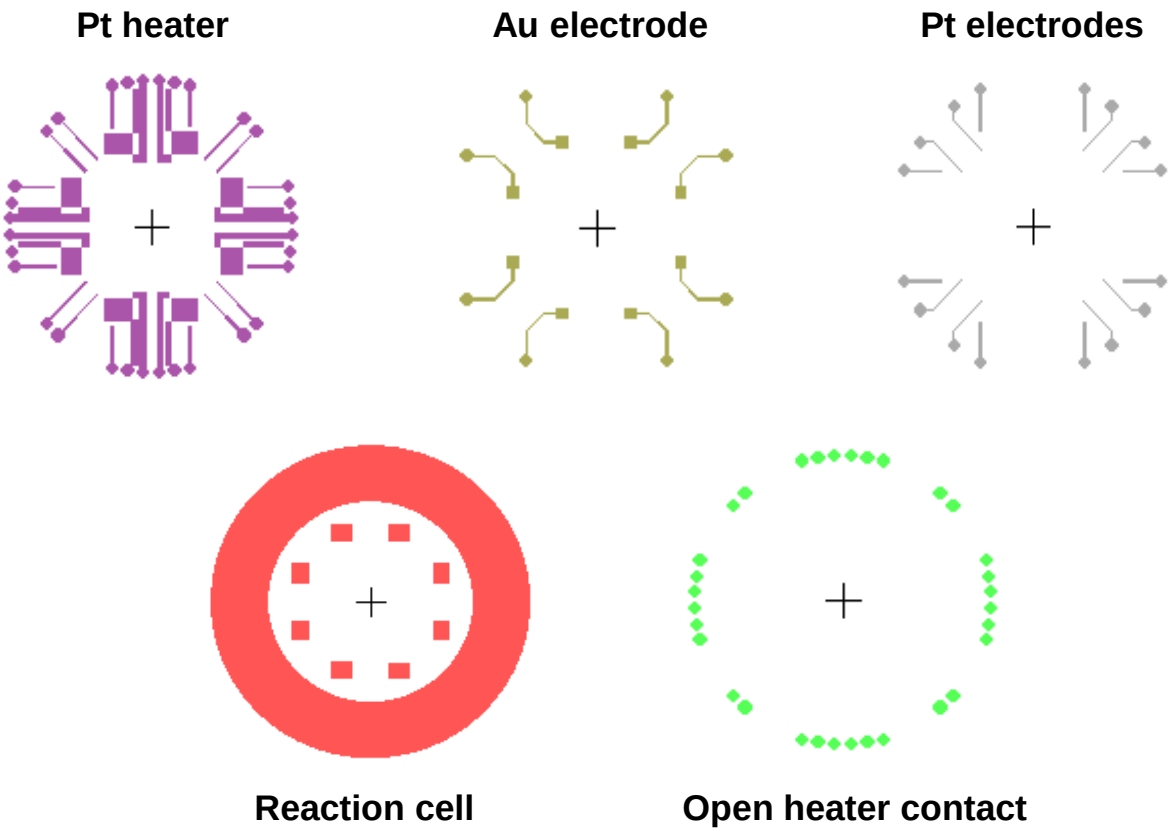

Figure 3.3. CAD drawings of each layer to create masks for employed in photolithographic fabrication to realize the layers of the microscale device platforms.

As described before, the 1st generation prototype device was built to help determine workable parameters for the device microheaters and to ensure that the electrodes functioned properly. Therefore, each Pt heater had its own design to create multiple heating profiles. Fig. 3.4 (and the associated Table 3.1) shows magnified views of the heater design; as indicated in the table, heater parameters varied in heater trace width (w) and trace separation (s). The width of the trace was varied to control the resistance of the Pt heater, and the separation between traces served to control the thermal distribution with the intention of creating a stable thermal profile. The desired thermal profile had a uniform heating area to cover the reaction well, capable of

rapidly heating liquid samples uniformly and achieving up to 100 °C, to fulfill the temperature requirement for analyzing the biochemical samples with small power consumption.

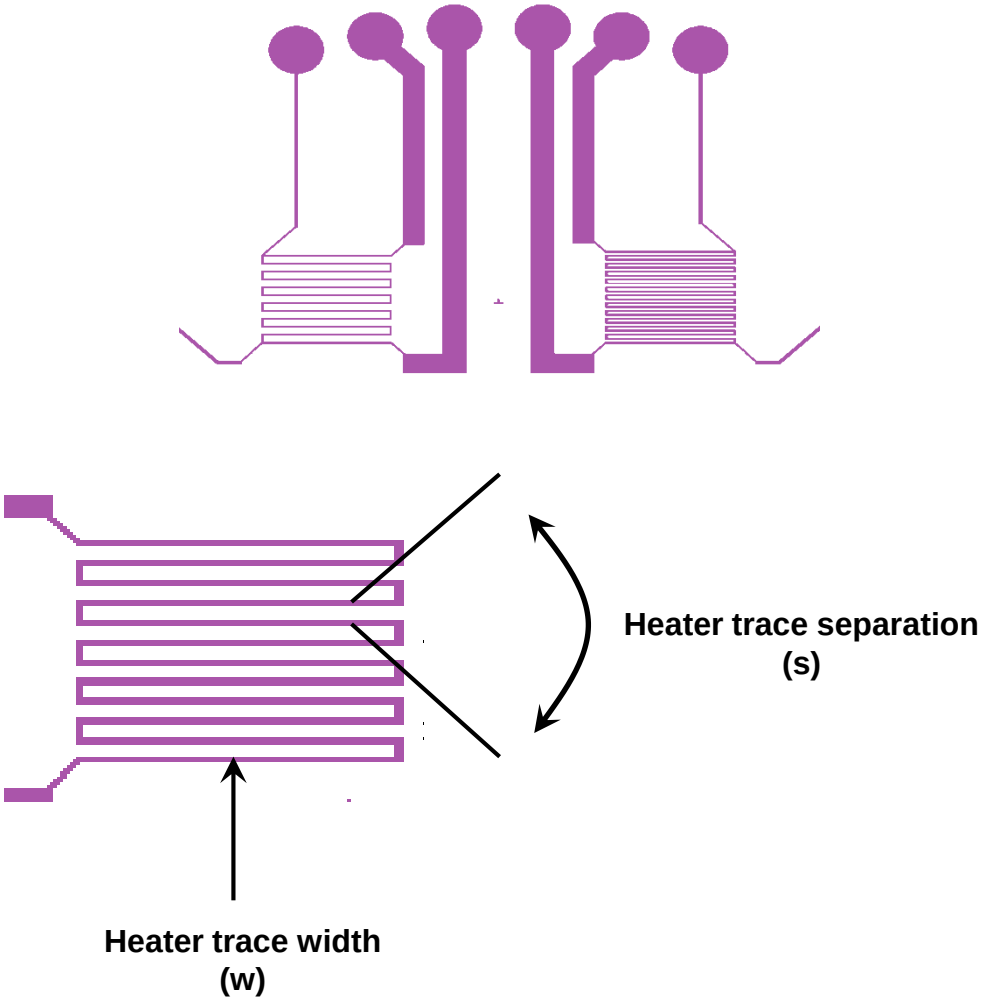

Figure 3.4. Magnified views of the Pt heater design, define the heater trace width (w) and heater trace separation (d).

The first pre-device wafer fabricated included only the Pt heater layer and SiO_2 insulating layer, and it was used to evaluate heater performance. During the initial heater testing, a water droplet was dispensed to cover the heating area. A source meter was used as a power supply to

control the voltage and current input to power up the heaters. An optical microscope was focused on top of the device surface to monitor the water droplet. Each heater was tested individually over a voltage range from 1-200 V, and a current range from 0-1 A with a maximum power of 200 W. Unfortunately, all the heater configurations showed no indication of an ability to boil water, and the internal water droplet temperature may not even have reached 60 -70 °C. Thus the first set of heater designs failed. One reason appeared to be that the heater trace separation was too large, so the heating was more concentrated near the heater trace edge. The separation limited the heat transfer from trace to trace, so the thermal distribution of the heater was poorly and caused overall low surface temperature. The conclusion reached was that the heater trace width needed to be adjusted to allow more trace loops at the heating area.

Table 3.1. Heater trace width and separation.

Heater #	Width (w) μm	Separation (s) μm
1	200	980
2	100	950
3	50	900
4	20	800
5	20	980
6	50	950
7	100	900
8	200	800

As a result, a redesign of the heater mask was carried out to decrease the heater trace separation by a large amount for a better trace to trace heat transfer, and adjust the heater trace by small amounts to form more loops. Table 3.2 showed the new heater parameters with much smaller trace separation for completing the 1st generation prototype device.

Table 3.2. Redesigned heater trace width and heater trace separation, as well as the resistances of each heater that were measured at room temperature.

Heater #	Width (w) μm	Separation (s) μm	Resistance (R) Ω
1	50	37.5	3880
2	50	37.5	3880
3	25	37.5	12290
4	25	37.5	12290
5	25	58.5	6180
6	25	58.5	6180
7	50	58.5	2689
8	100	33.5	1063

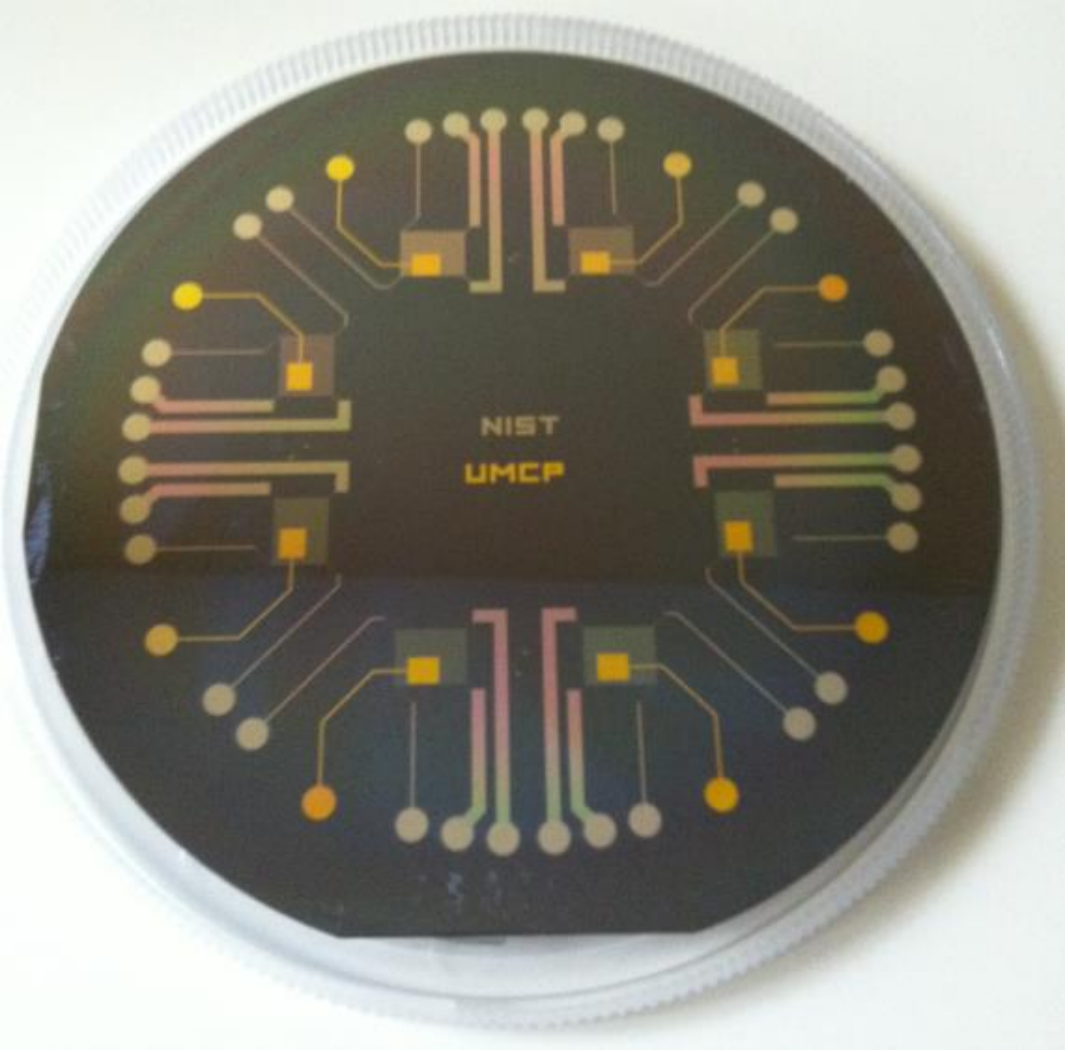

Figure 3.5. An image of microfabricated 1st generation prototype device with redesigned heater trace width and separation.

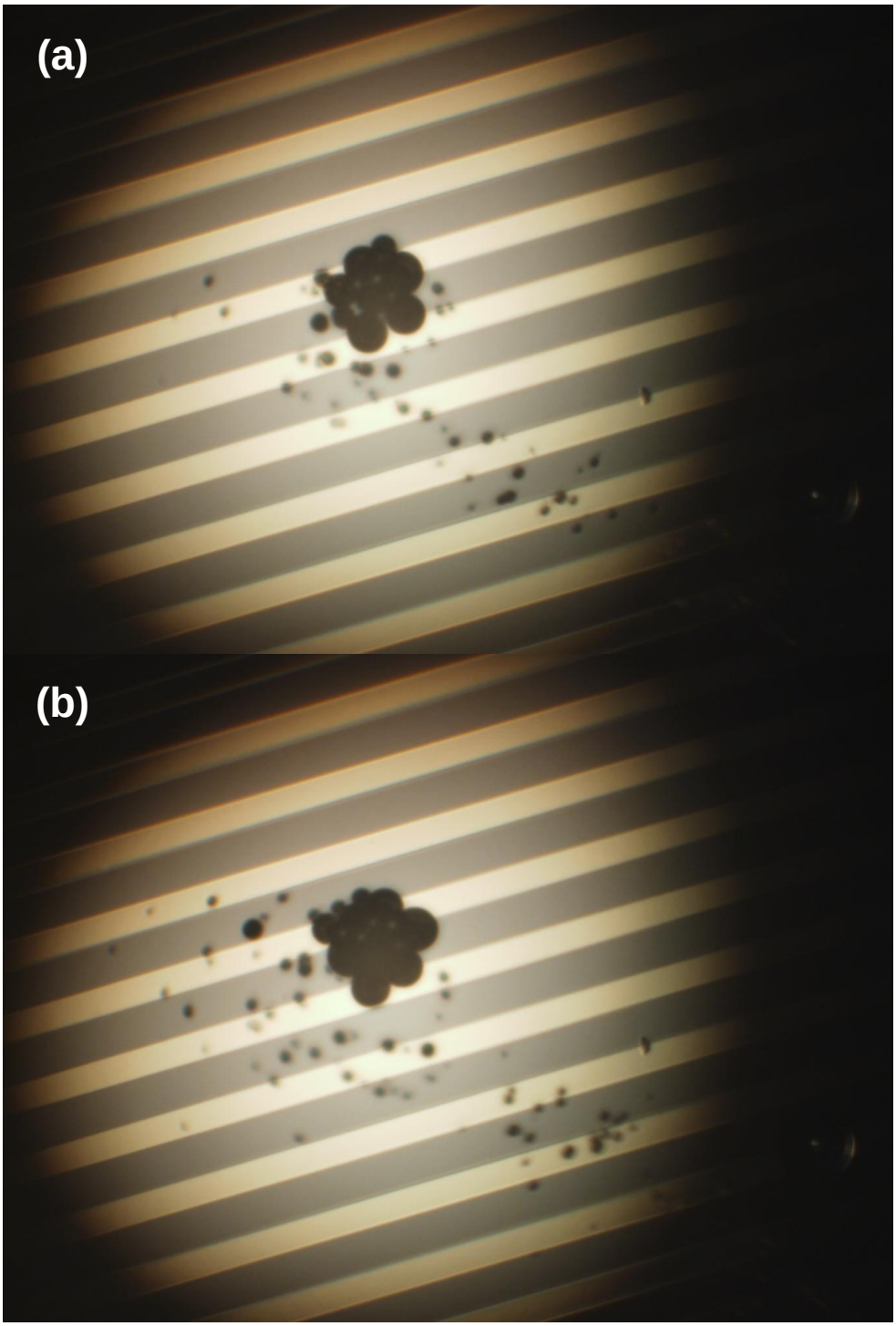

Figure 3.6. (a) Optical image showing water bubbling on the surface of heater #1 at 48 V; (b) optical image showing more rapid water bubbling on the surface of heater #1 around the max output power.

The redesigned mask with the new heater parameters was employed to fabricate the second wafer which would be retested to determine heating capability (see Fig. 3.5). After introducing a water droplet to cover the heating area, the heating evaluation was stared again. During the measurements, heaters #3 to #6 showed no proper sign indicating water boiling, but there were new observations from heaters #1, #2, #7 and #8. The voltage of heater #1 applied from the source meter was increased to reach the maximum output power. When the voltage reached 48 V, bubbles were observed forming at the edge of the droplet and migrated to the center of the heating area. Fig. 3.6(a) shows a captured image from an optical microscope providing evidence of the water bubbling inside a water droplet at the surface of the heater. By further increasing the voltage, more bubbles were created rapidly from the edge of the heater and again moved to the center. Another optical image taken with the optical microscope in Fig. 3.6(b) shows the result for increasing temperature of the water droplet. However, the maximum output power was reached shortly and the measurements could not be continued due to the limitation of the source meter. Similar water bubbling phenomena were observed at high output power using heater #7 and #8. Heater #7 required more output power than heater #1 in order to show the same amount of the water bubbling on the heater surface. And heater #8 started similar bubbling as heater #1 at 22.5 V, and more bubbling from the heater edge during the voltage increase. Because of the water droplet on the heater surface had a spherical shape, the droplet thickness at the edge was much less than at the middle of the droplet. The edges offer a smaller heat sink for heat transfer from the Pt heater and distributed to the liquid water. However, it was determined that we can only bring the full droplet to the boiling point if a more powerful power supply could be used.

Using an older power supply (which had no digital display) capable of heating with up to 300 V, studies could be done with a maximum output power at 100 W. Heater #1, #2 and #8

were evaluated using this power supply at increased voltage and larger output power. During the observation of the heating process of heater #1, a huge amount of water bubbles under rapid boiling could be observed by eye when the voltage was increased into the range of 180 V to 220 V. And the droplet evaporated in several seconds at a 220 V setting. The same phenomenon happened on heater #8 as the output power was increased, and the rapid evaporation process occurred at 200 V. The whole water droplet was successfully heated to its boiling point, the calculated power consumption was around 25-40 W, which is not ideal for microdevices. However, the redesign of the heater trace widths and separations did improve the heating results (from nothing to water bubbles). Useful data and further design options were acquired for the 2nd generation microdevice development. Another important observation involved the temperature of the whole silicon wafer during the heating with the high output power supply. When water droplets reached their boiling point around 200-220 V, besides noticeable heating in the heater area, considerable heating of the whole silicon wafer was noted (even to the point that would boil water). This heat from the microheater had been transferred and distributed to the whole silicon wafer instead of only the heater area. Thermal conduction within the silicon was the reason why the heaters required such a large output power to heat the water droplet to its boiling point. Due to the nature good thermal conductivity (1.3 W cm^{-1} °C^{-1}) of the Si, it became clear it was not a desirable substrate to fabricate Pt heaters. The devices required a substrate material with a low thermal conductivity in order to concentrate the heating at the heater area rather than distribute to the surrounding areas.

3a.2.2. Design and Fabrication of the 2nd Generation Prototype MicroDevice

After collecting all the valuable data described above from the 1st generation prototype device, we chose borosilicate glass wafer as the substrate material for the 2nd generation prototype device. Borosilicate glass is known to be chemically resistant, has a low thermal conductivity (1.14 W m^{-1} $°C^{-1}$) and the ability to withstand temperatures up to 450 °C, making it a good choice for applications which call for good temperature stability. As shown in Fig. 3.7, we maintained the general single-device configuration used for the 1st generation that had been fabricated on silicon, now with a microfluidic included. However, in moving to glass wafer devices, some adjustments were made in the layout, as shown in Fig 3.8 and Fig. 3.9. The three-electrode system (consisting of Au working, Pt counter and referening electrodes) and Pt heaters were miniaturized to fit a 2 mm diameter circle area to form a single element microdevice. The 10 µL reaction well could be formed by cutting a 2 mm diameter hole on the PDMS layer to introduce cylindrical chamber.

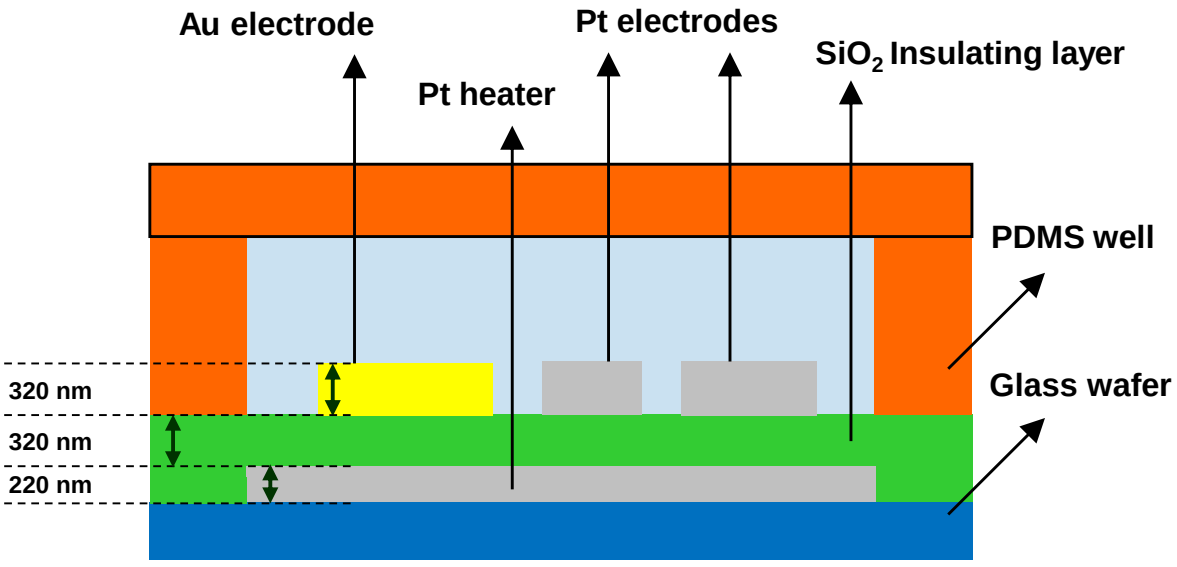

Figure 3.7. Schematic single element device architecture of the 2nd generation prototype microdevice.

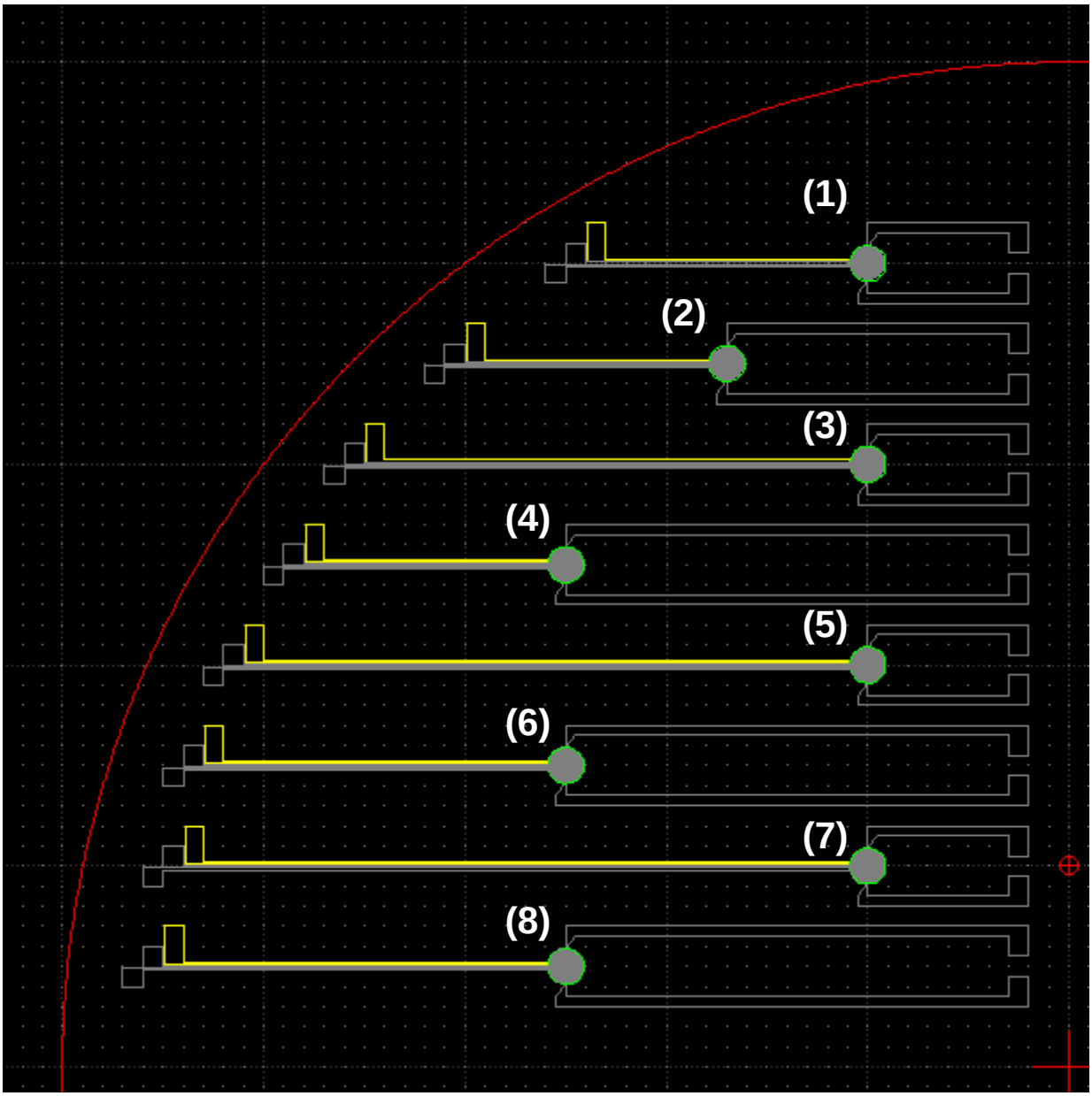

Figure 3.8. CAD drawing of a portion of the 2nd generation glass based prototype platform. The pictured wafer quadrant consists of eight individual single-element devices (labeled through 1-8). Each individual device has its own Pt heater with different parameters (width and separation) and three-electrode system (Au working electrode, Pt counter and reference electrodes).

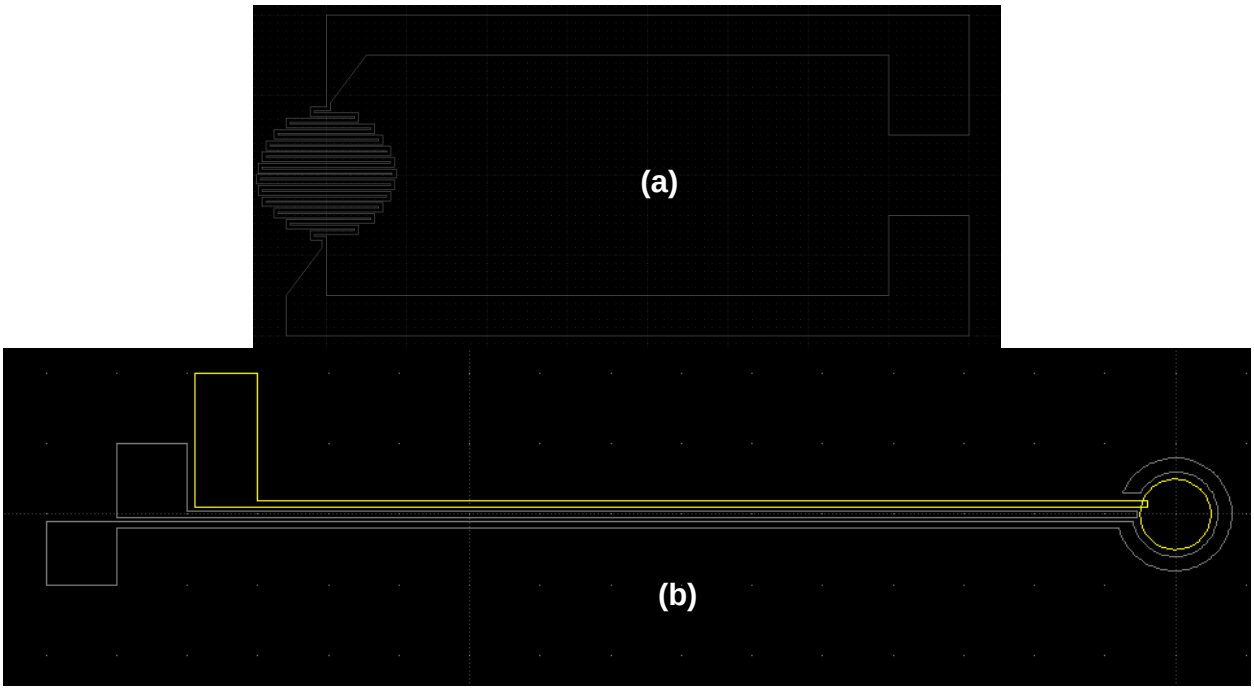

Figure 3.9. CAD drawing of (a) single Pt heater and (b) three-electrode system, the round gold electrodes were fabricated in one of two disc sizes (1 mm and 0.5 mm in diameter).

For this glass-based prototype microdevice, Pt heaters were also designed with different trace widths (10-50 µm) and trace separations (10-20 µm) based on the results obtained from studies on the 1st generation prototype devices. Table 3.3 lists all the parameters of the Pt heaters fabricated for each individual device in the glass-based 2nd generation.

Table 3.3. 2nd generation microdevice heater trace widths and heater trace separations, as well as the resistances of each heater measured at room temperature.

Heater #	Width (w) μm	Separation (s) μm	Resistance (R) Ω
1	50	20	552
2	50	10	648
3	40	20	812
4	40	10	965
5	30	20	1322
6	30	10	1618
7	20	10	3290
8	10	10	9660

As earlier, the 2nd generation prototype microdevice was fabricated with both Pt heater and three-electrode system included. Each single element on the microdevice was wired through the metal bond pad contact and made ready for heater calibration. The Pt resistive heater temperature calibration experiment was conducted using a 1100 °C box furnace to create a closed heating environment. The furnace was controlled to increase temperature in steps and the resistance values of all Pt heaters were recorded using a digital multimeter. After the calibration, we tested the heater by filling 10 μL of water inside the PDMS microwells, and then increased the voltage to elevate the temperature. Heater 1-4 could heat the water to boiling point with a relative low voltage based on the resistance reading during the measurements. The calibration indicated that at 96 °C, heaters 1-4 had resistance values equal to 662, 783, 974, 1172 Ω, respectively. When we increased the voltage to 12, 14, 16 and 18 V for heaters 1-4, the resistance values all passed

their value at 96 °C (668, 790, 975, 1194 Ω). It is clear that heaters 1 and 2 required lowest power to heat up, and were ideal for the low power thermal-electrochemical microdevice. Heater widths of 50 and 40 µm combined with 20 and 10 µm separations were demonstrated to be good combinations for a Pt resistive heater to power up the liquid sample to 100 °C. These width and separation values were important to use in the next platform, which is described in Section 3a.2.3.

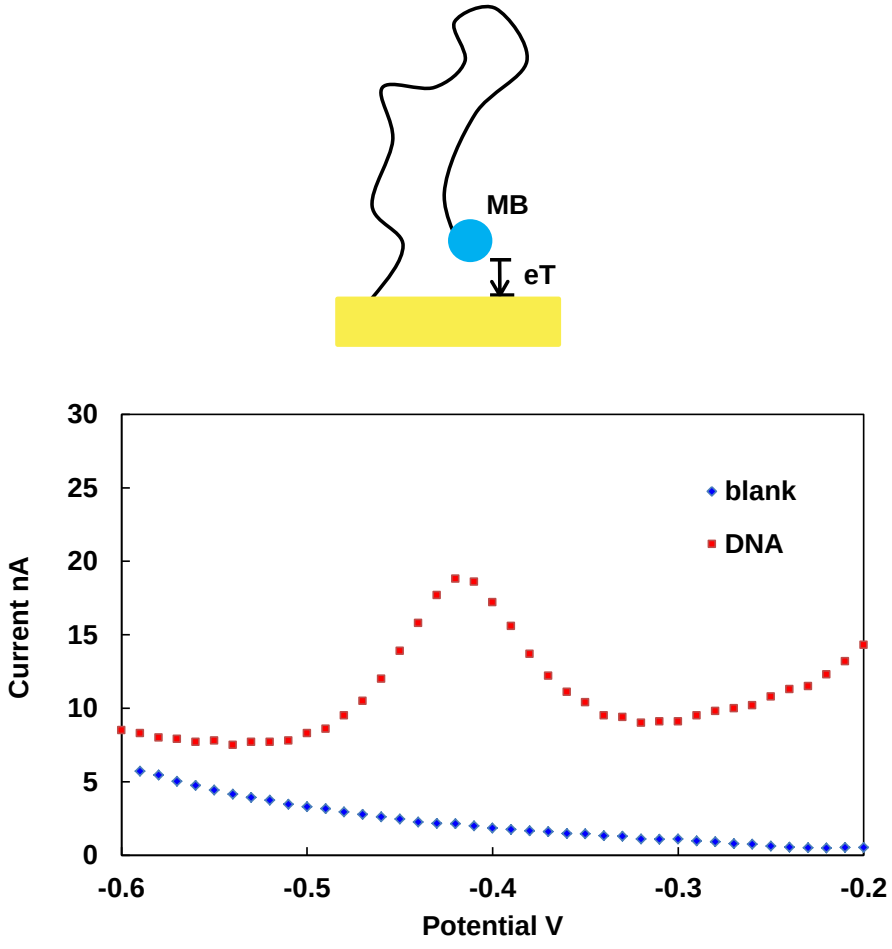

Figure 3.10. Red curve indicates SWV detection of MB-labeled DNA self-assembled on the gold electrode, and blue baseline is the SWV result without MB labeled DNA attached.

The three-electrode system of the 2nd generation device was also examined to ensure our electrode system design was capable of performing electrochemical detection based on attachment of MB-labeled DNA strands to the gold electrode. We first ran a blank SWV scan without DNA present on the gold electrode, and this resulted in the blue baseline in Fig. 3.10 which shows no electrochemical signal. Then MB labeled DNA was self-assembled on the gold working electrode using thiol attachment. SWV was carried out for detection of the redox MB signal. The peak current appeared at -0.41 V represented the electron-transfer between the redox MB and gold electrode. The signal was fairly stable and no further changes occurred as the SWV scans were repeated 3 times.

Based on these initial results for both heating and electrochemical detection, it appeared our 2nd generation platform would be able to perform electrochemical detection with temperature control at the same time for DNA samples ramped to temperature as high as 100 °C. However, before moving to that direction, we considered the possibility of a potential risk with the current Pt heater design. Because the Pt heater was powered by a source meter, and the current passing through the Pt heater could create magnetic field at the surface of the heater. This might affect not only the sensitivity of our electrochemical detection, but also the stability of the MB redox label. The concern comes in part due to the close proximity of the microdevice components and the samples to be studied using them. There seemed to be no literature that adequately addressed this possible issue, and we wanted to have our platform ready for temperature-controlled melting measurements without complications to the operation and measured signal. A redesign of the heater was developed with the objective of creating a magnetic field-cancellation heater to minimize the potential magnetic field issue during the heating. And the newer heater was designed using the energy saving combination of the trace width and separation.

3a.2.3. Temperature-Controlled Electrochemical Microscale Platform

Our temperature-controlled electrochemical microscale platform using the design of the field-cancellation Pt heater, was designed and fabricated. Schematic diagrams of the microscale electrochemical platform and associated fabrication steps are displayed in Fig. 3.11 (A)-(F). An optical micrograph of the microfabricated Pt heater and the three electrode system viewed from the top is shown in the Fig. 3.11 (G).

Our design objective for the microscale platform was realized-to produce a three-electrode electrochemical device with a small footprint, temperature control capabilities and relatively low thermal mass. Microfabrication processing used to produce structures like that pictured in Fig. 3.11(G) was performed at the National Institute Standards and Technology (NIST) Center for Nanoscale Science and Technology NanoFab Facility. Custom masks were designed in-house for all the required lithographic steps, and the masks were then fabricated at and purchased from the International Phototool Company LLC* (Colorado Spring, CO. USA). Feature sizes for our designed functional components, ranged from 10 to 50 μm. The first step involved fabricating Pt resistive heater traces on a 100 mm glass (borosilicate) wafer through a lift-off process using a front side contact aligner (MA8 Suss Microtec*, Sunnyvale, CA, USA) for contact lithography and an e-beam lithograhpy system (VB300 Vistec*, Best, Netherlands). S1813 and LOR3A photoresists were used to coat the wafer. The Pt heater pattern was created by exposing the wafer under UV light using the MA8 and followed by MF319 development. An e-beam was used next to deposit a 20 nm titanium (Ti) adhesion layer and then the 200 nm Pt heater layer. The 320 nm SiO2 insulating layer was formed using plasma-enhanced chemical vapor deposition (PECVD Unaxis 790 Plasmatherm*, Saint Petersburg, FL, USA). The Au electrodes (20 nm Ti layer and 300 nm Au layer) and Pt electrodes (20 nm Ti layer and 300 nm Pt layer) were fabricated on the

SiO_2 insulating layer using the similar lithographic steps to those for fabricating the Pt heater (described above). The heater metal contact pattern was created by exposing S1813 coated wafer under UV light using the MA8 followed by MF319 development. Then a reactive ion etching system (RIE Unaxis 790 Plasmatherm*, Saint Petersburg, FL, USA) was employed to create the heater metal contact. The 10 µL poly(dimethylsiloxane) (PDMS) (Sylgard 184 kit Dow Corning Corporation*, USA) chamber incorporated to hold liquid samples above the electrodes was formed using a 10:1 base-to-crosslinker ratio, and then cutting a 2 mm diameter hole using a metal punch to introduce a cylindrical chamber. The PDMS chamber was adhered to the SiO_2 insulating layer and centered on the Pt heater, three-electrode system. Analytes for electrochemical studies were introduced into the chamber using a 10 µL pipette. Finally the cylindrical chamber was closed by adding a PDMS lid before melting experiments were begun.

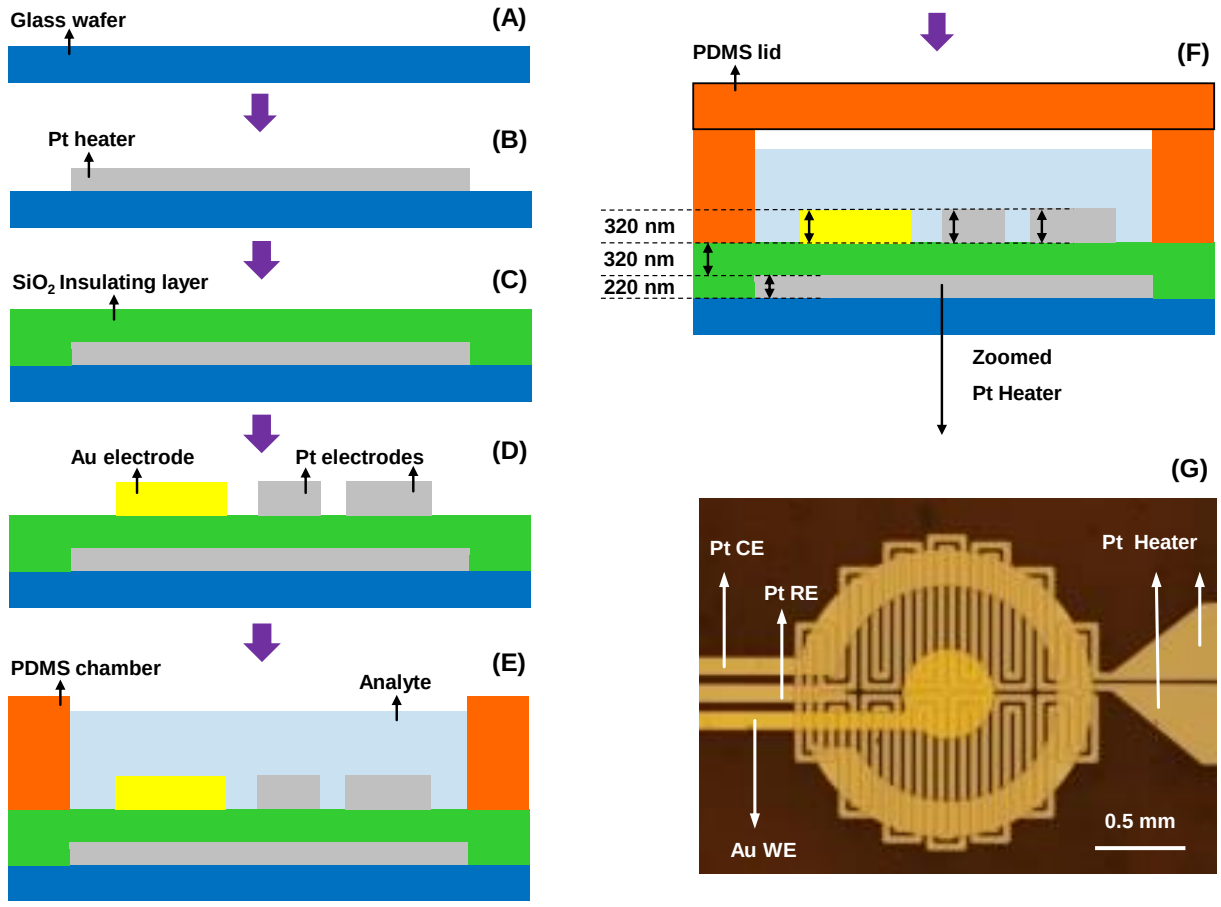

Figure 3.11. Schematic architecture of the electrochemical microscale platform. (A) Multiple versions of the platform were fabricated on a 100 mm glass wafer, but this schematic shows the steps for a single device section. (B) Pt heater lift-off deposition. (C) SiO_2 insulating layer chemical vapour deposition. (D) Au electrode lift-off deposition followed by Pt electrodes lift-off deposition. (E) PDMS chamber centered over the device on the insulating layer, and filled with analyte solution. (F) PDMS lid to close the chamber. (G) Optical micrograph showing a top view of the platform (without the PDMS well).

Our electrochemical platform provides rapid local temperature control (from an integrated thin-film Pt microheater) and electrochemical detection within a three-electrode chamber to perform melting curve analyses based on changes in electron transfer rates induced by conformational changes. The electrochemical chamber has an Au working electrode (WE), a Pt reference electrode (RE) and a Pt counter electrode (CE). The Pt heater was formed as an imbedded structure below the electrodes, and is separated from them by a thin 320 nm SiO_2 insulating layer. The glass-based platform is able to locally heat the electrodes to quickly create a stable heating profile due to the low thermal conductance of the intervening glass and the small area being heated (2 mm diameter). The heating characteristics were calibrated against the resistance of the Pt microheater in a temperature-controlled oven, so that temperatures during melting experiments could be determined from the heater resistance. No external heating source is required, and in an array configuration, each electrochemical microcell could have its own heating element to perform parallel, independent heating sequences. For the illustrative measurements in this study, we have used poly(dimethylsiloxane) (PDMS) to form a cylindrical 10 µL sample chamber centered on the microdevice. During the electrochemical melting process, direct heating was controlled and monitored via a source meter connected to the resistive microheater, so that we were able to incrementally raise the temperature by a selected step, and then measure the electrochemical characteristic in a total of approximately 20 seconds at each temperature value. The peak currents at each temperature were measured via SWV for melting-curve analysis.

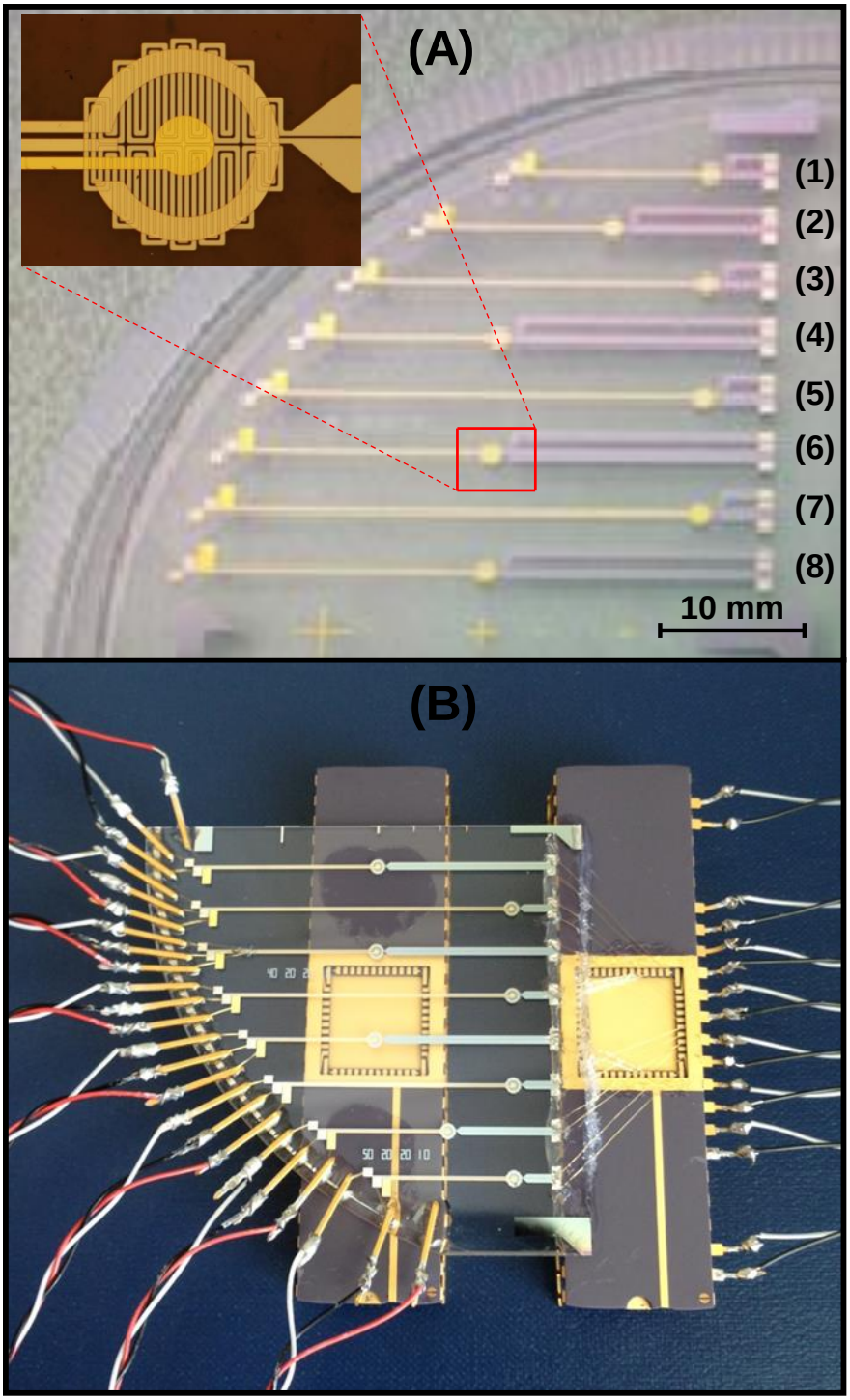

Figure 3.12. (A) 8 single-element microdevices fabricated on a quarter-section of a 100-mm diameter glass wafer. (B) Wired microdevices with electrode leads and heater connections.

Table 3.4. Temperature-controlled microscale platform heater trace width and heater trace separation, as well as the resistances of each heater measured at room temperature.

Heater #	Width (w) μm	Separation (s) μm	Resistance (R) Ω
1	50	20	463
2	50	20	496
3	50	20	463
4	50	20	531
5	40	20	701
6	40	20	776
7	40	20	700
8	40	20	771

The final-version microdevice is shown in Fig. 3.12 and the heater trace width and separation is listed in Table 3.4. There were only two heater widths used in this design which were 50 and 40 μm, with a 20 μm trace separation. It is believed these two offer the best characteristics for our field-cancellation heater within a surface coverage of 2 mm diameter circle. Before perfoming any temperature-controlled electrochemical measurements, the cancellation heaters were calibrated using the same furnace as for the 2nd generation device. The calibration resistance and temperature values were listed in Table 3.5.

Table 3.5. Temperature-controlled microscale platform heater trace width and heater trace separation, as well as the resistances of each heater measured at room temperature.

Temperature °C	Heater 1 Resistance Ω	2	3	4	5	6	7	8
27.7	471	504	470	540	714	790	710	786
32	478	511	476	548	723	800	720	796
38.1	487	520	485	558	737	815	733	811
43.8	495	530	493	567	751	832	746	826
49.4	503	538	501	577	762	844	758	839
55.1	511	547	510	586	775	857	770	857
62	521	558	520	597	790	873	785	870
67.6	529	566	528	606	802	887	797	883
73.5	537	574	536	616	814	901	810	896
79.2	545	583	544	625	827	914	822	909
84.8	553	592	552	634	839	927	834	922
90.1	561	600	559	643	850	940	846	936
96.5	569	609	568	652	863	955	859	950
102	577	618	576	662	876	969	871	964
107.5	585	626	584	670	887	981	882	976

After the heater calibration, we plotted the calibration curves and got linear equations for each of the Pt heaters (see Fig. 3.12). For example, heater 1 had a linear calibration equation of

y=1.427x+430.78 with a R^2 value of 0.9999 for a good linear fit. The resistances of the heater were measured (recorded the voltage and current value at each temperature for the resistance calculation) during the DNA heating process, and then the resistances were converted into the corresponding temperatures using the linear calibration equations to determine the temperature values for each electrochemical scan at the holding temperatures. Heaters #1 to #4 with a 50 μm trace width had much lower resistance than heaters #5 to #8 with a 40 μm trace width. When running DNA melting experiments, we found heaters #1 to #4 had better stability and required less energy to power up. Heaters #1 and #3 could heat up the liquid sample to 100 °C inside the microwell with 11 V. Finally, from these trials, the finalized heater design was determined (which can be used and improved in future microdevice fabrication); the design of heater #1 and #3 were reserved for building future next generation microarray high-throughput system.

The PDMS microwell was a 2 mm diameter cylindrical chamber that could be filled up with 10 μL of liquid sample for melting curve analysis. The chamber was closed by adhering a PDMS lid after introducing the liquid sample into the microwell using a 10 μL pipette. The 2 mm diameter cylindrical shape was designed to fit the all the liquid sample on top of the Pt heating area, so the liquid sample could be heated more uniformly with good heating distribution. A relative hot spot, created by the Pt heater on the glass-based substrate, was due to the low thermal conductivity of glass substrate which limited the heat loss to the surrounding area outside the sylindrical chamber.

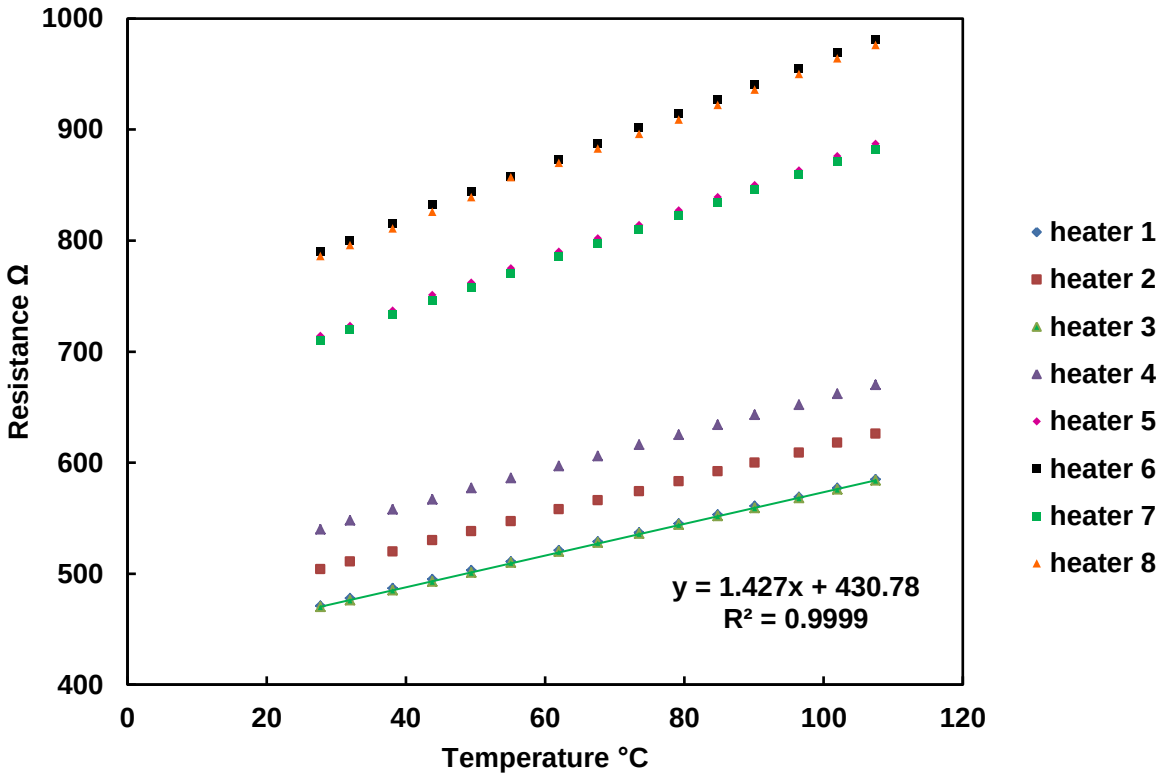

Figure 3.13. Heater 1-8 calibration lines (resistance vs. temperature) with linear equations of the heaters for temperature conversion.

3a.2.4. Rapid DNA Melting Analyses on Temperature-Controlled Electrochemical Platform

The final fabricated temperature-controlled electrochemical platform was ready for proof-of concept measurements for 10 µL DNA sample melting curve experiments.

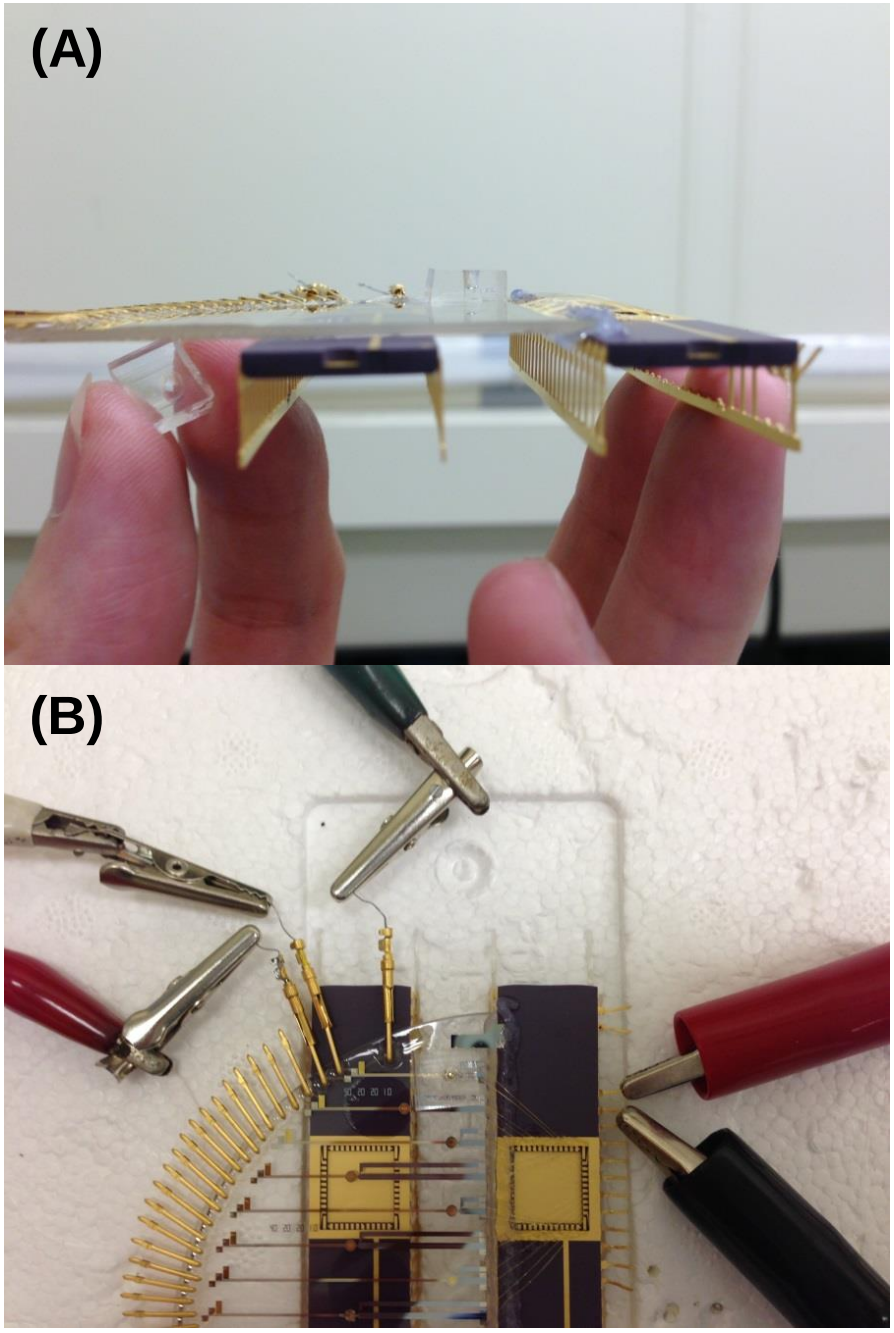

Figure 3.14. (A) The wired microdevice with a PDMS microwell adhered on the substrate and filled up with 10 µL DNA sample. Another PDMS lid piece would be adhered on the top to close the cylindrical chamber environment. (B) The microdevice was connected to the potentiostat on the left with green (WE), white (RE) and red (CE) clamps for electrochemical detection. The power supply was connected on the right with red and black clamps for heating controlling.

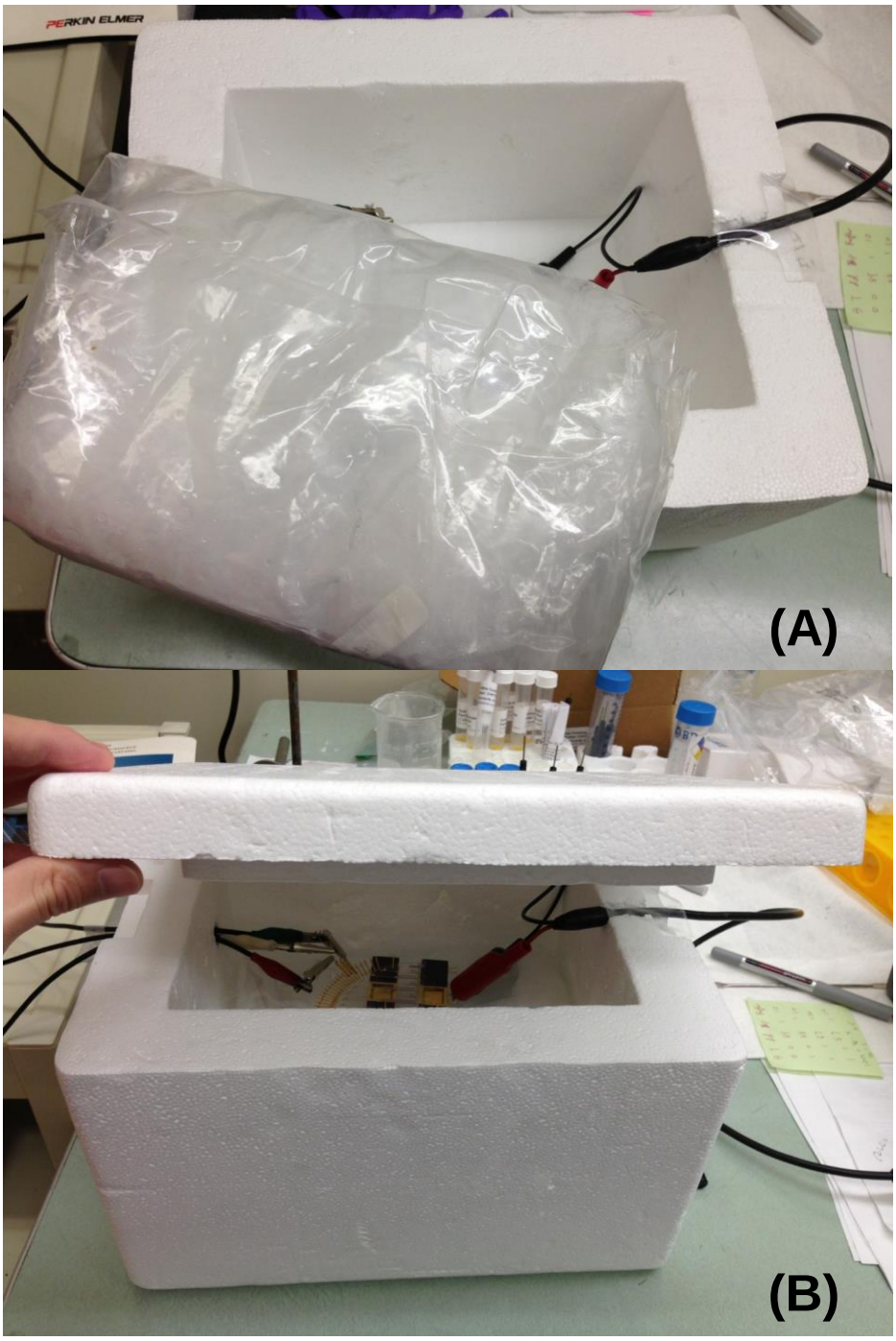

Figure 3.15. (A) The starting temperature of 4 °C was created by putting an ice pack at the bottom of an insulated box. (B) The microdevice was then laid on the ice pack and connected with potentiostat and power supply. The insulated box was closed at the experiment start and wouldn't be opened until the end of the melting curve analysis.

Fig. 3.14 and Fig. 3.15 showed the experimental setup for DNA melting analysis. The wire-bonded microdevice was filled up with DNA samples inside the PDMS microwell and a closed cylindrical chamber was created after closing the microwell with a PDMS lid. The three-electrode system was connected to the potentiostat for electrochemical measurements by the red, green and white labeled clamps. The Pt heater was connected with red and black clamps, and controlled by power supplier (source meter) to increase the temperature by steps. Voltage and current readings were recorded for Pt heater resistance calculations. The resistance values were converted to the corresponding temperature using the Pt heater calibration equation. In Fig. 3.15, in order to create a 4 °C starting temperature for cheap proof-of-concept purpose, we introduced an ice pack into the bottom of an insulated box. The microdevice filled with DNA solution inside PDMS chamber was placed on top of the ice pack and connected to the potentiostat and power supply. The box was insulated by closing the top to create a cold environment to insure the starting temperature was close to 4 °C. After brought down to the starting temperature, confirmed by a mercury thermometer inside the insulated box, the DNA melting experiment was ready to start. The whole melting procedures was completed inside the insulated box until the end to ensure no thermal contact from the outside.

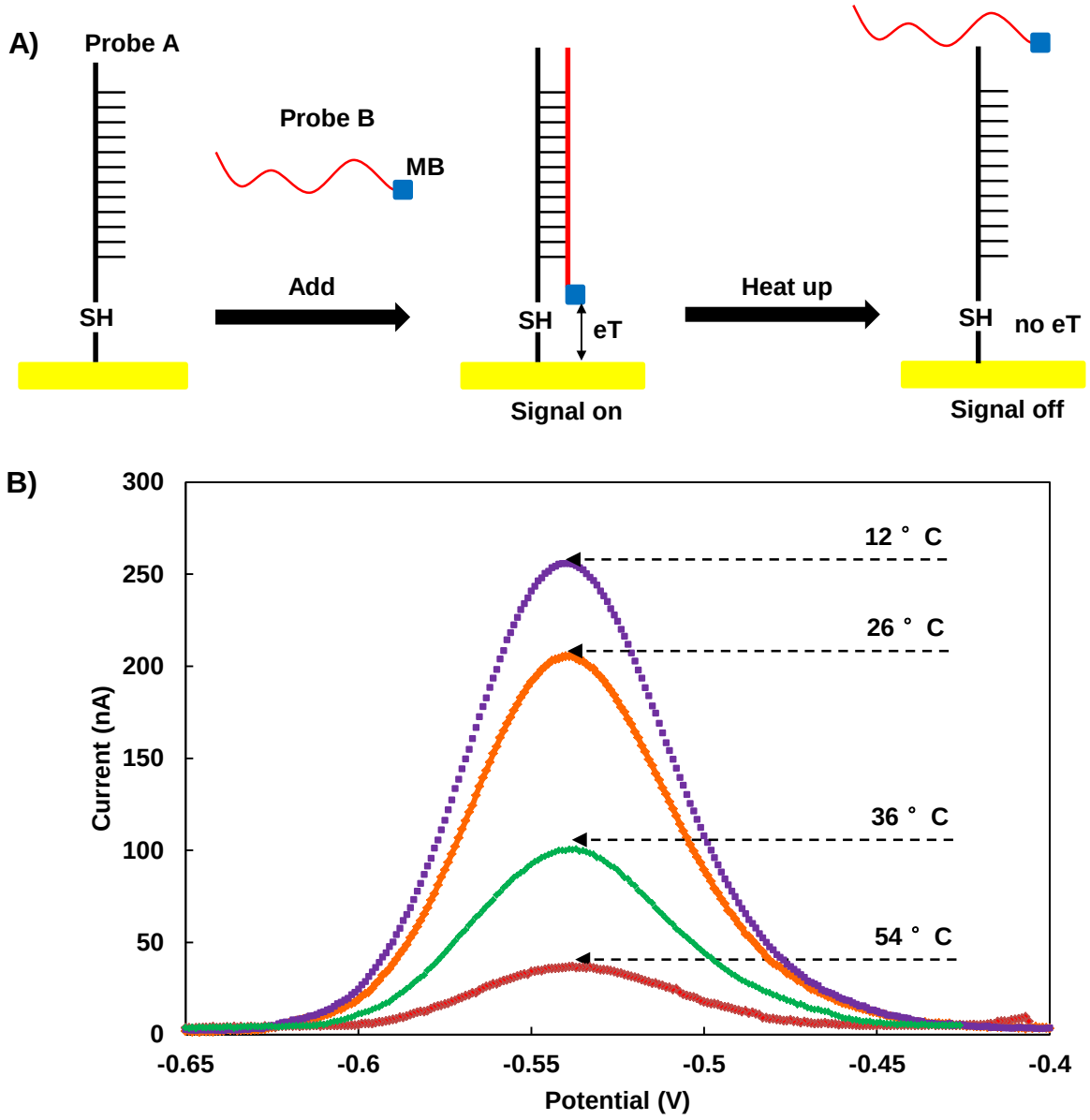

Figure 3.16. (A) The probe design and the electrochemical melting principle. Probe A (full-match): 5'-SH-C_6H_{12}-TTT ACC TTT ATT-3', Probe A1 (single-mismatch): 5'-SH-C_6H_{12}-TTT ACG TTT ATT-3', Probe A2 (double-mismatch): 5'-SH-C_6H_{12}-TTT AGG TTT ATT-3' and Probe B: 3'-MB-AAA TGG AAA TAA CC-5'. (B) Square Wave Voltammogram scan data at 12 °C, 26 °C, 36 °C and 54 °C shown for the potential range of -0.4 V to -0.65 V.

As a proof-of-concept demonstration of our microdevice for rapid electrochemical melting studies, a 5'-thiolated probe (designated as Probe A in Fig. 3.16A) was first self-assembled on the gold working electrode and a full-match (FM) complementary probe (designated Probe B), labeled with redox active methylene blue (MB) reporter, was added to form a stable duplex. We increased the temperature in 0.5 V increments using 5 seconds to reach thermal equilibrium, and then 15 seconds to obtain the Square Wave Voltammetry (SWV) scan on the Au electrode for that temperature. SWV was carried out in all studies from -0.2 V to -0.7 V with 0.001 V interval, 60 Hz frequency and 0.025 amplitude. The electron-transfer (eT) between the MB and gold electrode resulted in a 252 nA peak current after a SWV scan at 12 °C. The temperature was increased incrementally and SWV scans were taken after each successive temperature step. As we repeated the procedure, the temperature of the sample in the microchamber was increased incrementally and the current associated with the changing condition decreased monotonically (see Fig. 3.16B, which shows current features at several selected temperatures) from 252 nA (at 12 °C) to 25 nA (at 54 °C), after which no further significant current reduction was observed. This reduction to the final current value is apparently an indication of a sample in which bound duplexes have fully melted. Plotting the peak currents vs. temperature for this experiment led to a T_m (FM) value, determined by differentiation of the melting curve, to be 27.6 °C (see the day1 full-match plot in Fig. 3.17).

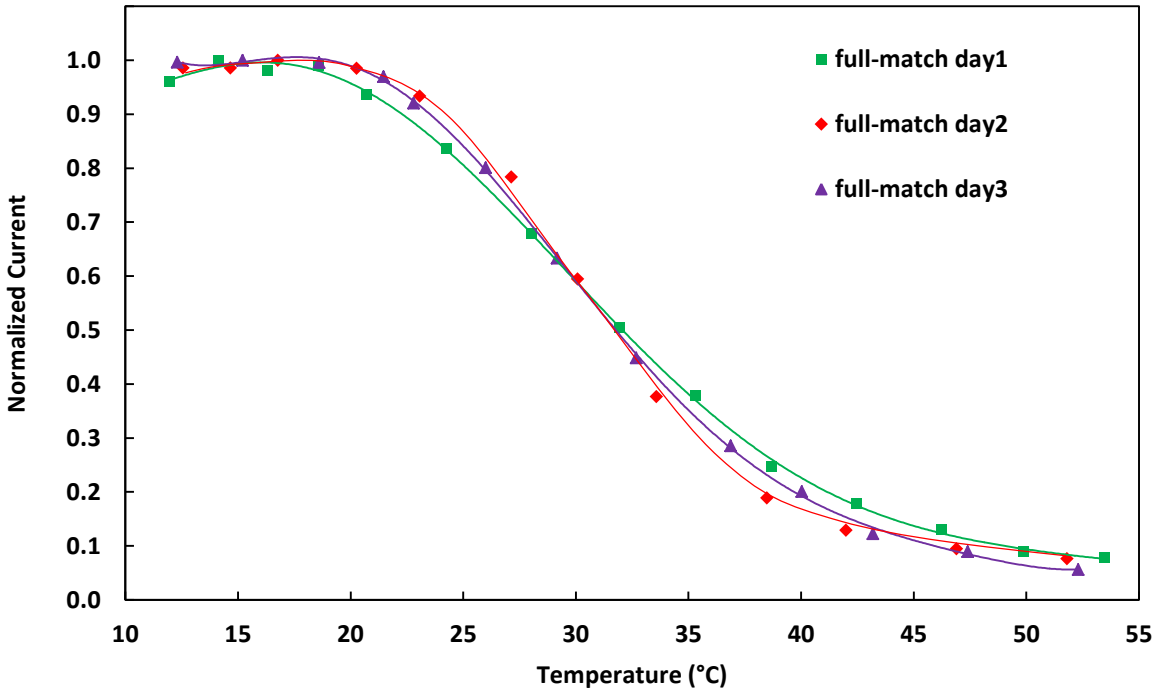

Figure 3.17. Melting curves (normalized) obtained using full-match probes on three different days. The Tm values for the three different melting curves were determined to be T_m (day1) = 27.6 °C, T_m (day2) = 27.1 °C and T_m (day3) = 28.0 °C. The average T_m for these measurements on full-match probes is 27.6 ± 0.4 °C.

In order to test the reproducibility of the device, we repeated the same procedure for the full-match DNA melting curve experiment on two additional days. The significant current decrease seen in all three cases was due to the melting of the duplex. Taking the 1st derivative of the data in each of the three melting curves (see Fig. 3.17) we found a T_m value of 27.6 ± 0.4 °C for the full-match probes, indicating the capability of our device to measure melting with a relatively small variance.

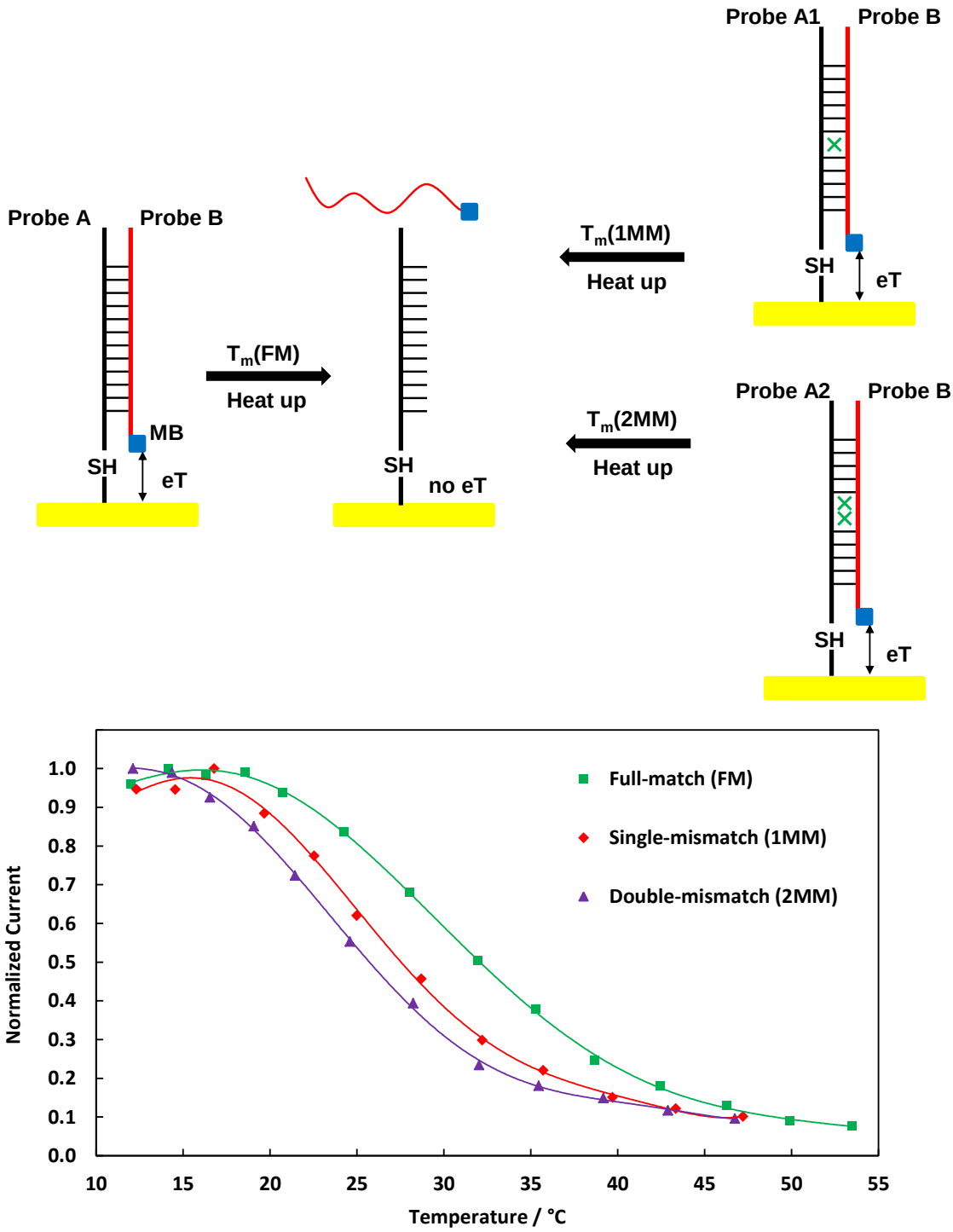

Figure 3.18. Melting curves (normalized) using full-match, single-mismatch and double-mismatch probes. The full-match duplex has a T_m at 27.6 °C, the single-mismatch duplex has a T_m at 22.5 °C and the double-mismatch duplex has a T_m at 20.3 °C.

Having demonstrated the proof-of-concept capability and reproducibility level of the microscale platform for performing melting curve measurements, we performed a related experiment involving a single-mismatch (1MM) Probe A1 with Probe B for SNP detection. This produced an electrochemical melting curve with a T_m (1MM) of 22.5 °C (Fig. 3.18). The value of ΔT_m (1MM) = -5.1 °C for the binding stability comparison between FM and 1MM duplexes is of the proper sign and magnitude for a surface-tethered DNA duplex. We note that this ΔT_m is significantly larger than the 0.4 °C variance we got in the repeated experiments for the full-match probes (mentioned for Fig. 3.17). Furthermore, we also performed a double-mismatch (2MM) Probe A2 melting curve measurement with Probe B. As shown in Fig. 3.18, we obtained a T_m (2MM) of 20.2 °C with a value of ΔT_m (2MM) = -7.3 °C, when compared to the full-match case.

It was discovered over the last 10 years that surface-DNA melting curve analysis would resultin a lower T_m compared to the T_m of solution-phased melting curve analysis using the same experimental conditions. The DNA T_m between solution-phase melting and surface melting had temperature differences of approximate 10 to 12 °C. And T_m comparisons between a planar-surface melting and spherical small particle surface melting had temperature differences around 6 °C [111,112,114-116] Our surface melting full-matched DNA had a 27.6 °C melting temperature value and the theoretical T_m value for this sequence in solution phase was 38.9 °C. (calculated by Integrated DNA Technologies OligoAnalyzer 3.1) The T_m difference of 11.3 °C from our experimental results agreed to the previously reported literature. Although the reason why surface melting has a lower melting temperature comparing to solution phased melting is still not clearly understood. This lower T_m phenomenon may be the result of factors such as surface chemistries and probe densities. If the experimental condition is the same, T_m obtained from planar surfaces has high probe density due to the thiolated self-assembly chemistry. And the

solution phase has the lowest probe density due to the equally distributed probes. The heavily packed probes on the surface may tense the steric and electrostatic interactions between neighboring DNA; thus decreasing the stability of the DNA and accelerating the DNA melting process that results in the lower melting temperature on surface than in solution.

However, such lowered T_m on surface melting is potentially good for DNA and small molecule binding studies. Because the stability of the small molecule bound DNA was increased, and the T_m is much higher if the small molecule binds to the DNA well. Water evaporation can become a critical issue if the melting temperature of the small molecule/DNA complex becomes too high. This may cause water losing during the melting process and change the small molecule and DNA concentration in the solution. Although microfluidic technology can reduce the sample volume, water evaporation could still be a key issue for high-throughput solution phased DNA melting analysis. Nowadays, microfabrication technology can incorporated into DNA surface melting measurements using electrochemical detection to build micro-array systems for high-throughput measurements, these microdevices can not only achieve what has been accomplished by solution phase optical DNA melting applications using microfabrication technology, but also worry less about the water evaporation issue. This can allow DNA melting analyses using electrochemical detection a powerful technique for biomolecular binding studies.

3a.3. Conclusion

In summary, we have designed and constructed a microfabricated platform to perform rapid electrochemical melting curve analyses on biomolecules. The built-in Pt heater in our device allows fast temperature ramping of the low-volume sample cell during melting studies. This newly developed platform can be used to analyze temperature-dependent conformational

changes for biomolecular samples that have been modified with electrochemically active moieties. It is likely this platform could also be used to examine and characterize stability changes induced by the binding of certain small molecules to nucleic acid structures. The advantage of this device architecture, fabricated using lithographic technology, is that it can be extended to produce multi-element arrays to be used with associated microfluidics for high-throughput, parallel measurements on biomolecular interactions and stability.

3a.4. Materials and Methods

Materials and oligonuicleotides

Three types of probes (A, A1, A2) and a complement Probe B (see Fig. 3.16 and Fig. 3.17) were used to demonstrate the characterization capabilities for our microdevice. A full-match (FM) Probe A, a single-mismatch (1MM) Probe A1 and a double-mismatch (2MM) Probe A2, synthesized to our specification were purchased from Integrated DNA Technologies* (Coralville, IA, USA). The methylene blue (MB)-labeled complementary Probe B was synthesized by and purchased from Biosearch Technology* (Novato, CA, USA). The sequences are as follows: Probe A is 5'-SH-(C_6H_{12})-TTT ACC TTT ATT-3'; Probe A1 is 5'-SH-(C6H_{12})-TTT ACG TTT ATT-3'; Probe A2 is 5'-SH-(C_6H_{12})-TTT AGG TTT ATT-3'; Probe B is 3'-(MB)-AAA TGG AAA TAA CC-5'. 6-mercaptohexanol was used for self-assembled monolayer formation and tris-(2-carboxyethyl) phosphine hydrochloride (TCEP) was used for disulfide bond reduction were purchased from Sigma-Aldrich* (St. Louis, MO, USA). All chemical reagents were of analytical grade or higher. Ultrapure water (18.2 MΩ•cm) was used in all preparations.

Fabrication of 1st generation temperature-controlled electrochemical platform

Microfabrication processing used to produce structures like that pictured in Fig. 3.1 and Fig. 3.2 was performed at the National Institute Standards and Technology (NIST) Center for Nanoscale Science and Technology NanoFab Facility. Custom masks were designed in-house for all the required lithographic steps, and the masks were then fabricated at and purchased from the International Phototool Company LLC* (Colorado Spring, CO. USA). Feature sizes for our designed functional components, ranged from 20 to 1000 μm. The first step involved fabricating Pt resistive heater traces on a 100 mm SiO_2 coated silicon wafer with single side polished through a lift-off process using a front side contact aligner (MA8 Suss Microtec*, Sunnyvale, CA, USA) for contact lithography and an e-beam lithograhpy system (VB300 Vistec*, Best, Netherlands). We used S1813 and LOR3A photoresists to coat the wafer. The Pt heater pattern was created by exposing the wafer under UV light using the MA8 and followed by MF319 development. An e-beam was used next to deposit a 20 nm titanium (Ti) adhesion layer and then the 200 nm Pt heater layer through a life-off process. The 320 nm SiO_2 insulating layer was formed using plasma-enhanced chemical vapor deposition (PECVD Unaxis 790 Plasmatherm*, Saint Petersburg, FL, USA). The Au electrodes (20 nm Ti layer and 300 nm Au layer) and Pt electrodes (20 nm Ti layer and 300 nm Pt layer) were fabricated on the SiO2 insulating layer using the similar lithographic steps to those for fabricating the Pt heater (described above). The heater metal contact pattern was created by exposing S1813 coated wafer under UV light using the MA8 followed by MF319 development. Then a reactive ion etching system (RIE Unaxis 790 Plasmatherm*, Saint Petersburg, FL, USA) was employed to create the heater metal contact.

Fabrication of 2nd generation temperature-controlled electrochemical platform

Microfabrication processing used to produce structures like that pictured in Fig. 3.7 and Fig. 3.8 was performed at the National Institute Standards and Technology (NIST) Center for Nanoscale Science and Technology NanoFab Facility. Custom masks were designed in-house for all the required lithographic steps, and the masks were then fabricated at and purchased from the International Phototool Company LLC* (Colorado Spring, CO. USA). Feature sizes for our designed functional components, ranged from 10 to 50 μm. The first step involved fabricating Pt resistive heater traces on a 100 mm glass (borosilicate) wafer with single side polished through a lift-off process using a front side contact aligner (MA8 Suss Microtec*, Sunnyvale, CA, USA) for contact lithography and an e-beam lithograhpy system (VB300 Vistec*, Best, Netherlands). We used S1813 and LOR3A photoresists to coat the wafer. The Pt heater pattern was created by exposing the wafer under UV light using the MA8 and followed by MF319 development. An e-beam was used next to deposit a 20 nm titanium (Ti) adhesion layer and then the 200 nm Pt heater layer through a life-off process. The 320 nm SiO_2 insulating layer was formed using plasma-enhanced chemical vapor deposition (PECVD Unaxis 790 Plasmatherm*, Saint Petersburg, FL, USA). The Au electrodes (20 nm Ti layer and 300 nm Au layer) and Pt electrodes (20 nm Ti layer and 300 nm Pt layer) were fabricated on the SiO2 insulating layer using the similar lithographic steps to those for fabricating the Pt heater (described above). The heater metal contact pattern was created by exposing S1813 coated wafer under UV light using the MA8 followed by MF319 development. Then a reactive ion etching system (RIE Unaxis 790 Plasmatherm*, Saint Petersburg, FL, USA) was employed to create the heater metal contact. The 10 μL poly(dimethylsiloxane) (PDMS) (Sylgard 184 kit Dow Corning Corporation*, USA) chamber incorporated to hold liquid samples above the electrodes was formed using a 10:1 base-to-crosslinker ratio, and then cutting a 2 mm diameter hole using a metal punch to introduce a

cylindrical chamber. The PDMS chamber was adhered to the SiO_2 insulating layer and centered on the Pt heater, three-electrode system. Analytes were introduced into the chamber using a 10 µL pipette. Finally the cylindrical chamber was closed by adding a PDMS lid before experiments were begun.

Electrochemical measurements (SWV) using the 2nd generation platform

The Au electrodes were cleaned before DNA self-assembly using a procedure that began by incubating the Au electrode with 50 mmol/L H_2SO_4. Then twenty cycles of cyclic voltammetry were run from 1.0 V to -0.1 V with a sample interval of 0.001 V. After the cleaning, 1 µL of 200 µmol/L Probe ZJP (5'-SH-C_6H_{12}-TTT TCC ACC GCC AAT ATT TTT GAT CTG TGG MB-3') was mixed with 2 µL of 10 mmol/L TCEP at room temperature in the dark for 45 minutes. The solution was then diluted to a concentration of 2 µmol/L with 100 µL PBS buffer (10 mmol/L phosphate-buffered saline pH 7.4 with 1 mol/L NaCl and 1 mmol/L Mg^{2+}). The Au electrode was incubated with 2 µmol/L Probe ZJP in 10 µL PBS for 30 mins in the dark. After rinsing with deionized water, followed by drying with a nitrogen gun, the electrodes were incubated in 200 mmol/L 6-mercaptohexanol solution (10 µL) for 1 hour at room temperature, in the dark. The electrode was rinsed for 1 minute using deionized water to remove any remaining 6-mercaptohexanol solution. The electrode was again dried using a nitrogen gun. The PDMS cell was filled with PBS buffer (10 µL) before SWV measurement start.

All SWV measurements were performed with a CHI 660 electrochemical workstation (CH Instrument, Inc,). SWV was carried out in the 10 mM PBS (pH 7.4) from -0.2 V to -0.7 V with 0.001 V interval, 60 Hz frequency and 0.025 amplitude.

Fabrication of temperature-controlled electrochemical microscale platform

In this microscale platform, the trace width of the Pt heaters were 40 and 50 μm, with one trace separation of 20 μm. Custom masks were designed in-house for all the required lithographic steps, and the masks were then fabricated at and purchased from the International Phototool Company LLC* (Colorado Spring, CO. USA). Feature sizes for our designed functional components, ranged from 10 to 50 μm. The first step involved fabricating Pt resistive heater traces on a 100 mm glass (borosilicate) wafer with single side polished through a lift-off process using a front side contact aligner (MA8 Suss Microtec*, Sunnyvale, CA, USA) for contact lithography and an e-beam lithograhpy system (VB300 Vistec*, Best, Netherlands). We used S1813 and LOR3A photoresists to coat the wafer. The Pt heater pattern was created by exposing the wafer under UV light using the MA8 and followed by MF319 development. An e-beam was used next to deposit a 20 nm titanium (Ti) adhesion layer and then the 200 nm Pt heater layer through a life-off process. The 320 nm SiO_2 insulating layer was formed using plasma-enhanced chemical vapor deposition (PECVD Unaxis 790 Plasmatherm*, Saint Petersburg, FL, USA). The Au electrodes (20 nm Ti layer and 300 nm Au layer) and Pt electrodes (20 nm Ti layer and 300 nm Pt layer) were fabricated on the SiO2 insulating layer using the similar lithographic steps to those for fabricating the Pt heater (described above). The heater metal contact pattern was created by exposing S1813 coated wafer under UV light using the MA8 followed by MF319 development. Then a reactive ion etching system (RIE Unaxis 790 Plasmatherm*, Saint Petersburg, FL, USA) was employed to create the heater metal contact. The 10 μL poly(dimethylsiloxane) (PDMS) (Sylgard 184 kit Dow Corning Corporation*, USA) chamber incorporated to hold liquid samples above the electrodes was formed using a 10:1 base-to-crosslinker ratio, and then cutting a 2 mm diameter hole using a metal punch to introduce a

cylindrical chamber. The PDMS chamber was adhered to the SiO_2 insulating layer and centered on the Pt heater, three-electrode system. Analytes were introduced into the chamber using a 10 µL pipette. Finally the cylindrical chamber was closed by adding a PDMS lid before experiments were begun.

Electrode cleaning and preparation of probes on microscale platform

The Au electrodes were cleaned before DNA self-assembly using a procedure that began by incubating the Au electrode with 50 mmol/L H_2SO_4. Then twenty cycles of cyclic voltammetry were run from 1.0 V to -0.1 V with a sample interval of 0.001 V. After the cleaning, 1 µL of 200 µmol/L Probe A was mixed with 2 µL of 10 mmol/L TCEP at room temperature in the dark for 45 minutes. The solution was then diluted to a concentration of 2 µmol/L with 100 µL PBS buffer (10 mmol/L phosphate-buffered saline pH 7.4 with 1 mol/L NaCl and 1 mmol/L Mg^{2+}). The Au electrode was incubated with 2 µmol/L Probe A in 10 µL PBS for 30 mins in the dark. After rinsing with deionized water, followed by drying with a nitrogen gun, the electrodes were incubated in 2 mmol/L 6-mercaptohexanol solution (10 µL) for 1 hour at room temperature, in the dark. The electrode was rinsed for 1 minute using deionized water to remove any remaining 6-mercaptohexanol solution. The electrode was again dried using a nitrogen gun. A similar preparation was used for molecular attachment in the experiments done with Probe A1 and A2. In each case, to allow hybridization interactions, the PDMS cell was filled with PBS buffer (10 µL) containing 2 µmol/L Probe B and left to stand for 30 mins in an insulated box held at 4 °C to allow for hybridization with the Probe B, after which the electrochemical melting curve measurements were taken.

Melting curve measurement procedures using the electrochemical microscale platform

All electrochemical measurements were performed with an electrochemical workstation (CHI660 BZ962 CH Instrument Inc*, Austin, TX, USA). During these measurements, sample temperature was controlled and monitored (as discussed below) using a source meter (B2962 Aglient Technologies*, CA, USA). The three electrodes and Pt heater were connected to the potentiostat and source meter, respectively. The temperature was increased incrementally with selected steps, we used 5 seconds to reach thermal equilibrium, and then 15 seconds to obtain the Square Wave Voltammetry (SWV) scan on the Au electrode for that temperature. SWV was carried out in all studies from -0.2 V to -0.7 V with 0.001 V interval, 60 Hz frequency and 0.025 amplitude. The sequence was repeated until the end of the melting curve measurements.

3b. Introduction to Studies on the Binding of Ligands at G-quadruplexes

3b.1. Introduction

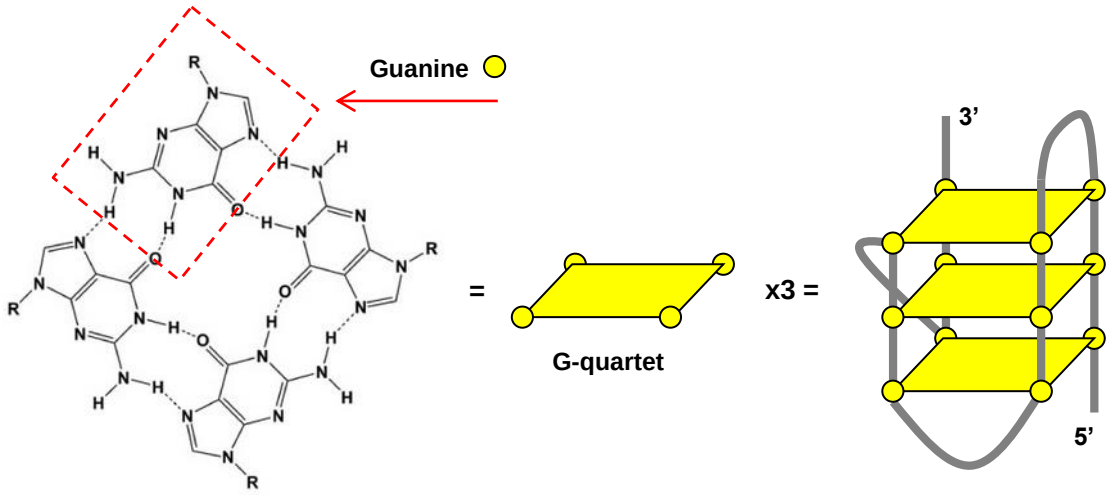

Figure 3.19. Structure of G-quadruplex.

The first defined anti-cancer drug target was DNA and this started the anti-cancer drug discovery research field that has been active during the past 20 years. G-quadruplexes are four-stranded DNA structures (shown in Fig 3.19) and can be formed at the ends of human chromosomes (called human telomeres). In humans, the telomere sequence is made up of repeats of TTAGGG at the 3' end of human chromosomes (in Fig. 3.20).[117] The telomere sequence is maintained by an enzyme called telomerase. In most cancer cells telomerase is over expressed and acts to prevent the natural shortening of the telomere.[118] The inhibition of telomerase by using small molecules to induce the 3' end of telomeric DNA to fold up into higher order G-quadruplexes structures can prevent the enzyme telomerase from extending the ends of chromosomes.[119] Many small molecules that bind to and stabilize G-quadruplexes have been

shown to inhibit cancer cells.[120] Telomestatin is an example of a small molecule that has been shown to have a high G-quadruplex affinity and also inhibit the actions of telomerase.[121]

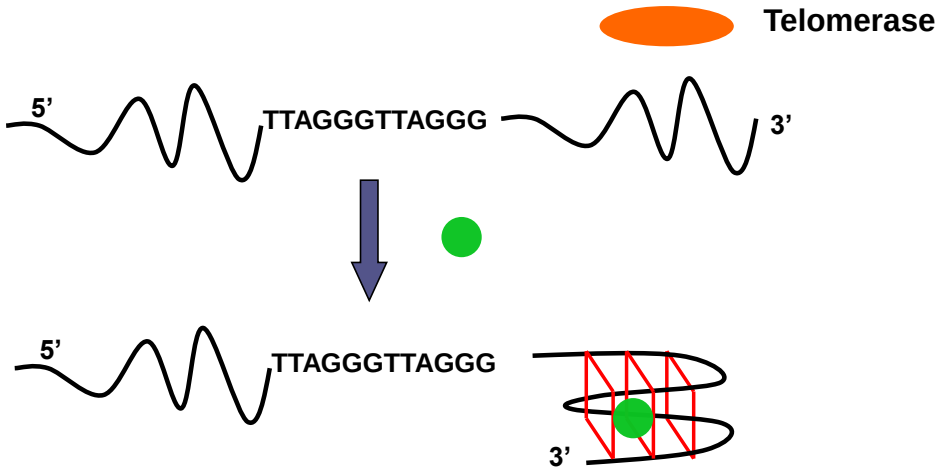

Figure 3.20. G-quadruplex stabilized agent binds to form a stable G-quadruplex structure at the end of 3' chromosome and this prevents telomerase from binding to the DNA.

Telomestatin has also been demonstrated to bind to G-rich sequences that are found near promoter regions.[122] These G-rich sequences are commonly found near some proto-oncogenes (such as MYC), and single-stranded DNA binding proteins, such as CNBP and hnRNBK, also bind near these sequences. Therefore it is expected that small molecules that could stabilize G-quadruplexes would also form stable quadruplex structures near the transcription start sites of proto-oncogenes, and hence prevent the binding of transcription factors and accessory proteins, such as CNBP and hnRNBK, thereby preventing the transcription of these cancer-promoting genes (see Fig. 3.21)[123,124]

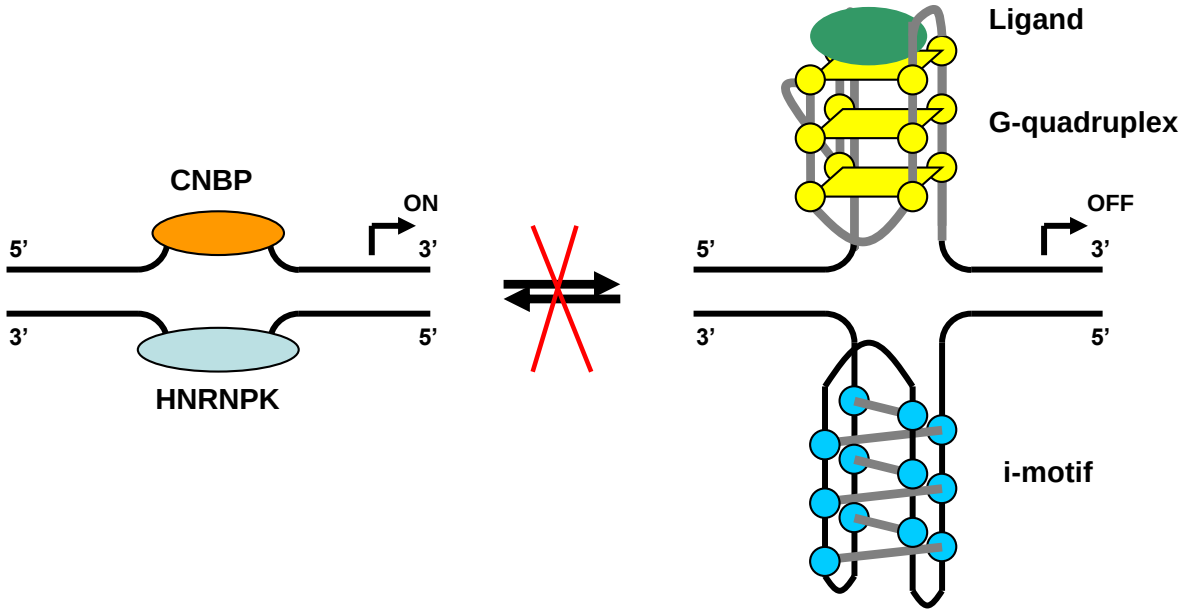

Figure 3.21. G-quadruplex ligand stabilized G-quadruplex structure in MYC promoter regions. This insures the silencing of the gene expression in this promoter site.

The importance of the G-quadruplex structure in chromosome maintenance as well as transcription regulation has spurred interest in finding new G-quadruplex stabilizing ligands as well as characterizing the interactions of known G-quadruplex ligands to the myriads of G-quadruplex structures found in humans. As we discussed in 3a.1, optical melting analysis is the traditional method for studying DNA binding by analyzing the shifts in melting temperatures as ligands bind to DNA. However, good melting curves, and hence good melting temperatures, can sometimes become difficult to achieve due to the competition between the ligand and the required chromophore. Additionally, it is challenging and costly to scale down these optical melting platforms to high-throughput systems.

Researchers have also begun examining other methods for detecting biomolecular conformational changes when these molecules are heated. These electrochemical measurements include the use of DNA-intercalator redox moiety. For analysis using nucleic acids, electrochemical faradic current can be measured by using electrochemical active molecules, which bind to double-stranded DNA. During the heating process, the double stranded DNA unfolds and the electroactive ligand dissociates from the DNA. As the single-stranded DNA that is left on the electrode does not contain the electrochemically active molecule anymore, the electrochemical signal is lost when the DNA unfolds.[109] There is considerable interest in designing new strategies to study the binding of small molecules to DNA. Xiao et.al developed an electrochemical detection of thrombin in blood serum using methylene blue (MB) labeled G-quadruplex based sensors.[25] In this thesis work, we have designed a new platform to achieve G-quadruplex/ligand melting curve analysis capability using electrochemical detection. As shown in Fig. 3.22, the G-quadruplex strand is labelled by redox MB and self-assembled on a gold electrode by a thiolated group. Without the binding of the small molecule ligand, the enhancement of the MB signal after melting analysis can establish a lower melting temperature, T_1. Upon ligand binding, a higher melting temperature, T_2, may result from the melting curve analysis of the G-quadruplex/ligand.

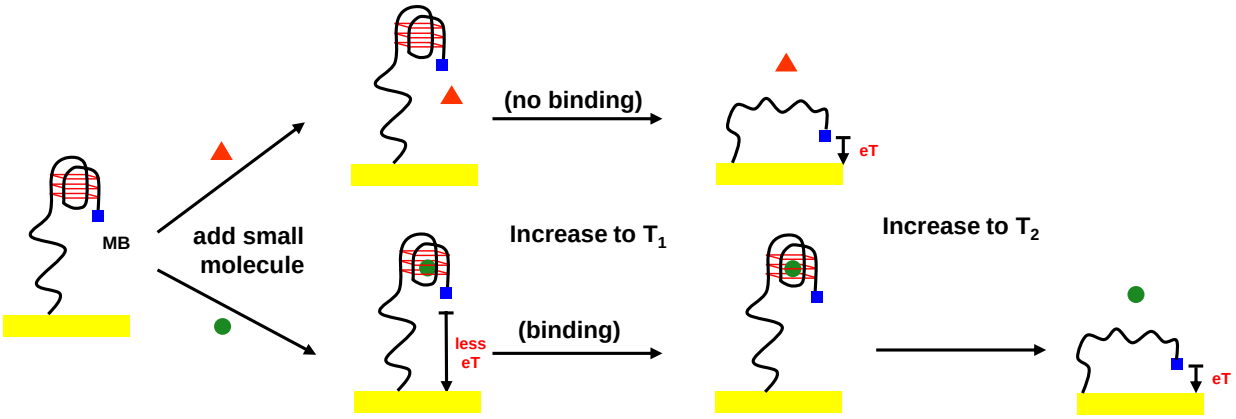

Figure 3.22. One strategy of G-quadruplex/ligand melting curve analysis using electrochemical detection of small molecule induced changes of stability.

3b.2. Preliminary Results and Discussion

The temperature-controlled electrochemical microscale platform (described in section 3a) was used for G-quadruplex/ligand-binding melting curve analysis. Fig. 3.23 shows our experimental setup for G-quadruplex $(TTAGGG)_4$ ligand stabilization using the strategy described in Fig. 3.22. SYUIQ-5 was picked as the binding ligand to stabilize the self-assembled G-quadruplex structure on the gold electrode. When SYUIQ-5 stabilized G-quadruplex through intercalation, the melting temperature of the stabilized G-quadruplex/SYUIQ-5 complex increased above the melting temperature of the G-quadruplex alone (control experiment). Collection of the melting curve is possible due to the enhancement of the redox MB signal on the G-quadruplex. The initial relative inhibition of the eT was due to the large distance between MB and the gold electrode surface at lower temperature. After the temperature was increased to reach the melting temperature for these structures, the eT was enhanced due to the melted single-stranded G-quadruplex sequence transforming to a lying down orientation on the gold electrode

surface. These varying electrochemical signals collected at different temperatures allow construction of the melting curve.

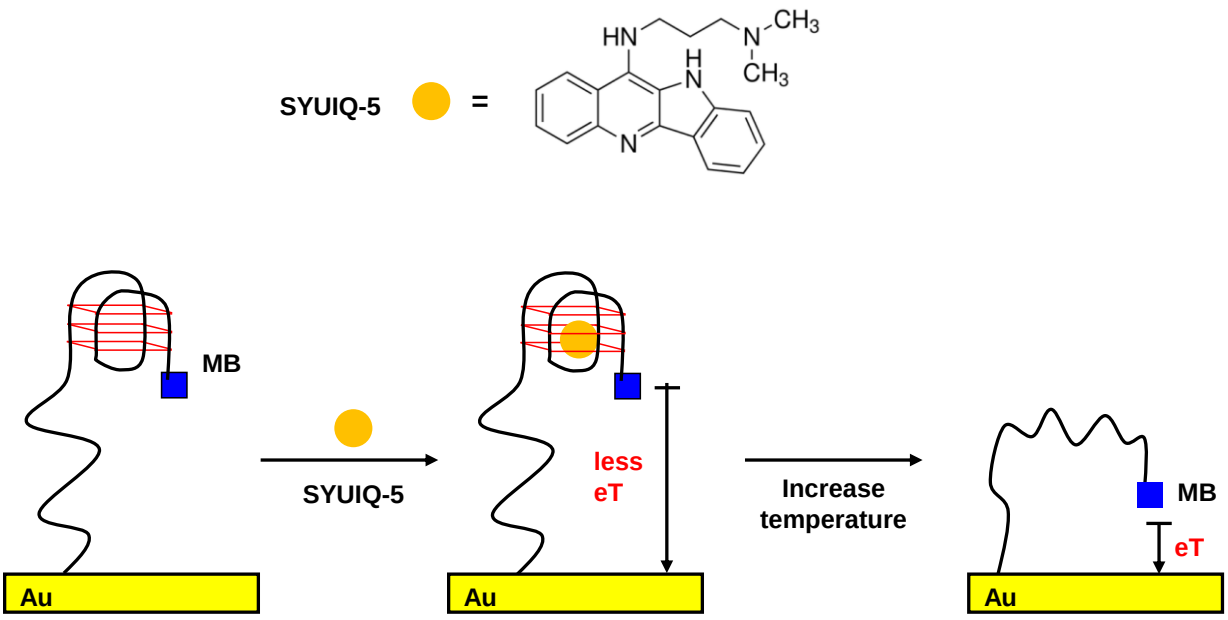

Figure 3.23. Schematic diagram of SYUIQ-5 as a G-quadruplex $(TTAGGG)_4$ binding ligand. The lower schematic shows the concept for for melting curve analysis using electrochemical detection to study ligand-induced stabilization.

A 5'-thiolated and 3' MB-labeled G-quadruplex strand (in Fig. 3.23) was first self-assembled on the gold working electrode; SYUIQ-5 was then added to stabilize the G-quadruplex structure. We started experimental measurements by increasing a selected temperature step, waited for 5 seconds to reach temperature equilibrium, and then took the SWV scan for 15 seconds. As we repeated the procedures, the temperature of the sample in the microchamber was increased incrementally from 30 °C to 62 °C and the current associated with the changing condition increased as shown in Fig. 3.24. A melting curve of G-quadruplex/SYUIQ-5 complex is plotted in blue, and a T_m value, determined by differentiation of

the melting curve, was found to be 52.1 °C. We also did a control experiment of melting electrode bound G-quadruplex without a stabilizing ligand present, which produced the orange melting curve shown in Fig. 3.24. We found a T_m value, determined by differentiation of the melting curve, to be 36.8 °C. By comparing the two melting temperature with and without the ligand SYUIQ-5 presenting, we obtained a value of ΔT_m of 15.3 °C. This indicates that the ligand can significantly increase stability for the telomere G-quadruplex $(TTAGGG)_4$.

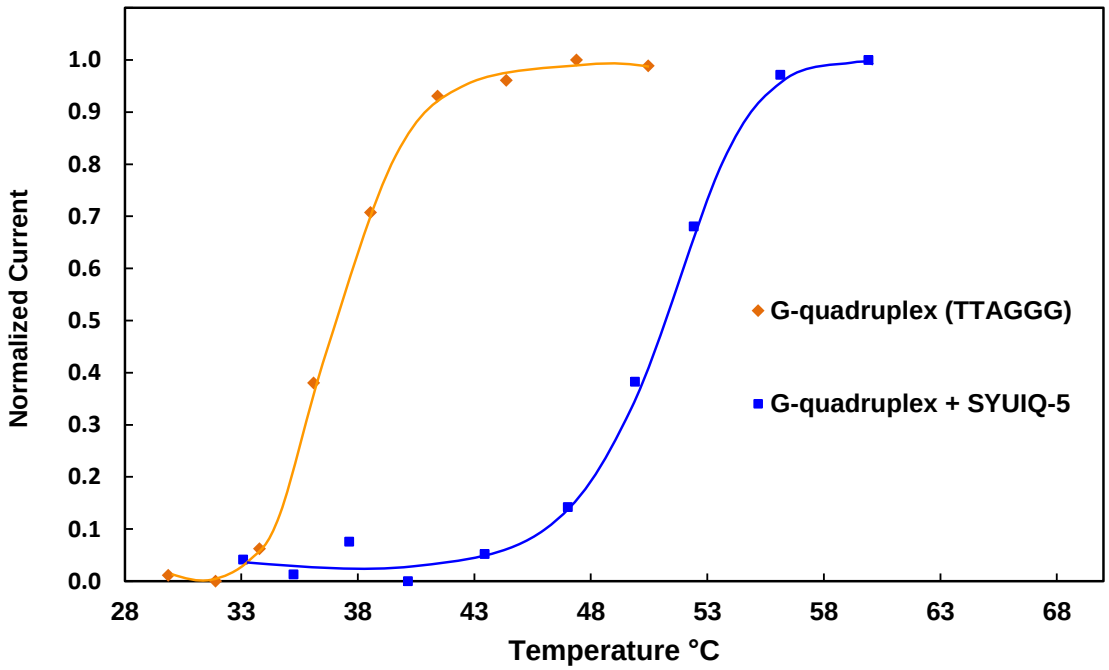

Figure 3.24. Melting curves (nomalized) using G-quadruplex $(TTAGGG)_4$ only in orange and G-quadruplex/SYUIQ-5 in blue. T_m (orange) = 36.8 °C, and T_m (blue) = 52.1 °C.

We also repeated the same procedure of the G-quadruplex and G-quadruplex/SYUIQ-5 melting curve experiment on two additional days. The significant current increase seen in all three cases was due to the melting of the G-quadruplex. Taking the 1st derivative of the data in

each of the three melting curves (see Fig. 3.25) we found a T_m value of 37.4 ± 0.9 °C for G-quadruplex, and a T_m value of 51.6 ± 0.5 °C for G-quadruplex/SYUIQ-5, indicating the capability of our device to measure melting with a relatively small variance.

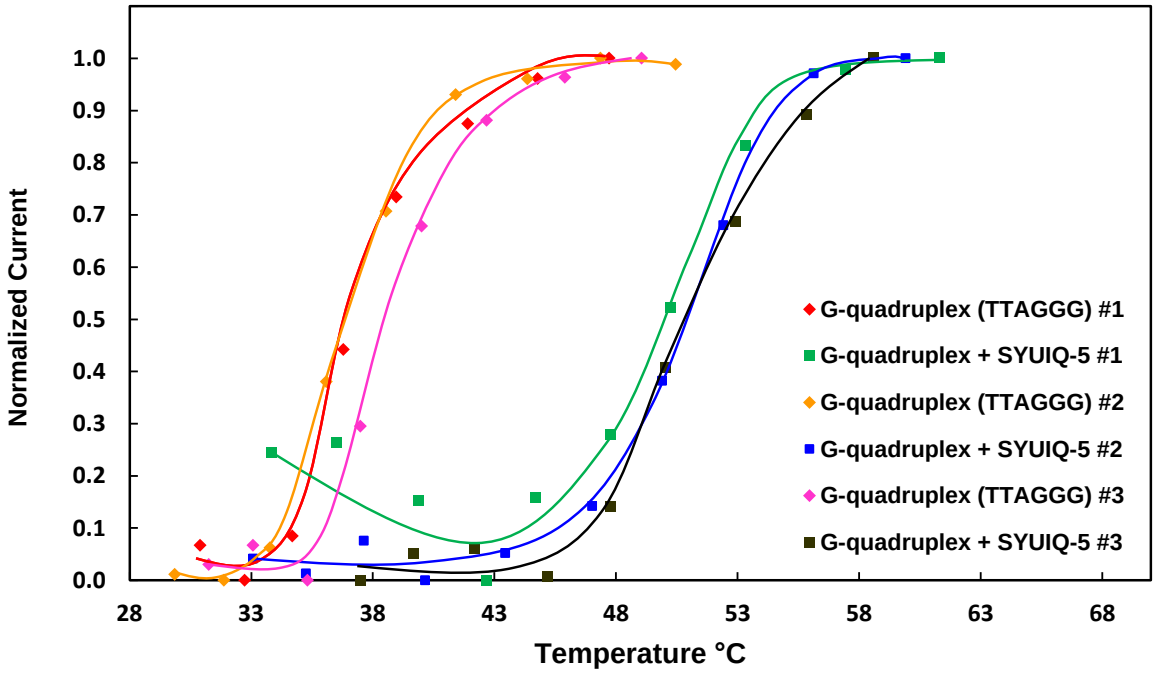

Figure 3.25. Melting curves (nomalized) of G-quadruplex $(TTAGGG)_4$ only, and G-quadruplex/SYUIQ-5, on three different days. The average T_m for G-quadruplex only is 37.4 ± 0.9 °C, and the average T_m for G-quadruplex/SYUIQ-5 is 51.6 ± 0.5 °C. (T_m (orange) = 36.8 °C, T_m (red) = 37.1 °C, T_m (pink) = 38.4 °C, T_m (blue) = 52.1 °C, T_m (green) = 51.2 °C, T_m (black) = 51.6 °C)

3b.3. Conclusion and Future Plan

These preliminary results show the capability of our temperature-controlled electrochemical microscale device to characterize interactional effects between G-quadruplex structure and

binding ligands. The melting curve analysis using electrochemical detection can determine the ΔT_m of the G-quadruplex after a stabilizing ligand binds. Future experiments are planned to demonstrate the melting temperature shifts that arise for different concentrations of the ligand. Also other commercial and lab-made G-quadruplex ligands will also be tested to find their effect on G-quadruplex melting temperatures. We have also proposed another strategy of using split G-quadruplex to achieve a signal-off melting curve analysis and this may become another useful approach.

3b.4. Materials and Methods

Materials and oligonuicleotides

The G-quadruplex stabilizing ligand SYUIQ-5 was purchased purchased from Sigma-Aldrich* (St. Louis, MO, USA). The 5'-thiolated and 3'-MB-labeled G-quadruplex was synthesized by and purchased from Biosearch Technology* (Novato, CA, USA). The sequences are as follows: 5'-SH-(C_6H_{12})-(TTA GGG)$_4$-MB-3'. 6-mercaptohexanol was used for self-assembled monolayer formation and tris-(2-carboxyethyl) phosphine hydrochloride (TCEP) was used for disulfide bond reduction were purchased from Sigma-Aldrich* (St. Louis, MO, USA). All chemical reagents were of analytical grade or higher. Ultrapure water (18.2 MΩ•cm) was used in all preparations.

Electrode cleaning and preparation of probes on microscale platform

The Au electrodes were cleaned before DNA self-assembly using a procedure that began by incubating the Au electrode with 50 mmol/L H_2SO_4. Then twenty cycles of cyclic voltammetry

were run from 1.0 V to -0.1 V with a sample interval of 0.001 V. After the cleaning, 1 µL of 200 µmol/L 5'-thiolated and 3'-MB-labeled G-quadruplex was mixed with 2 µL of 10 mmol/L TCEP at room temperature in the dark for 45 minutes. The solution was then diluted to a concentration of 2 µmol/L with 100 µL PBS buffer (10 mmol/L phosphate-buffered saline pH 7.4 with 1 mol/L NaCl and 1 mmol/L Mg^{2+}). The Au electrode was incubated with 2 µmol/L 5'-thiolated and 3'-MB-labeled G-quadruplex in 10 µL PBS for 30 mins in the dark. After rinsing with deionized water, followed by drying with a nitrogen gun, the electrodes were incubated in 2 mmol/L 6-mercaptohexanol solution (10 µL) for 1 hour at room temperature, in the dark. The electrode was rinsed for 1 minute using deionized water to remove any remaining 6-mercaptohexanol solution. The electrode was again dried using a nitrogen gun. The PDMS cell was filled with PBS buffer (10 µL) containing 2 µmol/L SYUIQ-5 and left to stand for 15 mins to allow G-quadruplex intercalation, after which the electrochemical melting curve measurements were taken.

Melting curve measurement procedures using the electrochemical microscale platform

All electrochemical measurements were performed with an electrochemical workstation (CHI660 BZ962 CH Instrument Inc*, Austin, TX, USA). During these measurements, sample temperature was controlled and monitored (as discussed below) using a source meter (B2962 Aglient Technologies*, CA, USA). The three electrodes and Pt heater were connected to the potentiostat and source meter, respectively. The temperature was increased incrementally with selected steps, we used 5 seconds to reach thermal equilibrium, and then 15 seconds to obtain the Square Wave Voltammetry (SWV) scan on the Au electrode for that temperature. SWV was carried out in all studies from -0.2 V to -0.7 V with 0.001 V interval, 60 Hz frequency and 0.025 amplitude. The sequence was repeated until the end of the melting curve measurements.

IV. Chapter 4: Summary and Future Outlook.

4.1. Summary

This thesis has discussed work to develop electrochemical junction probes detection of nucleic acids and rapid DNA melting analyses using a microfabricated electrochemical microscale platform related to detection of bioanalyte binding characteristics. Biomolecular binding studies represent a very important research area. Temperature is always a key parameter in these studies.

The work of signal-off and signal-on electrochemical junction probes detection used an isothermal amplification strategy to maintain the temperature for restriction endonucleases reaching their optimal rate of cleavage, so that the limited target concentration could be recycled into the cleavage reactions again and again to amplify the electrochemical signal. The work proved that the sensitivity of junction probe detection methods could be applied in SNP detection. Although the limit of detection isn't ideal for practical applications, improvements can be realized by screening more restriction endonucleases to find candidates for immobilized probes on the electrodes to increase the rate of cleavage and limit of detection.

A microfabricated, temperature-controlled electrochemical platform was developed and demonstrated as an alternative way to traditional optical detection methods for melting temperature studies. Temperature was controlled by microheater during the electrochemical detection and the electrochemical scans at different temperature were recorded. We looked into the nucleic acids binding studies and managed to determine the melting temperatures of nucleic acids using electrochemical detection methods in a relative short time period (less than 20 minutes).

We believe our research opens a new direction of biomolecular study research area. The simplicity, fabrication cost, inherent speed and robustness of the platform and measurements offer opportunities to build temperature-controlled microscale array-based high-throughput electrochemical systems with localized temperature control. These systems can potentially have big impacts in biomedical research and drug discovery.

4.2. Future Outlook

As mentioned above, the temperature-controlled electrochemical microscale platform has great potential for further development into array-based high-throughput systems for biomolecular binding screening. We have finished modifying our latest design (discussed in 3a.2.3) into 2x2, 4x1 and 4x2 array-based platform (see Fig. 4.1) in order to demonstrate parallel screening. The Pt-heaters in this version have a 50 μm trace width and 20 μm trace separation, as previous results showed this is to be the best combination for the Pt heaters. All the measurements to be done using this microscale platform will have same design parameter, allowing common experimental conditions to test the consistency between each individual devices. We can try to demonstrate 2x2 or 4x1 parallel measurements on this platform using a commercial, multi-channels potentiostat. Microfluidic PDMS channel delivery of samples would provide an ideal approach for array-based platforms to enable high-throughput screening.

Using microfluidic channels would allow one to work on lowering the microwell sample volume. The current volume is 10 μL, and microfluidic sample delivery structure may enable 1 μL or even lower volume (100 nL) in a completely sealed fluidic channel. If we are able to conduct melting curve analysis with such smaller volumes, this will further reduce the overall analyte volume, and reduce the cost for expensive samples. And it is possible to finish the

melting experiment in a much shorter time period since the lowered sample volume can be heated more quickly. Such efficiency is very important in the biomolecular screening in biomedical research and drug discovery fields.

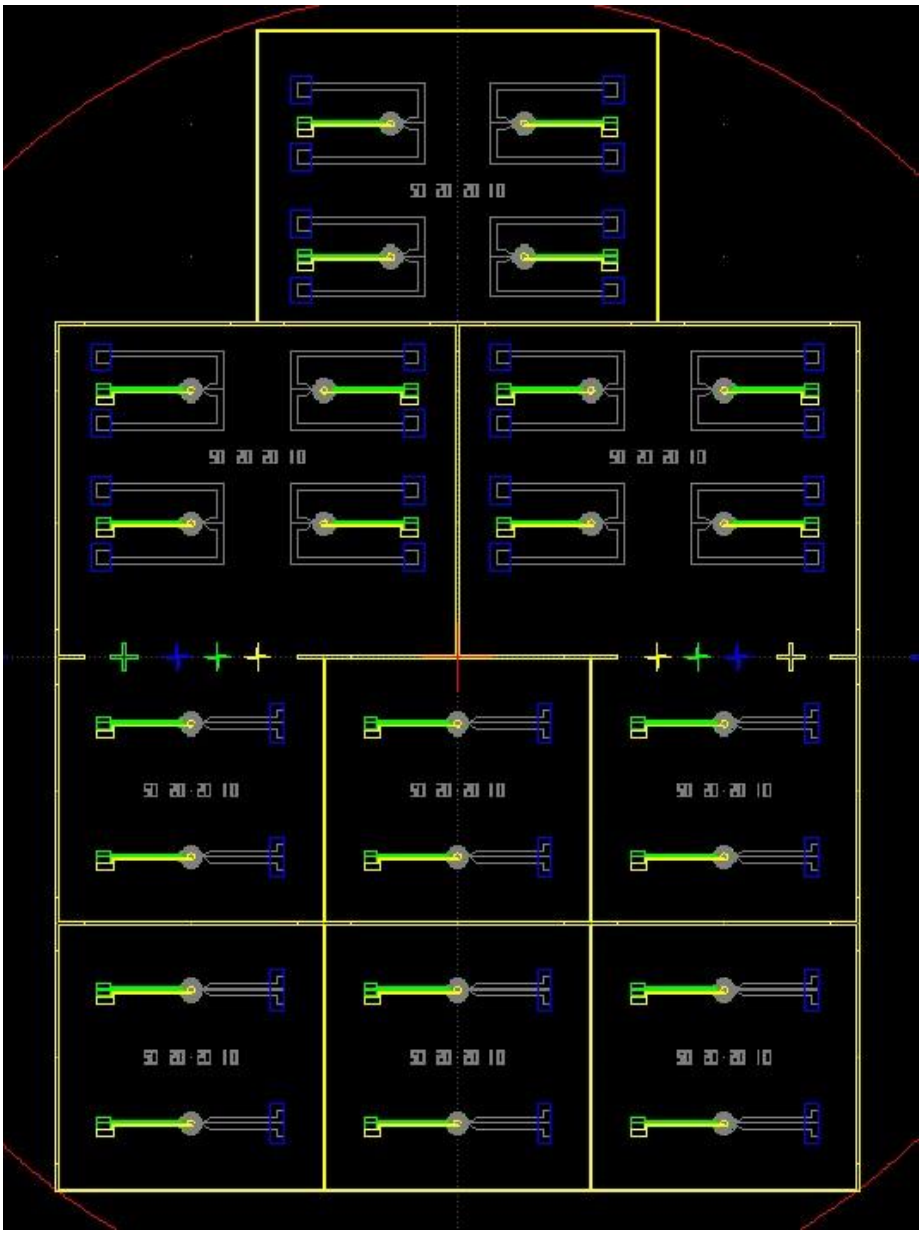

Figure 4.1. Newly designed 2x2, 4x1 and 4x2 array-based platform.

These advantages of the temperature-controlled electrochemical microscale platform technology can be very valuable in creating future analytical systems. Building smaller robust portable array-based microscale devices for different applications not only saves cost but also time. Plans have been made to build a 3x3 array-based temperature-controlled electrochemical automated system as a demonstration device for engineered commercialization (see Fig. 4.2). The system could consists of individually-controlled and powered heating source, three individual home-made micro potentiostats, a 3x3 array-based temperature-controlled electrochemical microchip mounted with microfluidic delivery system, and a micro-controller to be programmed to control the whole automated system on a motherboard

Such a system could be designed and fabricated to demonstrate automated parallel biomolecular melting curve analyses. With all the technology available including that demonstrated in this thesis work, the system shouldn't be too much of a challenge to assemble. Perhaps the most challenging part, the portable potentiostat, has already been addressed by Nemiroski et. al with their recent publication in early 2014.[125] The 3x3 microchip will be designed using on all best parameters according my previous versions built with low cost using microfabrication technology. The instrumentation components on the motherboard aren't consumable and can be made much simpler at relatively low cost compared to expensive instruments in the laboratory. The consumable low-cost microchip component can be disposable (one-time use) or it can be cleaned by special cleaning procedures for reuse.

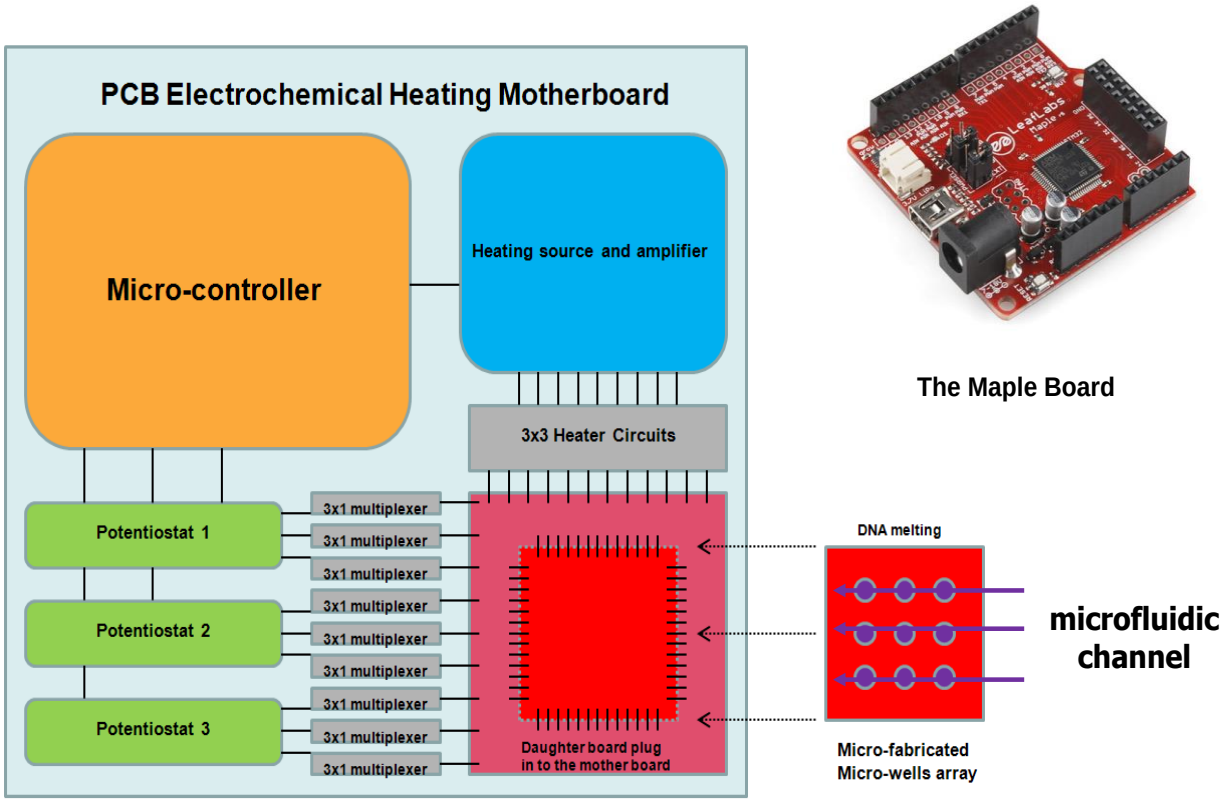

Figure 4.2. Scehmatic diagram for a PCB based 3x3 temperature-controlled electrochemical array platform.

Scale up to bigger array systems could occur after demonstrating the 3x3 automated microchip system. In Fig. 4.3, a 5x10, fifty-elements array system is proposed by using our temperature-controlled electrochemical microscale platform design. We can build a 5x10 motherboard with a micro-controller to program all the heating sources and individual potentiostats to do automated high-throughput biomolecular screening.

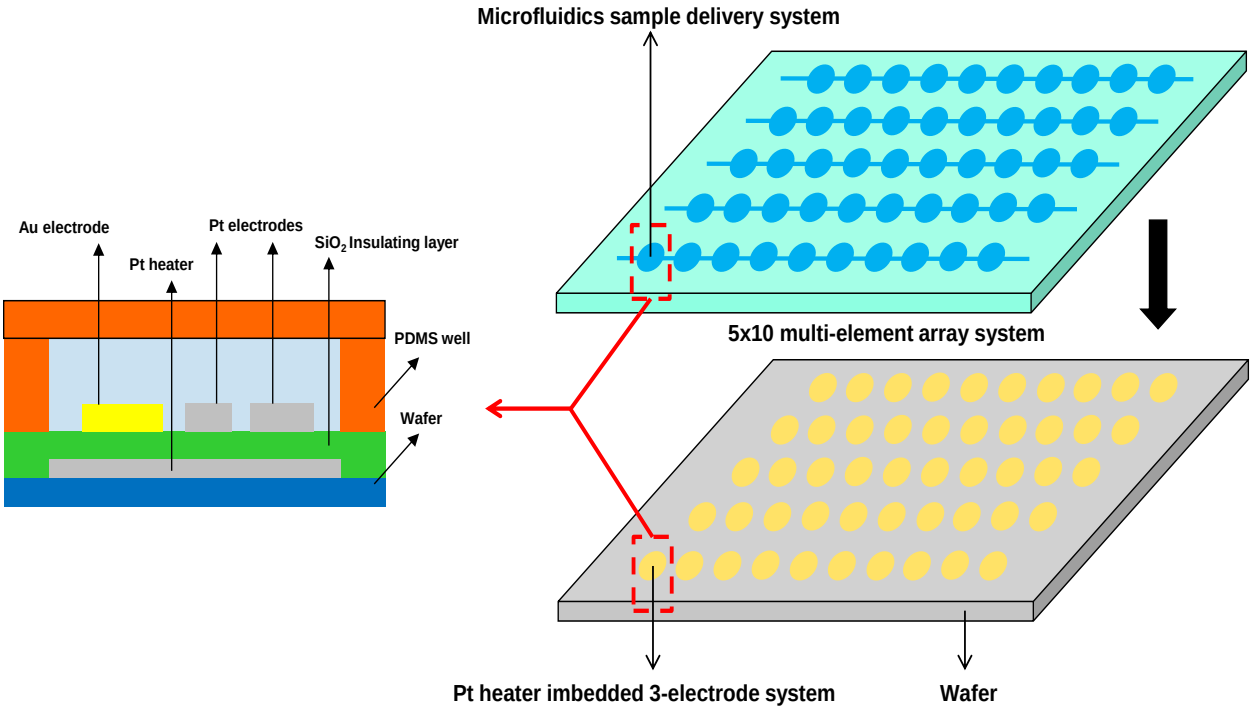

Figure 4.3. Schematic representation of a 5x10 muti-element array system with 50 identical single temperature-controlled electrochemical elements.

Our temperature-controlled electrochemical automated high-throughput system provides time saving, less labor, lower sample volume and low fabrication costs. These advantages will allow our system to have a big impact in drug discovery applications and biomolecular research.

References

1. Ronkainen, N. J.; Halsall, H. B.; Heineman, W. R. *Chem. Soc. Rev.* **2010**, 39, 1747-1763.
2. Ronkainen, N. J.; Thomas, J. H.; Halsall, H. B.; Heineman, W. R. *TrAC, Trends Anal. Chem.* **2002**, 21(4), 213.
3. Grieshaber, D.; MacKenzie, R.; Voros, J.; Reimhult, E. Sensors 2008, 8, 1400.
4. Wijayawardhana, C. A.; Halsall, H. B.; Heineman, W. R. *Electroanalytical Methods of Biological Materials*, ed. A. Brajter-Toth, J. Q. Chambers, Marcel Dekker, New York, **2002**, 329–365.
5. Yao, H.; Jenkins, S. H.; Pesce, A. J.; Halsall, H. B.; Heineman, W. R. *Clin. Chem. (Washington, D. C.)*, **1993**, 39, 1432.
6. *Laboratory Techniques in Electroanalytical Chemistry*, ed. P. T. Kissinger and W. R. Heineman, Marcel Dekker Inc, New York, NY, USA, **1996**.
7. *Bioelectrochemistry Fundamentals, Experimental Techniques and Applications,* ed. P. N. Bartlett, John Wiley & Sons, West Sussex, England, **2008**.
8. Wightman, R. M.; Wipf, D. O. *Electroanalytical Chemistry,* ed. A. J. Bard, Marcel Dekker, New York, USA, **1989,** 267.
9. Wightman, R. M. *Anal. Chem*, **1981**, 5, 1125A.
10. Heinze, J. *Angew. Chem., Int. Ed.* **1993**, 32, 1268.
11. Ronkainen, N. J.; Halsall, H. B.; Heineman, W. R. *Chem. Soc. Rev.* **2010**, 39, 1747-1763
12. Kissinger, P. T.; Heineman, W. R. *J. Chem. Educ*. **1983**, 60,702.
13. Eggins, B. R., *Chemical Sensors and Biosensors*, John Wiley & Sons, West Sussex, England, **2002**.

14. Debouck, C.; Goodfellow, P. N. *Nat. Genet.* **1999**, 21, 48-50.

15. Li, D.; Song, S.; Fan, C. *Acc, Chem. Res.* **2010**, 43, 631-641.

16. Palacek, E. *Nature* **1960**, 188, 656-657.

17. Millan, K. M.; Mikkelsen, S. R. *Anal. Chem.* **1993**, 65, 2317–2323.

18. Hashimoto, K.; Ito, K.; Ishimori, Y. *Anal. Chem.* **1994**, 66, 3830–3833.

19. Herne, T. M.; Tarlov, M. J. *J. Am. Chem. Soc*. **1997,** 119, 8916–8920.

20. Steel, A. B.; Herne, T. M.; Tarlov, M. J. *Anal. Chem*. **1998**, 70, 4670–4677.

21. Yu, C. J.; Wan, Y. J.; Yowanto, H.; Li, J.; Tao, C. L.; James, M. D.; Tan, C. L.; Blackburn, G. F.; Meade, T. J. *J. Am. Chem. Soc.* **2001**, 123, 11155–11161.

22. Fan, C.; Plaxco, K. W.; Heeger, A. J. *Proc. Natl. Acad. Sci. U.S.A.* **2003**, 100, 9134–9137.

23. Marcus, R. A. *Annu. Rev. Phys. Chem.* **1964**, 15, 155–196.

24. Zuo, X.; Song, S.; Zhang, J.; Pan, D.; Wang, L.; Fan, C. *J. Am. Chem. Soc.* **2007**, 129, 1042–1043.

25. Xiao, Y.; Lubin, A. A.; Heeger, A. J.; Plaxco, K. W. *Angew. Chem., Int. Ed.* **2005**, 44, 5456–5459.

26. Zhang, J.; Wan, Y.; Wang, L.; Song, S.; Li, D.; Fan, C. *Electrochem. Commun.* **2008**, 10, 1258–1260.

27. Zayats, M.; Huang, Y.; Gill, R.; Ma, C. A.; Willner, I. *J. Am. Chem. Soc.* **2006**, 128, 13666–13667.

28. Xiao, Y.; Piorek, B. D.; Plaxco, K. W.; Heeger, A. J. *J. Am. Chem. Soc.* **2005**, 127, 17990–17991.

29. Liu, G.; Wan, Y.; Gau, V.; Zhang, J.; Wang, L.; Song, S.; Fan, C. *J. Am. Chem. Soc.* **2008**, 130, 6820–6825.

30. Tyagi, S.; Kramer, F. R. *Nat. Biotechnol.* **1996**, 14, 303–308.

31. Zhang, J.; Song, S.; Zhang, L.; Wang, L.; Wu, H.; Pan, D.; Fan, C. *J. Am. Chem. Soc.* **2006**, 128, 8575–8580.

32. Eckermann, A. L.; Feld, D. J.; Shaw, J. A.; Meade, T. J. *Coord. Chem. Rev.* **2010**, 254, 1769–1802.

33. Mir, M.; Homs, A.; Samitier, J. *Electrophoresis* **2009**, 30, 3386-3397.

34. Manz, A.; Fettinger, J. C.; Verpoorte, E.; Ludi, H.; Widmer, H. M.; Harrison, D. J. *Trends Anal. Chem.* **1991**, 10, 144–149.

35. Burns, M.; Johnson, B.; Brahmasandra, S.; Handique, K.; Webster, J.; Krishnan, M.; Sammarco, T. et al. *Science* **1998**, 282, 484–487.

36. Janasek, D.; Franzke, J.; Manz, A. *Nature* **2006**, 442, 374–380.

37. Farkas, D. H. *Clin. Chem*. **2001**, 47, 1871–1872.

38. Liu, R. H.; Grodzinski, P.; Yang, J.; Lenigk, R. *Integrated Biochips DNA Anal*. **2007**, 46–67.

39. Lee, T. M. H.; Carles, M. C.; Hsing, I. M. *Lab Chip* **2003**, 3, 100–105.

40. Pavlovic, E.; Lai, R. Y.; Wu, T. T.; Ferguson, B. S.; Sun, R.; Plaxco, K. W.; Soh, H. T. *Langmuir* **2008**, 24, 1102–1107.

41. Shiddiky, M. J. A.; Shim, Y. B. *Anal. Chem*. **2007**, 79, 3724–3733.

42. Triroj, N.; Lapierre-Devlin, M. A.; Kelley, S. O.; Beresford, R. *IEEE Sensors J*. **2005**, 6, 1395–1402.

43. Ertl, P.; Emrich, C. A.; Singhal, P.; Mathies, R. A. *Anal. Chem*. **2004**, 76, 3749–3755.

44. Wee, E. J. W.; Rauf, S.; Koo, K. M., Shiddiky, M. J. A.; Trau, M. *Lab Chip* **2013**, 13, 4385-4391.

45. Liu, D. J.; Perdue, R. K.; Sun, L.; Crooks, R. M. *Langmuir* **2004**, 20, 5905–5910.

46. Sadik, O. A; Aluoch, A. O.; Zhou, A. *Biosens. Bioelectron*. **2009**, 24, 2749–2765.

47. Ghindilis, A. L.; Smith, M. W.; Schwarzkopf, K. R.; Roth; K. M.; Peyvan, K.; Munro, S. B.; Lodes, M. J. et al. *Biosens. Bioelectron*. **2007**, 22, 1853–1860.

48. Berti, F.; Laschi, S;, Palchetti, I.; Rossier, J. S.; Reymond, F.; Mascini, M.; Marrazza, G. *Talanta* **2009**, 77, 971–978.

49. Gabig-Ciminska, M.; Holmgren, A.; Andresen, H.; Barken, K. B.; Wumpelmann, M., Albers, J.; Hintsche, R. et al. *Biosens. Bioelectron*. **2004**, 19, 537–546.

50. Gao, C.; Sun, X.; Gillis, K. *Biomed Microdevices* **2013**, 15, 445-451.

51. Sakata, T.; Kamahori, M.; Miyahara, Y. *Japanese J. Appl. Phys*. **2005**, 44, 2854–2859.

52. Star, A.; Tu, E.; Niemann, J.; Gabriel, J.-C. P.; Joiner; C. S.; Valcke, C. *Proc. Natl. Acad. Sci. USA* **2006**, 103, 921–926.

53. Xue, Q.; Bian, C.; Tong, J.; Sun, J.; Zhang, H.; Xia, S. *Biosens Bioelectron*. **2011**, 26, 2689-2693.

54. Mir, M.; Jenkins, A. T. A.; Katakis, I. *Electrochem. Commun*. **2008**, 10, 1533–1536.

55. Dawoud, A. A.; Kawaguchi, T.; Jankowiak, R. *Anal. Bioanal. Chem*. **2007**, 388, 245–252.

56. Branton, D.; Deamer, D. W.; Marziali, A.; Bayley, H.; Benner, S. A.; Butler, T., Di Ventra, M. et al. *Nat. Biotechnol*. **2008**, 10, 1146–1153.

57. Allen, T. *Particle Size Measurement.* Chapman & Hall, London, UK, **1990**.

58. Kasianowicz, J. J.; Brandin, E.; Branton, D.; Deamer, D. W. *Proc. Natl. Acad. Sci. USA* **1996**, 93, 13770-13773.

59. Maglia, G.; Restrepo, M. R.; Mikhailova, E.; Bayley, H. *Proc. Natl. Acad. Sci. USA* **2008**, 105, 19720–19725.

60. Clarke, J.; Wu, H. C.; Jayasinghe, L.; Patel, A.; Reid, S.; Bayley, H.; *Nat. Nanotechnol*. **2009**, 4, 265–270.

61. Cagnin, S.; Caraballo, M.; Guiducci, C.; Martini, P.; Ross, M.; SantaAna, M.; Danley, D.; West, T.; Lanfranchi, G. *Sensors* **2009**, 9, 3122–3148.

62. Ronkainen, N.J.; Halsall, H. B.; Heineman, W. R. *Chem. Soc. Rev.* **2010**, 39, 1747–1763.

63. Sassolas, A.; Leca-Bouvier, B. D.; Blum, L. J. *Chem. Rev.* **2008**, 108, 109–139.

64. Abe, H.; Kool, E.T. *J. Am. Chem. Soc.* **2004**, 126, 13980–13986.

65. Kolpashchikov, D. M. *Chem. Rev.* **2010**, 110, 4709–4723.

66. Franzini, R. M.; Kool, E. T. *J. Am. Chem. Soc*. **2009**, 131,16021–16023.

67. Kolpashchikov, D. M. *J. Am. Chem. Soc*. **2008**, 130, 2934–2935.

68. Hsieh, K.; Xiao, Y.; Soh, H. T. *Langmuir* **2010**, 26, 10392–10396.

69. Wu, D.; Yin, B. C.; Ye, B. C. *Biosens. Bioelectron.* **2011**, 28, 232–238.

70. Chen, J.; Zhang, J.; Li, J.; Fu, F.; Yang, H.; Chen, G. *Chem. Commun*. **2010**, 46, 5939–5941.

71. Chen, J.; Zhang, J.; Guo, Y.; Li, J.; Fu, F.; Yang, H.; Chen, G. *Chem. Commun.* **2011**, 47, 8004–8006.

72. Wu, D.; Yin, B. C.; Ye, B. C. *Biosens. Bioelectron*. **2011**, 28, 232–238.

73. Nakayama, S.; Yan, L.; Sintim, H. O. *J. Am. Chem. Soc*. **2008**, 130, 12560–12561.

74. Yan, L.; Nakayama, S.; Yitbarek, S.; Greenfield, I.; Sintim, H. O. *Chem. Commun.* **2011**, 47, 200–202.

75. Wang, Q.; Yang, L.; Yang, X.; Wang, K.; He, L.; Zhu, J.; Su, T. *Chem. Commun*. **2012**, 48, 2982–2984.

76. Collard, D. M.; Fox, M. *Langmuir* **1991**, 7, 1192–1197.

77. Hsieh, K.; White, R. J.; Ferguson, B. S.; Plaxco, K. W.; Xiao, Y.; Soh, H. T. *Angew. Chem., Int. Ed.* **2011**, 50, 11176–11180.

78. Brown, T.; Hunter, W. N.; Kneale, G.; Kennard, O. *Proc. Natl. Acad. Sci. USA* **1986**, 83, 2402–2406.

79. Liu, D.; Daubendiek, S.; Zullman, M.; Kool, E. T. *J. Am. Chem. Soc*. **1996**, 118, 1587–1594.

80. Ohmichi, T.; Maki, A.; Kool, E. T. *Proc. Natl. Acad. Sci. USA* **2002**, 99, 54–59.

81. Hartig, J.; Kool, E. T. *Nucleic Acids Res.* **2004**, 32, e152.

82. Pomerantz, A.; Moerner, W.; Kool, E. T. *J. Phys. Chem. B.* **2008**, 112, 13184–13187.

83. Nakayama, S.; Sintim, H. O. *J. Am. Chem. Soc.* **2009**, 131, 10320–110333.

84. Nakayama, S.; Wang, J.; Sintim, H. O. *Chem.–Eur. J.* **2008**, 130, 12560–12561.

85. Cai, S.; Lau, C.; Lu, J. *Anal. Chem*. **2010**, 82, 7178–7184.

86. Spencer, S. M.; Lin, L.;Chiang, C.; Peng, Z.; Hesketh, P; Salon, J.; Huang, Z. *ChemBioChem*. **2010**, 11, 1378–1382.

87. Xiang, Y.; Lu, Y. *Anal. Chem*. **2012**, 84, 1975–1980.

88. Zheng, D.; Zou, R.; Lou, X. *Anal. Chem.*, **2012**, 84, 3554–3560.

89. Zhang, J.; Chen, J. H.; Chen, R. C.; Chen, G. N.; Fu, F. F. *Biosens. Bioelectron*. **2009**, 25, 815–819.

90. Hara, Y.; Fujii, T.; Kashida, H.; Sekiguchi, K.; Liang, X.; Niwa, K.; Takase, T.; Yoshida, Y.; Asanuma, H.; Hiroyuk. *Angew. Chem., Int. Ed*. **2010**, 49, 5502–5506.

91. Gerasimova, Y. V.; Peck, S.; Kolpashchikov, D. M. *Chem. Commun.* **2010**, 46, 8761–8763.

92. Gottesfeld, J. M.; Neely, L.; Trauger, J. W.; Baird, E. E.; Dervan, P. B. *Nature* **1997**, 387, 202.

93. Belozerova, I.; Levicky, R. *J. Am. Chem. Soc*. **2012**, 134, 18667-18676.

94. SantaLucia, J. Jr. *Proc. Natl. Acad. Sci. USA* **1998**, 95, 1460-1465.

95. Warren, C. L.; Kratochvil, N. C. S.; Hauschild, K. E.; Foister, S.; Brezinski, M. L.; Dervan, P. B.; Phillips, G. N.; Ansari, A. Z. *Proc. Natl. Acad. Sci. USA* **2006**, 103, 867.

96. Alzeer, J; Luedtke, N. W. *Biochemistry*. **2010**, 49, 4339.

97. Senqupta, B.; Pahari, B.; Blackmon, L.; Senqupta P. K. *PLoS One*. **2013**, 8, e65383.

98. Zhou, J.; Le, V.; Kalia, D.; Nakayama, S.; Mikek, C.; Lewis, E. A.; Sintim, H. O. *Mol. Biosyst*. **2014**, 10, 2724.

99. Glass, L.S.; Bapat, A.; Kelley, M. R.; Georgiadis, M. M.; Long, E. C. *Bioorg. Med. Chem. Lett*. **2010**, 20, 1685.

100. Hauschild, K. E.; Stover, J. S.; Boger, D. L.; Ansari, A. Z. Bioorg. Med. Chem. Lett. 2009, 19, 3779.

101. Puckett, J. W.; Muzikar, K. A.; Tietjen, J.; Warren, C. L.; Ansari, A. Z.; Dervan, P. B. J. Am. Chem. Soc. 2007, 127, 12310.

102. Pope, L. H.; Allen, S.; Davies, M. C.; Roberts, C. J.; Tendler, S. J. B.; Williams, P. M. *Langmuir* **2001**, 17, 8300.

103. Broeck, T. V.; Joniau, S.; Clinckemalie, L.; Helsen, C.; Prekovic, S.; Spans, L.; Tosco, L.; Poppel, H. V.; Claessens, F. *Biomed. Res. Int.* **2014**, 627510.

104. Kim, S.; Annu. M. A. *Rev. Biomed. Eng*. **2007**, 9, 289-320.

105. Peterlinz, K. A.; Georgiadis, R. M.; Herne, T. M.; Tarlov, M. J. *J. Am. Chem. Soc*. **1997**, 119, 3401-3402.

106. Herne, T. M.; Tarlov, M. J. *J. Am. Chem. Soc*. **1997**, 119, 8916-8920.

107. Fan, C.; Plaxco, K. W.; Heeger A. J. *Proc. Natl. Acad. Sci. USA* **2003**, 100, 9134-9137.

108. Lumley-Woodyear, T.; Caruana, D. J.; Campbell, C. N.; Heller, A. *Anal Chem*. **1999**, 71, 394-398.

109. Meunier-Prest, R.; Raveau, S.; Finot, E.; Legacy, G.; Cherkaoui-Malki, M.; Latruffe, N. *Nucleic Acids Res*. **2003**, 31, e150.

110. Li, D.; Song, S.; Fan, C. *Acc. Chem. Res*. **2010**, 43, 631.

111. Flechsig, G.; Peter, J.; Hartwich, G.; Wang, J.; Grundler, P. *Langmuir* **2005**, 21, 7848-7858.

112. Surkus, A.; Flechsig, G. *Electroanalysis* **2009**, 21, 1119-1123.

113. Yang, A. H.; Hsieh, H.; Patterson, A. S.; Ferguson, B. S.; Eisenstein, M.; Plaxco, K. W.; Soh, H. T. *Angew. Chem. Int. Ed*. **2014**, 53, 3163-3167.

114. Russom, A.; Haasl, S.; Brookes, A. J.; Anderson, H.; Stemme, G. *Anal. Chem*. **2004**, 76, 1778-1787.

115. Nasef, H.; Ozalp, V. C.; Beni, V.; O'Sullivan, C. *Anal. Biochem*. **2010**, 406, 34-40.

116. Brewood, G. P.; Rangineni, Y.; Fish, D. J.; Bhandiwad, A. S.; Evans, D. R.; Solanki, R.; Benight, A.S. *Nucleic Acids Res*. **2008**, 36, e98.

117. Blackburn, E. H. *Cell* **2001**, 106, 661-673.

118. Harley, C. B. *Curr. Mol. Med*. **2005**, 5, 205.

119. Neidle, S. *The FEBS Journal* **2010**, 277, 1118-1125.

120. Balasubramanian, S.; Hurley, L. H.; Neidle, S. *Nat. Rev. Drug Discov*. **2011**, 10,261.

121. Kim, M. Y.; Vankayalapati, N.; Shin-Ya, K.; Wierzba, K.; Hurley, L. H. *J. Am. Chem. Soc*. **2002**, 124, 2098-2099.

122. Brooks, T. A.; Hurley, L. H. *Genes & Cancer* **2010**, 1, 641-649.

123. Balasubramanian, S.; Hurley, L. H.; Neidle, S. *Nature. Rev. Drug. Discovery.* **2011**, 10, 261-275.

124. Siddiqui-Jain, A.; Grand, C. L.; Bears, D. J.; Hurley, L. H. *Proc. Natl. Acad. Sci. USA* **2002**, 99, 11593-11598.

125. Nemiroski, A.; Christodouleas, D. C.; Hennek, J. W.; Kumar, A. A.; Maxwell, E. J.; Fernandez-Abedul, M. T.; Whitesides, G. M. *Proc. Natl. Acad. Sci. USA* **2014**, Early Ed, 1-6.